TRANSFER LENGTH, DEVELOPMENT LENGTH, FLEXURAL STRENGTH, AND PRESTRESS LOSS EVALUATION IN PRETENSIONED SELF-CONSOLIDATING CONCRETE MEMBERS

By

Justin D. Trent

Thesis submitted to the Faculty of the Virginia Polytechnic Institute and State University in partial fulfillment of the requirements for the degree of

MASTER OF SCIENCE

In

CIVIL ENGINEERING

APPROVED:

Thomas E. Cousins, Co-Chairperson

Carin L. Roberts-Wollman, Co-Chairperson

Linbing Wang

May 10, 2007

Blacksburg, Virginia

Keywords: self-consolidating concrete, transfer length, development length, prestress losses

TRANSFER LENGTH, DEVELOPMENT LENGTH, FLEXURAL STRENGTH, AND PRESTRESS LOSS EVALUATION IN PRETENSIONED SELF-CONSOLIDATING CONCRETE MEMBERS

Justin D. Trent

ABSTRACT

The first objective of this thesis was to determine the effect of using self-consolidating concrete versus normal concrete on transfer and development lengths, and flexural strengths of prestressed members. Three small rectangular members were made, two cast with SCC mixes and one cast with a conventional mix, to determine the transfer length of each mix. Transfer lengths of both ends of each member were determined by measuring the concrete surface strains. The change in the transfer length was monitored by determining the transfer length of each member at prestress release, 7 days after release, and 28 days after release. All concrete mixes had lower than code determined transfer lengths at prestress release. Each concrete mix showed between a 12 to 56 percent increase in transfer length after 28 days. One SCC mix exceeded the ACI code stipulated 50 strand diameters 7 days after prestress transfer. The other SCC mix was consistently below the transfer length of the conventional concrete.

Separate development length members were cast in a stay-in-place steel form used for creating structural double tees. Each development length member was a stub tee. Iterative load testing was performed to determine the development length of each SCC and conventional mix. Development lengths for both SCC mixes were approximately 20 percent shorter than ACI and AASHTO code predictions. A development length for the conventional concrete was not determined due to non-repeating test data. The flexural strength of each member was determined during load testing. All concrete mixes achieved higher than the ACI predicted strengths.

The second objective of this thesis was to experimentally measure prestress losses and compare these experimental values to theoretical models. Crack initiation and crack reopening tests were performed to experimentally determine the prestress losses in each member. Three theoretical models were evaluated, the sixth edition PCI Design Handbook suggested model, a 1975 PCI Committee on Prestress Losses model, and the AASHTO LRFD prestress loss model. The crack initiation experimental values tended to be between 10 and 15 percent lower than theoretical models. In general, the crack reopening prediction of the effective prestress had a

good correlation with theoretical models. This suggests crack reopening tests can be used as predictors of effective prestress, and as such, predictors of prestress losses in future experimental research. Additionally, the concrete type was shown to affect the prestress losses determined in the development length members. The SCC members tended to have higher effective prestress forces than the conventional concrete members, and thus had less prestress losses due to creep and shrinkage than the conventional concrete members.

ACKNOWLEDGEMENTS

First I want to thank my fiancée, Mary Sullivan, my twin daughters, Megan and Micayla, and the rest of my family who have supported me through my educational journey. Each of you has sacrificed tremendous amounts of time while patiently waiting for me to complete my undergraduate and graduate studies. I thank you from the bottom of my heart for all the love and kindness you have shown me.

Secondly, I want to thank the Charles E. Via, Jr. Department of Civil and Environmental Engineering at Virginia Tech for the opportunity to earn my Master's Degree. I extend my gratitude to the forward thinking engineers and managers at The Shockey Precast Group who helped provide and fund my research. I must also thank Dr. Cousins and Dr. Wollmann for their help in setting up my research and advising me throughout the project. I would also like to thank Dr. Wang for being my other committee member and patiently attempting to understand my research.

Finally, I would like to thank all of those who helped me complete testing at the Structures and Materials Laboratory at Virginia Tech. Often I was uncertain of what step to take next and you provided insight and physical help in finishing the tests.

TABLE OF CONTENTS

LIST OF FIGURES

LIST OF TABLES

1. INTRODUCTION

1.1 Background

Precast, prestressed concrete is a specialty application of structural concrete, where concrete members are manufactured off site and shipped to the construction site to be erected. The members are prestressed in order to counter the effects of service loads encountered during the member's lifetime. Prestressed concrete is effectively used in many applications, ranging from bridges and buildings to parking garages. A major portion of the cost of precast concrete members is the production and quality control.

In a traditional prestressed concrete plant, precast pieces are formed with either wood or steel formwork. Prestressing strand is run along the length of the formwork and is then stressed to its initial design stress. After placement of mild reinforcement, the concrete is brought to the plant and placed and vibrated in the form by numerous laborers. This process is time consuming, noisy, strenuous, and requires stringent quality control procedures which are often difficult to achieve. However, a relatively new type of concrete, self-consolidating concrete (SCC), has the ability to eliminate the need for exhaustive labor used in placing and vibrating concrete into precast forms.

Self-consolidating concrete is a highly flowable concrete mix which has the ability to fill voids around reinforcement under its own weight and without segregating or losing stability. Use of SCC has recently become an important topic in the precast/prestressed concrete industry. Self consolidating concrete has the potential to reduce the cost of producing precast/prestressed concrete product. SCC uses smaller aggregate and admixtures that allow the concrete mix to flow. When SCC is poured into the form, the concrete mix rises around the prestressed strand and mild reinforcement without the need of vibration. The elimination of vibration, which is used for placing most other regular concrete mixes, will reduce the cost of producing the concrete members by decreasing the amount of labor used and the amount of equipment needed to create the concrete members. However, with the use of smaller aggregate a question regarding the bond strength of the SCC mix with the prestressing strand as compared to regular concrete mixes has arisen. Some believe the bond strength of a SCC mix may not be as strong as the bond strength of normal concrete mixes, which could cause a reduction in member strength for members made with SCC as opposed to members made with normal mix concretes.

Aiming to take advantage of the properties of SCC mixes, The Shockey Precast Group (SPG) decided to investigate the bond strength of two SCC mixes compared to one of Shockey's primary mix designs. To this end, a research program was setup by SPG in collaboration with Virginia Tech that will compare the properties of the two SCC mixes with Shockey's regular mix concrete design.

The major objective of this research experiment is to compare the design characteristics of SCC mixes with those of SPG's regular concrete mix. Since SCC has the potential to be used extensively in the production of the Shockey's double tee parking structures, the members tested in this experiment were stub double tee members. The stub double tee members were fabricated at SPG's Winchester, VA precast plant and were shipped to the Virginia Tech Structures and Materials Lab in Blacksburg, VA. SPG's stay-in-place steel forms were utilized to fabricate the development length members. Therefore, gauge points could not be installed along the length of the beams and measurement of the transfer length was not possible. Additional small scale rectangular members were cast and used to determine the transfer length of each mix. The transfer length members were cast and tested at SPG's Winchester, VA plant.

1.2 Research Objectives

This thesis documents a research program sponsored by SPG. The overall goal of the project was to determine if the mechanical bonding characteristics (transfer length and development length) of potential SCC mixes are comparable to or better than the mechanical characteristics of a conventional concrete mix used by SPG. In addition to this, the flexural strength of SCC members was investigated. Furthermore, this thesis will compare theoretical models for computing prestress losses to experimentally determined values of effective prestress.

1.2.1 Transfer Length

The first objective of this thesis is to investigate the transfer length of self consolidating concrete mixes as compared to a conventional concrete mix. The region at the end of a member where the effective prestress force is transferred from the prestressing strands to the concrete is called the transfer length. In this study, three prismatic members (one of each mix design), ten feet long and 6 in. by 6 in. in cross section were created to determine the transfer length. Concrete surface strains were measured on all of the members at various times and were used to determine the transfer length of each mix design. These members were fabricated, instrumented, and tested at SPG's Winchester plant.

1.2.2 Development Length

The shortest length of bond between the concrete and prestressing steel required to achieve the critical stress at that section is known as the development length. In prestressed concrete members, there are two regions which make up the development length. These two regions are the transfer length and the flexural bond length. The flexural bond length is an additional length past the transfer length which is required to reach the ultimate flexural capacity of the member.

In order to determine development length, twelve stub tee beams were created and loaded until failure at various embedment lengths. These embedment lengths were used to determine the development length and the flexural capacity of the members. Theoretically, the development length is the shortest distance of embedment length (L_e) for which a flexural failure will occur. Figure 1.1 shows the schematic for the development length and flexural strength testing layout.

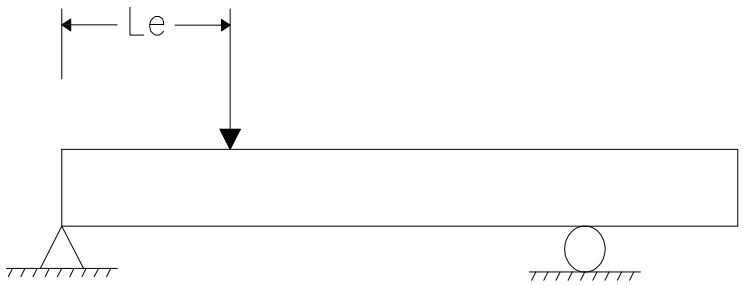

Figure 1.1: Development Length Testing Schematic

1.2.3 Flexural Strength

The ability of a structural member to withstand bending is known as flexural capacity. During the course of development length testing, ultimate moment capacities were determined. These ultimate moments were compared to ACI's theoretical predictions of flexural strength for precast concrete members.

1.2.4 Evaluation of Effective Prestress

The last objective of this research project is to compare experimentally determined values of the effective prestress in the strand to the theoretically determined values. The effective prestress is an important parameter to know when designing prestressed concrete members because it impacts service parameters such as deflection, camber, and crack widths. In addition to these service parameters, the effective prestress can also affect the calculation of concrete shear strength.

Using basic theory of mechanics, the effective prestress in the steel can be experimentally determined. This was done by finding the bending moment required to crack the extreme tensile fiber of the concrete member. The stresses in the member caused by the bending moment were then equilibrated to the internal stresses in the member, and thus the stress in the steel. In addition, the moment required to reopen the crack was used to determine the effective prestress by the same process. These values were then compared to prestress loss models found in the Precast Prestressed Concrete Institute Sixth Edition Design Handbook (PCI 2004), Precast Prestressed Concrete Institute Committee on Prestress Losses (PCI 1975), and the American Association of State and Highway Transportation Officials (AASHTO 2006).

1.3 Thesis Organization

This thesis is organized into five chapters. Chapter one is an introduction of the thesis and research objectives. Chapter two will provide an overview of self-consolidating concrete as well as a discussion of current code provisions and research findings regarding transfer length, development length, flexural strength, and prestress losses. Next, chapter three will discuss the dimensions, material properties, production and testing of the precast members. Chapter four consists of the results from testing and an analysis of the results compared to current code models and research models. Finally, chapter five includes a conclusion of the thesis with a section on recommendations for further research.

2. LITERATURE REVIEW

2.1 Self-Consolidating Concrete

Self-consolidating concrete is a type of high performance concrete which has the ability to flow around dense reinforcement and properly consolidate under its own weight. SCC was first developed in Japan in the 1980's as an underwater concrete and was then expanded to conventional concrete applications to increase casting efficiency and reduce dependency on a low skilled labor supply. Use of SCC has been adopted by several European countries since its development. However, the spread of the technology has been slow to reach the United States (Hamilton et al. 2005).

Recently there has been an increased interest in self-consolidating concrete technology amongst precast producers. The ease of placement of SCC has the potential for producers to redeploy their laborers and potentially create quicker, more efficient casting processes. However, there have been concerns over the bonding strength of SCC to steel prestressing strand. Since SCC technology is just now becoming of interest to most commercial users in the United States, there is little testing data relating the bond strength of SCC to prestressing strand as compared with traditional concrete mixes. Therefore, a brief review of available literature is provided below.

2.1.1 Schindler et al.

This research study was completed in order to evaluate the engineering properties of self-consolidating concrete in precast applications. Twenty-one different SCC mixes were designed and manufactured along with two conventional slump concretes which served as a control group. Variables in the design of the SCC mixes include the use of other cementitious materials (Type III cement with 30 percent Class C fly ash, 30 to 50 percent Ground Granulated Blast Furnace (GGBF) slag, or a blend of 22 percent Class C fly ash with 8 percent densified silica fume), water to cementitious material ratio (0.28, 0.32, 0.36, and 0.40), and the sand to aggregate ratio (by volume – 0.38, 0.42, and 0.46). Fresh concrete properties, such as slump/flow, T-50 (time it takes for the slump/flow to spread out 20 in. in diameter), and visual stability index were performed. Compressive strength, modulus of elasticity, and drying shrinkage were among the hardened concrete properties measured in this study. 4 in. by 8 in. match cured cylinders were created and tested at 18 hours, 21 hours, 7 days, and 28 days. 6x in. by 12 in. moist-cured

cylinders were cast and tested at longer time intervals of 7 days, 28 days, and 56 days. Drying shrinkage specimen was cast and readings were made at 28 days and 112 days.

Compressive strengths of the SCC mixes at 18 hours ranged from 5470 psi to 9530 psi while the two control mixtures had a compressive strength of 6280 psi and 7480 psi. There was no apparent correlation between the initial compressive strength and the sand to aggregate ratio, nor did the sand to aggregate ratio affect the long term compressive strength. As expected, an increase in the water to cementitious material ratio decreased the strength of each concrete mix. The different combinations of cementitious materials appeared to affect the concrete strength only at higher levels of water to cementitious material ratios. This led the authors to suggest that cementitious materials other than Portland cement is can be feasibly used for certain ranges of the water to cementitious material ratio.

The eighteen hour value of the initial modulus of elasticity of the SCC mixes ranged from 4700 ksi to 5900 ksi, while the two control mixes had values of 5330 and 6100 ksi. Fifty-six day modulus of elasticity measurements yielded results ranging from 6650 to 7600 ksi for the SCC mixes and 6500 ksi and 7000 ksi for the control mixes. The initial modulus of elasticity for the SCC concretes was less than values obtained for normal concrete of similar compressive strength. However, the final modulus of elasticity of the SCC concretes was comparable to the control mixes of similar compressive strength. It appeared there was a lag in the stiffness gain in the SCC mixes. Researchers found the sand to aggregate ratio did not affect the modulus of elasticity when the fine and coarse aggregate have comparable elastic modulus and the total aggregate volume is held constant. In addition, the SCC mixes tended to have modulus of elasticity slightly greater than ACI code predicted values which are based on the compressive strength of the concrete.

The last objective of this research was to identify the drying shrinkage properties of SCC. It appears from the data that an increase in the sand to aggregate ratio did correspond to an increase in drying shrinkage at 112 days. In addition, drying shrinkage results compared reasonably well to ACI 209R and AASHTO theoretical model predictions. It was concluded by the authors that these models can be used for predicting drying shrinkage in large scale SCC members (Schindler 2007).

2.1.2 Christian Druta

The author of this research study compared the tensile strength and compressive strength values of self-consolidating concrete and normal concrete specimens as functions of the water to cement ratio. In addition, the bond between the aggregate and the cement paste was investigated with the use of a Scanning Electron Microscope. Twenty-eight day compressive concrete strengths ranged from 4207 psi to 9514 psi for self-consolidating concrete and from 2558 psi to 5924 psi for the normal concrete. The significantly higher compressive strengths were attributed to the use of chemical admixtures in the SCC mixes. Split tensile strengths ranged from 340 psi to 545 psi and from 255 psi to 423 psi for the SCC and normal concrete, respectively.

The split tensile strength and compressive strength tests found a negative correlation between the water to cement ratio and the tested strengths. As the water to cement ratio increased, the tensile and compressive strengths of both the normal and self-consolidating concrete mixes decreased. Since there was such a large difference in concrete compressive strengths, it is hard to compare the split tensile strength of the SCC mix with the normal concrete mix of similar water to cement ratios. Comparing the values of the split tensile strength to ACI code predictions of the tensile strength of concrete gives a correlation between the normal concrete mix and the SCC mix. The tensile strength of both mixes was typically 68 to 75 percent less than the ACI prediction which is based on the concrete compressive strength (Druta 2003).

2.1.3 Chan Y., Chen Y., and Liu, Y.

In this study, researchers sought to determine the effects of concrete consolidation on the bond strength of reinforcement. Three types of concrete were used, a normal concrete (NC) with a low slump (slump approximately 3 in.), a HPC with a high slump (slump greater than 8 in.), and self-consolidating concrete. Different styles of concrete placement were used in this research including vibrating the concrete mix in a manner consistent with standard practice, over vibrating the mix, vibrating the mix by hitting the reinforcing bar with the vibrator, and no vibration. Each of these vibration techniques was used on a specimen cast with each concrete mix. The concrete mixes were cast into pullout test formwork which included three No. 10 reinforcing bars. Specimens were moist cured for 28 days prior to testing. Single reinforcing bar pullout test were performed at 28 days.

Before testing, the condition of each pullout member was visually evaluated. The low slump without vibration and high slump concrete vibrated against the bar did not consolidate

well. The SCC concrete mix consolidated well in all instances. Once each member was tested, correlations between vibration practices and bond strength of the concrete were found. Under normal vibrating conditions, the SCC mix performed the best in terms of bond strength, followed by the HPC. As vibration is applied to each mix, the SCC mix begins to drop in strength, while the HPC and NC mixes increase in bond capacity. When the HPC was over vibrated, its strength was significantly reduced. It was found that HPC concrete is stronger in bond with no vibration than with over vibration or improper vibration. The NC mix bond strength did not seem to degrade with over vibration. It was the findings of this study that improperly vibrating HPC or SCC can significantly reduce the bond capacity of each concrete mix. Therefore, when using these concrete mixes in design, there must be a level of quality control in placing the concrete in order to prevent degradation of concrete strength (Chan et al. 2003).

2.2 Transfer Length

Precast prestressed concrete members are created by stressing steel strands within a formwork, placing concrete around the strands, allowing the concrete to mature to an acceptable strength, then releasing the force in the strand. The force is then transferred from the strand to the concrete through friction and mechanical interlock. The length of the region where the effective prestress force is delivered from the strand to the concrete is known as the transfer length. The stress in the strand varies from zero at the end of the member to the effective prestress at the transfer length. Figure 2.1 below depicts theoretically accepted relationship between strand stress and distance along a prestressed concrete member.

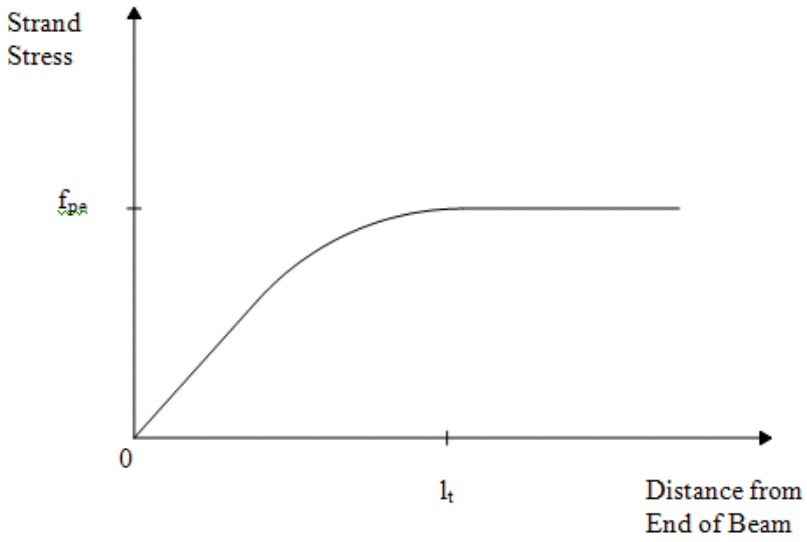

Figure 2.1 Strand Stress versus Member Length

Bond stresses in end regions of prestressed transfer zones are primarily a result of friction and mechanical interlock. In traditional reinforced concrete structures, a third component of bond stress is chemical adhesion. However, in prestress applications this chemical adhesion is broken due to the slip of the prestressing strand at release. Friction develops in the concrete member when the strand force is released and the strand tries to shorten. Due to Poisson's Effect, the diameter of the strand decreases when the strand is initially stressed along its length. As the concrete hardens, it conforms to the reduced strand diameter. When the force is released, the strand attempts to shorten along its length and the diameter tries to increase. This shortening of the strand length and enlarging of the strand diameter create an increase in the normal forces from the strand to the concrete. This increase in normal force in turn increases the bond stresses due to friction. This is known as the Hoyer effect. In addition to frictional bond stresses due to the Hoyer Effect, transfer region stresses are provided by mechanical interlock. Seven wire strand, which is typically used in prestressed applications, has a helical shape. When the strand is released, it attempts to twist as it is pulled through the concrete. Mechanical interlock between the helically shaped strand and the concrete causes more bond stresses to form (Barnes, et al 2003).

Transfer length is important in many design aspects of prestressed concrete, such as deflections, camber, crack widths, and shear design. It is particularly important in shear design since high levels of shear occur in the end regions of prestressed members. If the transfer length is underestimated, the design could become unconservative.

2.2.1 Code Provisions

The American Concrete Institute (ACI) document 318, Building Code Requirements for Structural Concrete, allows two means for calculating the transfer length of a prestressed member. The first is related to shear design and is located in Section 11.4.4. The prestress force should vary from zero at the free end to the effective prestress force at the end of the transfer zone when calculating the concrete web shear strength V_{cw} for a critical section within the transfer region. For this calculation, the transfer length is assumed to be 50 strand diameters.

The second method for determining the transfer length is found in Section 12.9.1 as Equation 12-4, which is as follows:

$$l_d = \left(\frac{f_{se}}{3000}\right) d_b + \left(\frac{f_{ps} - f_{se}}{1000}\right) d_b \qquad 2.1$$

Where:

l_d = development length (in.)

f_{se} = effective stress in prestressing steel (psi)

d_b = strand diameter (in.)

f_{ps} = stress in steel at nominal flexural strength (psi)

ACI Section R12.9 states that the first term of equation 2.1 above is known as the transfer length. The second term in equation 2.1 is the flexural bond length and the summation of the two lengths is the development length, which will be discussed later. When grade 270 strands are stressed at 75 percent of ultimate stress and approximately 25 percent losses are assumed, the transfer length term will reduce to approximately 50 strand diameters, which is the transfer length value used in shear design (ACI 2005).

AASHTO defines the transfer length in Article 5.11.4.1 as 60 strand diameters (AASHTO 2006). This increase from 50 strand diameters to 60 strand diameters is to allow for using larger effective prestress which is the current practice in design (Nassar 2002).

2.2.2 Tabatabai & Dickson

In the process of reviewing the development length equation Tabatabai and Dickson have also dealt with the transfer length equation, which is a part of the development length equation. In their review process, they have identified the rule of thumb value for the transfer length of 50 strand diameters as results from research data on flexural bond by Hanson and Kaar in 1959 and Kaar et al. in 1963. Both of these research initiatives were conducted by the Portland Cement Association (PCA).

The transfer length was found by equating the bond forces along the strand to the force in the prestressing strand:

$$U_t \sum_0 L_t = A_{ps} f_{se} \qquad 2.2$$

Where:

U_t = average bond stress

$\sum_0$ = circumference of prestressing strand = $4/3\pi D$

L_t = transfer length

A_{ps} = area of prestressing strand = $0.725\pi D^2/4$

D = nominal strand diameter

f_{se} = effective prestress

Hanson and Kaar, based on numerous studies at the PCA, suggested the average bond stress should be 400 psi. Using correction factors of 0.725 and 4/3 to account for the difference between actual circumference and area of prestressing strand and the nominal values, and assuming ultimate tensile strength equal to 250 ksi, equation 2.2 will reduce to:

$$L_t \cong \frac{1}{3} f_{se} d_b \qquad 2.3$$

If the effective stress in the strands is 150 ksi, as it was in the tests at PCA, then equation 2.3 reduces to approximately 50 strand diameters.

It is important to note that equation 2.3 was derived for stress relieved strands with ultimate strength of 250 ksi. It is more likely today that grade 270 low relaxation strands will be used. Also, maximum strand diameters used in the tests were equal to ½ in. and all tests were performed in normal weight concrete. In addition, the above equation was derived to give an average value of the transfer length, not an upper bound (Tabatabai & Dickson 1993).

2.2.3 Russell and Burns

In this study, 44 pretensioned prestressed concrete members were tested to determine the transfer length of each member. Of these 44 members, twelve were scaled models of AASHTO cross sections, while the rest were rectangular prismatic members. There were numerous variables considered in this research, including the following: number of strands, diameter of strand, bonded or debonded strand, presence of confining reinforcement, and cross section. The members were created in a manner to simulate precast plant fabrication methods. As such, all the members were torch cut at release, although a few strands in the rectangular sections were detensioned to 70 percent of their original stress before being torch cut. The initial concrete compressive strengths ranged from 3850 to 5580 psi with an average strength of 4460 psi. Final concrete compressive strengths ranged from 5110 to 7530 psi with an average of 6500 psi. Strand spacing in the tested members was 2 in., except for three rectangular members, which were spaced at 2.25 in. to simulate current AASHTO provisions. Concrete cover was either 2, 2.25, or 2.5 in., depending on the cross section.

Concrete surface strain, end slip, and steel strain were the three parameters measured in this research. Concrete surface strains were measured with detachable mechanical strain gages (DEMEC gauges) and were used with DEMEC target points. End slip was measured using dial gages and steel rules. Electrical resistance strain gauges were attached to the strands to measure steel strain, but were deemed unsuccessful due to numerous problems.

Transfer lengths were determined using the 95 percent average maximum strain method (95 % AMS). The procedure for the 95 % AMS method is as follows: 1) the beginning of the strain plateau is visually observed on the strain versus member length plot 2) all strain values within this plateau are averaged 3) this average value is reduced by 5 percent 4) the 95 percent AMS line is plotted on the strain versus member length plot 5) the intersection of the 95 percent

AMS line with the strain profile gives the transfer length. The average transfer length for a 0.5 in. fully bonded strand was 29.5 in. with a standard deviation of 6.85 in. The average transfer length for fully bonded 0.6 in. diameter strands was 40.0 in. with a standard deviation of 6.80 in. During this study, it was determined that the transfer length is not linearly proportional to the diameter of the strand. The code equation for the transfer length would predict a 20 percent increase in transfer length with a 0.1 in. increase in strand diameter. However, this study found a 36 percent increase resulted from a 0.1 in. increase in diameter. Therefore, the authors proposed the following equation to relate the transfer length to the strand diameter:

$$l_t = K d_b^{\alpha} \tag{2.4}$$

Where:

l_t = transfer length (in.)

K = constant

d_b = strand diameter (in.)

α = constant

Through regression analysis, an α of 1.68 was found to best fit the data in this study. After normalizing the data, average transfer lengths were 59 strand diameters and 67 strand diameters for 0.5 in. and 0.6 in. diameters strands, respectively. A conservative transfer length equation was proposed as

$$l_t = \frac{f_{se}}{2} d_b \tag{2.5}$$

Where:

l_t = transfer length (in.)

f_{se} = effective prestress (ksi)

d_b = strand diameter (in.)

Several other parameters were assessed in this study including an end slip relation to transfer length, spacing of strands, and transfer length of debonded strands, effect of cross section on transfer length, and effect of confinement reinforcement on transfer length. This study showed a relationship between the end slip and the transfer length of prestressed concrete members.

$$l_t = \frac{2E_{ps}}{f_{si}} L_{es} \qquad 2.6$$

Where:

l_t = transfer length (in.)

E_{ps} = prestressing strand modulus of elasticity (ksi)

f_{si} = strand stress immediately prior to release (ksi)

L_{es} = end slip

Strand spacing of 2 in. was found to be adequate for 0.6 in. diameter strands, as opposed to the rule of thumb spacing of 2.25 in. The effect of the cross sectional area was significant since transfer lengths of scale AASHTO shapes were 25 percent less than the rectangular members. Finally, confining reinforcement seemed to have no significant affect on transfer lengths (Russell & Burns 1996).

2.2.4 Barnes, Grove, and Burns

This study measured transfer lengths of 36 plant-cast AASHTO Type I girders with 0.6 in. diameter prestressing strands spaced at 2 in. on center. Two thirds of the strands in the girders were subjected to varying debonding lengths. This resulted in creating 192 different transfer length zones. Of these 192 transfer zones, 184 transfer lengths were determined. Several factors were investigated to determine their effect on the transfer length, including concrete strength, time, surface condition of the strand, and type of prestress release. Three concrete mixes were used and were designated as L, M, and H. The target initial strengths for L, M, and H concrete mixes were 4000, 7000, and 9000 psi, respectively. The target range for 28 day compressive strengths were 5000 to 7000 psi for mix L, 9500 to 11,500 psi for mix M, and 13,000 to 15,000 psi for mix H. Transfer length measurements were determined at various time frames after casting to determine the time dependence of transfer length. Some strands used in

the testing exhibited a rusted surface, while others were clean. This strand surface condition was taken into account during testing. Finally, release methods were used to correlate release conditions to transfer length. In the first release method, strands were torch cut at both ends of a member to simulate sudden release, whereas in the second method, strands were cut from one end at a time to simulate a gradual release of prestress force at the second end of the member.

Results of this research showed that all 184 transfer lengths measured were less than the AASHTO stipulation of 60 strand diameters. Only three of the transfer lengths actually eclipsed the ACI provision of 50 strand diameters used in shear design. The following equation was used in this study:

$$l_t = \alpha \frac{f_{pt}}{\sqrt{f'_{ci}}} d_b \qquad 2.7$$

Where:

l_t = transfer length (in.)

α = proportionality constant ($ksi^{-0.5}$)

f_{pt} = tendon stress after release (ksi)

f'_{ci} = initial concrete compressive strength (ksi)

d_b = strand diameter (in.)

From equation 2.7 we find that the transfer length is inversely proportional to the concrete compressive strength. In the study an α value equal to 0.57 produced an upper bound line for the transfer length equation. As time proceeded from prestress release, the transfer length increased approximately 10 to 20 percent. It is noted, however, that the majority of this increase occurred within 28 days of prestress release. The surface condition of the strand did affect the transfer length measured. Rusted strands in concretes with lower compressive strengths had 13 percent smaller transfer lengths than bright strands. However, the effect in higher strength concretes was negligible since rusted strand transfer lengths were widely variable and were sometimes longer than bright strand transfer lengths. As a result, researchers do not recommend using weathering as a means to decrease transfer lengths. Type of prestress release (sudden or gradual) had little effect on the transfer length of bright strands. However, the transfer length of rusted strands

increased 30 to 50 per cent when comparing the live end values to the dead end values. Researchers attributed this effect to the concrete bonding to the rust and not the whole strand. When the strand is released, the rust breaks free and reduces the frictional bond stresses. Finally, researchers recommended using a lower bound approach to determining the transfer length when checking release stresses in the concrete. A value of α equal to 0.17 corresponds to this lower bound value (Barnes, et al 2003).

2.2.5 C. Dale Buckner

This report, sponsored by the Federal Highway Administration (FHWA), was completed in 1994 to resolve conflicting recommendations on transfer length and development length from various research studies. In 1988, FWHA issued a memorandum prohibiting the use of 0.6 in. diameter strand in pretensioned precast concrete. In addition, FHWA required a minimum strand spacing to be at least 4 strand diameters. This was done in response to research by Cousins et al. at North Carolina State University which measured very long transfer lengths (1990). The report reviewed numerous studies and recommended new design criteria.

Buckner recommended the following transfer length equation:

$$l_t = \frac{1250 f_{si} d_b}{E_c} \qquad 2.8$$

Where:

l_t = transfer length (in.)

f_{si} = initial strand stress (ksi)

d_b = strand diameter (in.)

E_c = elastic modulus (ksi)

For normal weight concrete with concrete strength at release greater than 3500 psi, equation 2.8 reduces to:

$$l_t = \frac{f_{si} d_b}{3} \qquad 2.9$$

It is important to note Shahawy et al. were the first to propose the use of equation 2.9 in determining the transfer length.

2.2.6 Girgis and Tuan

This study was undertaken to determine the bonding capacity of self-consolidating concrete. Transfer length testing was performed on three bridge girders, two of which were cast with self-consolidating concrete (SCC), and the other was made with a conventional concrete mix. In addition to the transfer length tests performed, Moustafa style pullout tests were performed on 0.6 in. diameter strands.

The three girders tested were various I-shaped bridge girders which were to be used in actual bridge construction. The bridge girder in project I, which was an SCC mix project, had a depth of 44.3 in. and a web thickness of 5.9 in. It was 72.5 ft long with 14, 0.6 in. diameter straight strands spaced at 2 in., with 2 harped strands and four top strands. The girder of project II, also a SCC project, had a depth of 35.4 in. with a web thickness of 5.9 in. It was 90.0 ft long with 26, 0.6 in diameter straight strands, eight harped strands, and four top strands. The girder of project III, the conventional concrete mix project, had a depth of 53.6 in. and a web width of 5.9 in. The girder was 124.0 ft long with 44, 0.5 in diameter straight strands, ten harped strands, and four top strands. Initial concrete compressive strengths for Projects I, II, and II were 6492, 5977, and 6970 psi, respectively. The 28 day compressive strengths were 10,887 psi, 8033 psi, and 9523 psi for project I, project II, and project III, respectively.

Transfer length measurements were taken at release and at 3, 7, 14, and 28 days. Measurements were made using DEMEC gage points and a measuring caliper. The 95 percent average maximum strain value method was used to determine the transfer length of each girder. To take into account the different compressive strengths of each concrete girder, Equation 2.7 was used to normalize the data. The measured transfer lengths of each girder were as follows: 38 in. for Project I, 46 in. for Project II, and 21 in. for Project III. From this data, the authors concluded the transfer length of SCC girders may be longer than expected when compared to transfer lengths of conventional concrete girders. The authors noted that lower early strengths experienced by the SCC mixes may have been the cause of the longer transfer lengths.

Eighteen Moustafa pullout tests were performed on each mix with 0.6 in. diameter strands embedded at 18 in. depths. The concrete block was 80 in. long with a 24 in. by 24 in cross section. The strands were spaced at 8 in. The pullout capacities of each mix were as follows: 43.4 kip with a standard deviation of 2.8 kip at two days for Mix 1 (corresponding to Project I), 54.2 kip with a standard deviation of 5 kip at one day for Mix 2 (corresponding to

Project II), and 48 kip with a standard deviation of 8.6 kip for Mix 3 (corresponding to Project III). The benchmark for Moustafa pullout test is considered to be 36 kip, which shows that all mixes had adequate bond strength. Interestingly, Mix 2 was tested again at 28 day and had significantly increased values of bond strength (65.9 kip with a standard deviation of 2.9 kip). This finding led the researchers to suggest that flexural bond lengths in SCC may be smaller than in conventional concrete mixes.

2.3 Development Length

Development length is the shortest length of embedded strand required to produce the necessary stress in the steel (f_{ps}) for nominal flexural strength. There are two components to the development length. The first component is the transfer length (discussed in section 2.2). The second portion of the development length is the flexural bond length. The sum of the transfer length and flexural bond length is the development length. The stresses in the flexural bond region differ from stresses in the transfer bond region. Flexural bond stresses are created by variation in the bending moment along the length of the member due to externally applied loads. When cracking occurs, these flexural bond stresses increase significantly. The strand diameter decreases with the increase in stress due to Poisson's effect. The stresses are high enough to cause localized slipping of the strand at the crack due to loss of chemical adhesion between the strand and the concrete and loss of frictional bond stresses. This slip causes stress increases adjacent to the crack. When the stress reaches a value large enough to cause slip, the chemical adhesion is broken and the frictional resistance is decreased at that location and stresses are redistributed as before. This continued redistribution results in a bond stress wave from the initial crack towards the ends of the member. Once the stress wave reaches the transfer region, general bond failure occurs and the maximum strand stress has been reached. Due to the helical shape of the strand, mechanical interlock between the strand and the concrete can allow the member to continue to attain load and deform (Nilson 1987). Figure 2.2 below shows the variation of steel stress with distance along the member.

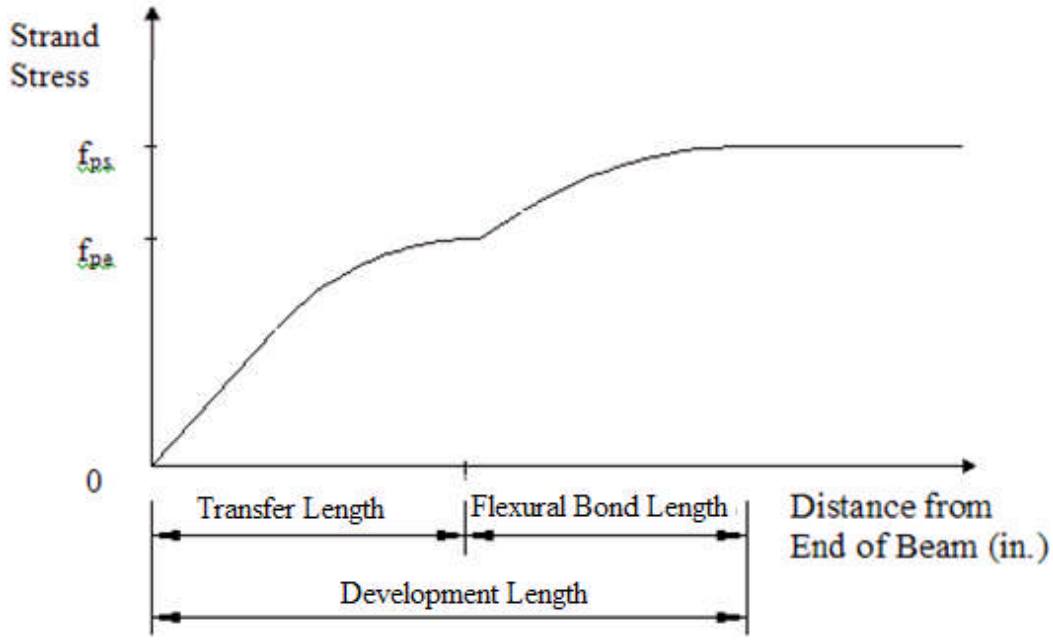

Figure 2.2 Strand Stress versus Member Length

2.3.1 Code Provisions f_{ps}

ACI recommends the use of Equation 2.1 for the calculation of development length. Per ACI Section 12.9.1, the length of embedded strand must be longer than Equation 2.1 in order to use the full strength of the member. However, if the length of embedded strand is less than the development length, ACI Section 12.9.1.1 allows for a reduction in strand stress, and thus a reduction in flexural capacity, to account for the shorter embedment length (ACI 2005).

AASHTO recommends equation 5.11.4.2-1 from Article 5.11.4.2 for the development length of prestressing strand

$$l_d \geq \kappa\left(f_{ps} - \frac{2}{3} f_{pe} \right) \qquad 2.10$$

Where:

l_d = development length (in.)

d_b = nominal strand diameter (in.)

f_{ps} = average stress in prestressing steel required for nominal resistance (ksi)

f_{pe} = effective stress in prestressing steel after losses (ksi)

κ = 1.0 for pretensioned members with depth less than or equal to 24.0 in.

κ = 1.6 for pretensioned members with depth greater than 24.0 in.

If κ is set equal to 1.0, then Equation 2.10 becomes the ACI recommended equation for development length determination. In addition, AASHTO recommends a bilinear relationship for determining maximum strand stress at locations with embedment lengths less than the development length. The bi-linear relationship is shown in Figure 2.3 (AASHTO 2006).

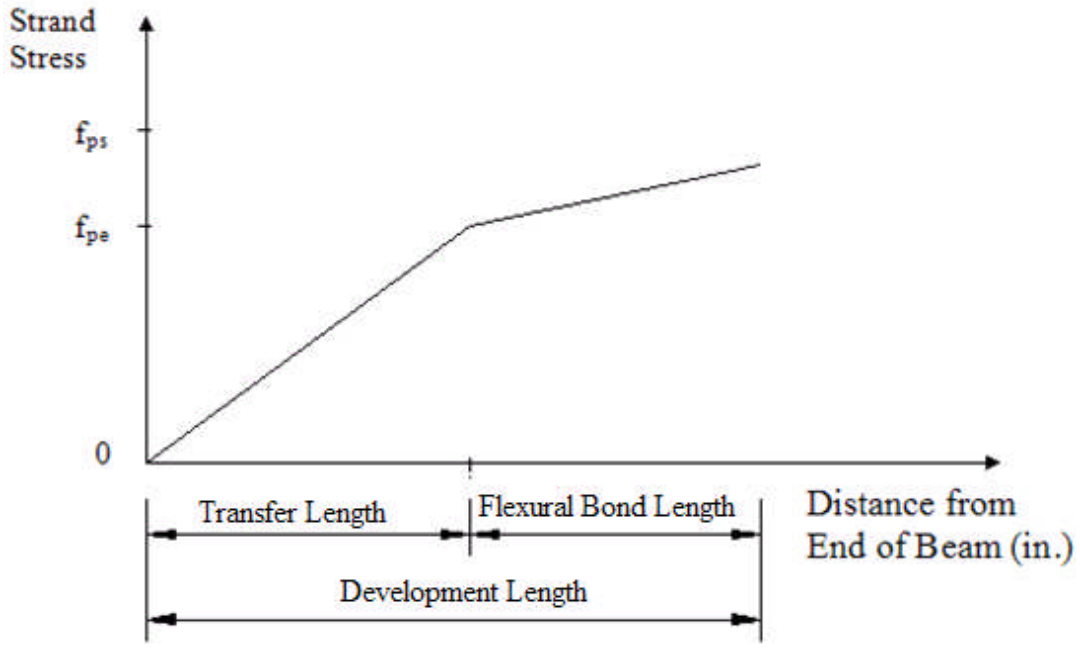

Figure 2.3 Bi-linear Approximation of Strand Stress

2.3.2 Tabatabai and Dickson

Tabatabai and Dickson, through an intense literature review process, determined the origins of the development length equation to be a result of pioneering research completed by Hanson and Kaar in 1959. The creation of the development length equation was attributed to Alan H. Mattock, who was employed at PCA. The original form of the development length equation proposed by Mattock was

$$f_{ps} - f_{se} = 0.9\left(\frac{L_d - L_t}{d_b}\right) \quad 2.11$$

ACI suggested rearranging the equation and dropping the 0.9 factor. If Equation 2.3 is substituted for the transfer length (L_t) of the rearranged equation suggested by ACI, the following results:

$$l_d = \left(\frac{f_{se}}{3}\right)d_b + \left(f_{ps} - f_{se}\right)d_b \quad 2.12$$

Equation 2.12 is identical to Equation 2.3, except that the units are in ksi instead of psi. This equation was derived using grade 250, stress relived strand with a maximum diameter of ½ in. As was noted in section 2.2.2, the equation is designed to give an average development length as supported by the research data at the time of derivation (Tabatabai & Dickson 1993).

2.3.3 C. Dale Buckner

As discussed in section 2.2.5, FHWA required strand spacing to be 4 strand diameters in response to research findings by Cousins et al. Numerous research initiatives sought to prove 2 in. strand spacing was adequate for 0.6 in. diameter strand, instead of the FHWA requirement of 2.25 in. (four strand diameters). Buckner reviewed the research data presented in these experiments and recommended the following equation:

$$l_d = \frac{f_{si}d_b}{3} + \lambda\left(f_{ps} - f_{se}\right)d_b \quad 2.13$$

Where:

l_d = development length (in.)

f_{si} = strand stress immediately after release (ksi)

d_b = strand diameter (in.)

$\lambda = [0.6 + 0.4\varepsilon_{ps}]$ (ε_{ps} is the strain corresponding to f_{ps}

f_{ps} = stress in steel at nominal flexural strength (ksi)

f_{se} = effective stress in prestressing steel (ksi)

There are two differences between Equation 2.13 and the AASHTO LRFD development length equation. The first difference is the change from f_{se} to f_{si} in the transfer length term (see 2.2.5). The second change is the additional multiplier, λ, to the flexural bond length term. The suggested lower and upper limits on λ are 1.0 and 2.0, respectively. These λ values correspond to steel strains of 0.01 and 0.035 respectively, and are considered reasonable design limits.

2.3.3 Mohsen Shahawy

In this study, the researcher reviewed results from numerous tests of prestressed slabs, piles, and girders tested at the Florida Department of Transportation (FDOT) Structures Research Center (FSRC). For this study, twelve AASHTO Type II girders were created with initial concrete strength of 4000 psi and final concrete strength of 5000 psi. Each girder had a cast in place reinforced concrete deck with a 28 day design concrete strength of 5000 psi. Variables tested in this experiment include strand diameter, embedment length, and confinement reinforcing.

Development length tests concluded the AASHTO provision at the time of research (Equation 2.10 without the 1.6 factor) was unconservative, and the proposed AASHTO equation modifier of 1.6 was overly conservative. During testing, researchers discovered that initial slippage occurred nearly simultaneously with the appearance of the first shear crack. This led the researchers to believe there was a correspondence between shear cracking and bond failures. For members with depths greater than 24 in., development lengths were consistently longer than the AASHTO provision at the time. A new development length equation was proposed to take into account the shear bond interaction. The new equation is as follows:

$$l_d = \left(\frac{f_{si}}{3}\right)D + \frac{\left(f_{su}^{\ *} - f_{se}\right)D}{4u_{ave}} + d\cot\theta \qquad 2.14$$

Where:

l_d = development length (in.)

f_{si} = strand stress immediately after release (ksi)

D = strand diameter (in.)

$f_{su}^{\ *}$ = strand stress required for ultimate strength (ksi)

f_{se} = effective prestress (ksi)

u_{ave} = average bond stress (ksi)

d = distance to critical section (in.)

θ = angle of shear failure

The first two terms of Equation 2.14 are the flexural development length terms, whereas the third term is the shear development length term. If the average bond stress is assumed to be 300 psi, the angle of shear failure is assumed to be 30 degrees, and the critical section is assumed to be 85 percent of the section height, Equation 2.14 becomes:

$$l_d = \left(\frac{f_{si}}{3}\right)D + \frac{\left(f_{su}^{*} - f_{se}\right)D}{1.2} + 1.47h \qquad 2.15$$

Where:

h = section height

This equation was recommended by the researcher in place of the AASHTO equation at the time of research. Equation 2.15 was shown to offer conservative values of the development length with a mean development length 20 percent greater than measured values and a standard deviation of 0.15. The equation was therefore conservative, but not as conservative as the 1.6 factor that is currently used in AASHTO (Shahawy 2001).

2.4 Flexural Strength

A brief review of code provisions and related research on flexural strength will be provided in the following subsections.

2.4.1 Code Provisions

The flexural strength of pretensioned concrete members where the assumed compressive stress block has a depth less than the thickness of the flange is as follows:

$$M_n = A_{ps} f_{ps}\left(d_p - \frac{a}{2}\right) + A_s f_y\left(d - \frac{a}{2}\right) + A_s' f_s'\left(\frac{a}{2} - d'\right) \qquad 2.16$$

Where:

M_n = nominal moment strength (in.-kip)

A_{ps} = area of prestressing strand(s) (in^2)

f_{ps} = stress in prestressing steel at ultimate strength (ksi)

d_p = depth from extreme compression fiber of concrete to centroid of prestressing steel (in.)

a = depth of compressive stress block (in.)

A_s = area of positive flexural reinforcing steel (in^2)

f_y = yield stress of mild reinforcement (ksi)

d = depth from extreme compression fiber of concrete to centroid of positive reinforcement (in.)

A_s' = area of negative flexural reinforcing steel (in^2)

f_s' = stress in negative flexural reinforcing steel (ksi)

d' = depth from extreme compressive fiber of concrete to centroid of negative reinforcement (in.)

This equation assumes a prismatic member.

In order to determine the stress in the prestressing steel, f_{ps}, at ultimate strength, ACI defines equation 18-3 for fully bonded prestressing strands in section 18.7.2 as the following:

$$f_{ps} = f_{pu}\left\{1-\frac{\gamma_p}{\beta_1}\left[\rho_p\frac{f_{pu}}{f_c'}+\frac{d}{d_p}(\omega-\omega')\right]\right\} \qquad 2.17$$

Where:

f_{ps} = stress in prestressing steel at ultimate strength (ksi)

f_{pu} = ultimate stress of prestressing steel (ksi)

γ_p = factor relating strand yield stress to ultimate strand stress

β_1 = factor related to concrete strength

ρ_p = ratio of A_{ps} to bd_p

f_c' = concrete compressive strength (ksi)

d_p = depth from extreme compression fiber of concrete to centroid of prestressing steel (in.)

ω = tension reinforcement index ($\rho f_y/f_c$')

ω' = compression reinforcement index ($\rho' f_y/f_c$')

AASHTO provides the same guidance as ACI in determining the flexural strength of prestressed concrete members.

2.4.2 Natio, Parent, & Brunn

Full scale testing was performed on bulb-tee cross sections to determine the flexural and shear behaviors of SCC as compared to a conventional concrete mix made of high early strength concrete (HESC). Three girders were cast with SCC and three other girders were cast with HESC concrete. The girders had a depth of 45 in. with a web thickness of 7 in., a top and bottom flange width of 47 in. and 32 in., respectively, and were 35 ft long. There were a total of 26 strands in each of the full cross section girders. Three different load conditions were analyzed, compressive flexural failure, web shear failure, and tensile flexural failure. Concrete compressive strengths ranged from 9183 psi to 10,037 psi for the HESC mix and from 8930 psi to 10,720 psi for the SCC mix. The average values of the concrete compressive strengths for the HESC and the SCC were 9639 psi and 9993 psi, respectively.

To analyze the compressive flexural failure, the load application was set up at an embedment length equal to one development length plus the depth of the section. This location ensured enough development length of the strands to result in a flexural failure mode. The web shear failure setup required the load to be closer to the support, so the point of load application was reduced to under a development length. For the tensile flexural failure, the bottom layer of strands were severed at the point of load application by chipping the bottom concrete cover away and then flame cutting the strands.

In each case the experimental results yielded higher flexural capacities and shear capacities than theoretically predicted. The range for flexural capacity in the HESC girders was from 1 percent to 4 percent greater than theoretical values and the range for SCC was 1 percent to 2 percent greater than theoretical values. The web shear capacity of the HESC was 7 percent greater than theoretical values and the web shear capacity for the SCC was 6 percent greater than theoretical values. In addition, flexural and shear deformation was as expected, and the HESC and SCC damage profiles were comparable. The researchers concluded the SCC mixture used in their work outperformed current design requirements and would be a viable option for implementation (Natio et al. 2006).

2.4.3 Hamilton, H.R., Labonte, T., & Ansley, M.H.

In this research project, the plastic and hardened properties of self-consolidating concrete were examined in field and laboratory testing. The portion of the research highlighted here is the examination of flexural and shear behavior of AASHTO Type II girders cast with SCC and

normal concrete. Eight AASTHO Type II girders (four with SCC mixes and four with normal concrete mixes) were cast along the same line of prestressing strands. Each girder had a concrete cap cast compositely with the girder to simulate the presence of a bridge deck. The concrete cap was 2 ft wide and 1 ft deep with No. 5 grade 60 mild reinforcement used for temperature and shrinkage steel. One girder of each mix was tested to produce a flexural failure mode, while the other was tested to produce a shear failure mode. Four more AASHTO Type II girders (one of each SCC mix and one of each normal concrete mix) were cast without deck caps and were tested to produce shear failures. To design the girders, the AASHTO LRFD Bridge Design Specification was used to design a fictitious bridge with a span of 40 ft and girders spaced evenly at 6 ft. The prestressing tendon consisted of twelve 0.5 in. diameter grade 270 prestressing strands with 2 strands debonded for a length of 6 ft. The average concrete strength of the SCC girder at the time of testing was 10,030 psi, while the average strength of the normal concrete mix was 7490 psi. The average concrete strength of the cap cast on the SCC girder and the normal concrete girder was 8350 psi and 7405 psi, respectively.

Shear tests were performed on four AASHTO Type II girders made of four separate mixes, two SCC and two normal concrete. The cracking behavior of each mix was nearly identical and each beam failed as a result of compression failure of the top flange. The standard concrete mix out performed one of the SCC mixes by carrying 8.7 percent more load and deflecting 22 percent more. The second SCC girder and the second normal concrete girder performed almost identically in the shear tests.

Shear-flexure tests were also performed to characterize the flexural behavior of SCC when compared to a standard concrete mix. The test was setup to create web shear cracking, followed by a ductile flexural failure mode in each specimen. In all four shear-flexure tests, the concrete cap failed in compression due to flexural bending of the composite section. Visual inspection of each member showed the cracking behavior of SCC beams was similar to the cracking behavior of normal concrete beams. The flexural load capacity of all the beams was very similar. However, the deflection of the first standard mix girder was 41.5 percent greater than the deflection of the first SCC mix girder. The second standard mix girder had a 9.3 percent greater deflection than the second SCC mix girder. These results led the author to conclude the ductility of an SCC girder may be significantly less than the ductility of a normal concrete girder.

Finally, four shear-slip tests were completed, one for each SCC and normal concrete mix girder. An embedment length for the point of load application shorter than the development length of each strand was used for this test. Additionally, the end of the beam being tested was placed so it overhung the bearing support by 6 in. in order to promote shear cracking and bond failure of the strand. With the exception of one SCC mix girder, the failure mode was again compression failure of the cap due to flexural bending stresses. As with the shear-flexure tests, the load capacities of the SCC and normal concrete girders were similar, except for the strand slip failure of the second SCC mix girder. Again, the ductility of the normal concrete girder was much greater than the ductility of the SCC girder with the normal concrete girder deflecting 18 percent more. The second SCC mix girder failed in a strand slip manner and thus its load capacity and ductility was reduced. That particular girder was positioned on the end of the casting line of girders in which the strands were torch cut at prestress transfer, while the normal concrete members were not subjected to the sudden prestress transfer. It is the author's belief that this resulted in a longer transfer length for the second SCC girder, which in turn resulted in a longer development length. The long development length did not allow the girder to reach its full load carrying capacity (Hamilton et al. 2005).

2.5 Prestress Losses

Prestress losses in pretensioned concrete members occur as a result of two different phenomena. The first is instantaneous loss of prestress, which is caused by elastic shortening of the concrete member at the transfer of prestress force from the steel to the concrete, and by slip of the strand. The second is a long term loss of prestress force due to creep and shrinkage of the concrete member, and from relaxation of the steel strand. Below is an overview of the various prestress loss models available within codes or the literature.

2.5.1 ACI 318-05

The ACI 318 code does not give a specific model to use for calculating prestress losses in pretensioned concrete members. Instead, the commentary refers the reader to various references in order to determine prestress losses. The ACI code simply stipulates that prestress loss calculations should consider prestressing steel seating at transfer, elastic shortening of the concrete, creep of the concrete, shrinkage of the concrete, and relaxation of the steel.

2.5.2 AASHTO LRFD 2006

AASHTO has two methods for computing prestress losses. The first is an approximate method which applies to standard precast members which undergo normal loading and exposure conditions. This approximate method is restricted to normal weight concrete members that are moist or steam cured and made with prestressing steel that has low or normal relaxation properties (AASHTO 2006). The second method is a time dependent method, where prestress losses are evaluated at various time steps to determine the effective prestress in the member at any particular time. The time step method is used mostly for precast members that act compositely with a deck, but it can be used on noncomposite members as well. An outline of the time step method for prestress loss determination is given in Chapter 4.

2.5.3 PCI Prestress Loss Recommendations

Two separate models have been put forth by PCI as models for predicting prestress losses. The first model was introduced in 1975 by the CPI Committee on Prestress Losses. The method put forth by this committee utilizes a time stepping model similar to AASHTO. The losses are broken into initial losses and time dependent losses. Elastic shortening is the initial prestress loss considered in this model. The long term prestress losses used in this model are shrinkage of the concrete, creep of the concrete, and relaxation of the prestressing steel.

The second theoretical model addressed by PCI is the model provided in the sixth edition PCI design handbook. This model allows the user to determine various types of prestress losses, including elastic shortening, creep, shrinkage, and relaxation. One interesting aspect of this model is the time independence of the model. There is no term in this prestress model which affiliates the time effects of creep or shrinkage. Specific details of each PCI model are provided in Chapter 4.

2.5.4 Baran, Shield, & French

Researchers in this study performed experimental studies to evaluate the use of high strength concrete in bridge applications. Two MnDOT 45M I-girders were cast along 46 0.6 diameter grade 270 prestressing strands, which were either draped or debonded at the ends to prevent tensile cracks at release. The initial compressive strengths of girder I and girder II were 9300 psi and 10,400 psi, respectively. The 28 day compressive strength of each girder was 12,100 psi for girder I and 11,100 psi for girder two. Each girder had a composite deck cast on its top. Prestress losses were determined by vibrating wire gauges and by flexural load testing.

Flexural load testing was used to calculate the effective prestress in each girder, which could then be used to determine the amount of prestress losses. The loads required to initiate and reopen cracks were used to calculate the effective prestress. Equation 2.18 below gives the effective prestress for a given load.

$$\sigma = -\frac{P_e}{A_{nc}} - \frac{P_e e_{nc} c_{nc}}{I_{nc}} + \frac{(M_o + M_d) c_{nc}}{I_{nc}} + \frac{M_{applied} c_c}{I_c} \qquad 2.18$$

Where:

σ = stress in concrete (ksi)

P_e = effective prestress force (kip)

A_{nc} = non-composite area (in.^{2})

e_{nc} = non-composite eccentricity (in.)

c_{nc} = non-composite distance to extreme fiber (in.)

I_{nc} = non-composite moment of inertia (in.^{4})

M_o = self weight moment (in.-kip)

$M_{applied}$ = applied moment during load testing (in.-kip)

c_c = composite distance to extreme tension fiber (in.)

I_c = composite moment of inertia (in.^{4})

When performing the crack initiation test, the concrete stress at the centroid of the prestressing force is set equal to the concrete tensile strength and the corresponding cracking moment and prestressing force is determined. When a crack reopening test is performed, the concrete stress at the same location is determined and the corresponding applied moment and prestressing force is determined. Values of the total prestress losses measured by crack initiation and crack reopening tests were 7.7 percent and 12.0 percent higher than the losses determined using the vibrating wire gauges for girder I and girder II, respectively. The authors concluded that prestress losses occur prior to transfer of the prestress force.

2.5.5 Hunter T. Hodges

This research study was performed to investigate the effect of casting orientation of prestressing strand on its bonding capacity and to determine prestress losses experimentally. Twenty four bulb tee prestressed concrete members were cast with three prestressing strands in the bottom flange. Four different strand types were used including ½ in. diameter grade 270, ½ in. diameter grade 300, ½ in. special diameter grade 270, and ½ in. special diameter grade 300

strand. Initial concrete strength averages ranged from 4850 psi to 5970 psi. Final average concrete strengths at testing ranged from 6420 psi to 8190 psi. Transfer and development length testing found strands cast with a significant depth of concrete below their location had longer transfer and development lengths than normally cast strands. A modifying factor similar to the reinforcing bar location factor for deformed bar development length was suggested.

Three methods were used to experimentally determine prestress losses. The first was the use of vibrating wire gauges. The second and third methods consisted of the use of flexural testing to initiate and reopen cracks. When compared to code determined values of the prestress losses, the vibrating wire gauge upper bound was within 4 percent on average of the theoretical loss model provided by AASHTO. However, the lower bound value of prestress loss, on average, was only 75 percent of the AASHTO model. Crack initiation and crack reopening tests also had larger measured losses than AASHTO's code values. The crack initiation model resulted in 5 percent more prestress losses and the crack reopening model resulted in 19 percent more prestress loss than the AASHTO model, on average. As with Baran, Shield, and French, the author of this study suggests prestress losses are occurring before transfer of the prestress force (Hodges 2006).

2.6 Literature Review Digest

This literature review has been provided to familiarize the reader with the current code guidance for the transfer length, development length, and flexural strength of pretension concrete members. In addition, current and past research work has been presented to expose the reader to proposed alternative equations for transfer length of both conventional concrete and SCC members, as well as equations for the development length of convention concrete members. Furthermore, current research on the behavior of self-consolidating concrete members in flexure has been presented. Prestress loss models will be presented in chapter 4 of this thesis.

While many research programs have been setup to determine the transfer length, development length, and flexural strength of conventional concrete member, there is little research results currently available for transfer length and flexural strength of SCC pretensioned members and even less literature on the development length of SCC members. This thesis will add a little more data to the pool of transfer length data currently available. The development length testing performed in this research program will add significantly needed statistics on the development length and flexural strength of SCC to the research community. Experimental

prestress loss methods used in this thesis will attempt to confirm the ability to use crack initiation and crack re-opening tests to monitor prestress losses. Additionally, prestress losses due to creep and shrinkage in SCC mixes will be compared to the same prestress losses in the conventional concrete mix.

3. TEST MEMBER FABRICATION AND TESTING

3.1 Introduction

This chapter provides details on member design, reinforcement, casting processes, curing, instrumentation, and testing. Twelve prestressed concrete stub tee members were cast at the SPG's Winchester, VA plant, and shipped to the Virginia Tech Structures and Materials Laboratory for testing. These twelve stub tee members were used to determine the development length and flexural capacity of the various mixes. A timeline for fabrication and testing a typical stub tee specimen is given below.

1. Block out form work was created and installed to utilize the current double tee bed at SPG.
2. Strands were tensioned and mild reinforcement was added.
3. Concrete was placed/poured; double tee bed was covered and subjected to a 12 hour cure with approximately six hours of additional heat transferred from the precast bed.
4. Prestress force was released once the concrete strength was adequate. The beam was removed from the double tee bed and placed in the lay down yard until shipment.
5. At approximately two weeks from pour, the beams were shipped to the Virginia Tech Structures and Materials Laboratory and unloaded.
6. An individual beam was placed into loading position and load was applied until the presence of the first crack appeared. The beam was then unloaded and reloaded until the crack reopened.
7. The beam was then loaded until a flexural failure or a bond failure occurred.

In addition to the twelve stub tee members used to characterize the development length and flexural strength of the concrete mixes, three square, prismatic members were created to determine the transfer length of the individual concrete mixes. All casting and testing for the transfer length members took place at the Winchester plant of SPG. A typical timeline for a transfer length specimen is given below.

1. Formwork was created on a wall panel prestressing bed at SPG's Winchester plant.
2. The strand was tensioned and the concrete was poured/placed into the formwork.
3. Members were covered and allowed to cure at ambient temperature overnight.
4. Formwork was removed and DEMEC gage points were installed along the length of each side of the member. Gage distances were measured.

5. The strand was detensioned and transfer length measurements were taken.
6. The strand was cut and the members were placed in a storage warehouse with relatively constant temperature and humidity.
7. Transfer length measurements were taken at seven days and twenty-eight days after prestress release.

3.2 Nomenclature

A unique name was given to each test on each specimen. Figure 3.1 shows a typical member designation for the stub tee and the transfer length member, respectively. The WT designation is common to all development length testing members. The number following the WT designation indicates the concrete mix type. The fourth term in the beam name depicts an individual member. The fifth and sixth terms indicate which end is being tested (development length members were tested at each end). For example, a WT3C WE designation indicates a test is being performed on the west end of a development length member made with S1CCM2 concrete.

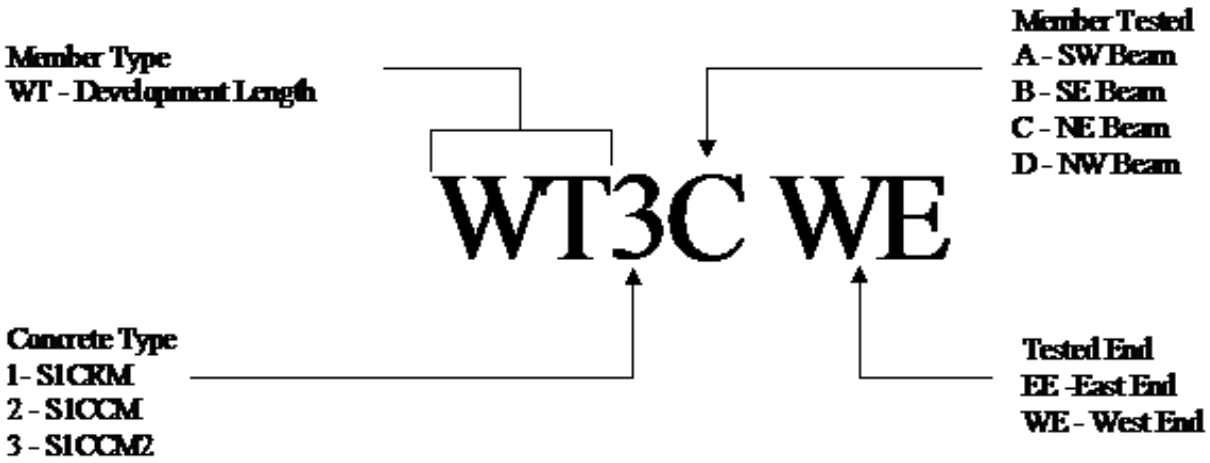

Figure 3.1 Member Nomenclature

3.3 Prestressed Concrete Beam Fabrication

This section discusses the fabrication of the transfer length and development length members.

3.3.1 Transfer Length Member Fabrication

Three prestressed members were cast and poured along a single strand on November 27, 2006. This eliminated any differences in steel properties between concrete mixes and allowed a head to head comparison of the transfer length of each concrete mix. All beams were cast along a single 9/16 in. diameter grade 270 low relaxation strand. The nominal cross sectional area of the strand was 0.196 $in.^2$. All members had the same cross sectional area.

3.3.2 Development Length Member Fabrication

Twelve prestressed beams were cast in three separate pours of three different concrete mixes. All beams were prestressed with a single 9/16 in. diameter grade 270 low relaxation strand. Members made of concrete mix S1CCM, a self consolidating concrete mix, were cast on the first day of casting. Members made with S1CCM2, another self consolidating concrete mix, were cast on the second day, and members made of S1CRM, a conventional concrete mix, were cast on day three. On each day, one set of two beams shared one prestressing strand and the other two beams shared a second prestressing strand. The cross sectional area of the strand varied depending on the strand pack used to create the member. The nominal cross sectional area of the strand was 0.196 $in.^2$. All members had the same cross sectional properties. Table 3.1 shows the date each beam was cast, as well as the strand pack used in stressing the beam.

Table 3.1 Beam identification information

Beam Name	Pour Date	Strand Pack #
WT1A	7/27/2006	800239301
WT1B	7/27/2006	800239301
WT1C	7/27/2006	800238701
WT1D	7/27/2006	800238701
WT2A	7/25/2006	800205702
WT2B	7/25/2006	800205702
WT2C	7/25/2006	800149702
WT2D	7/25/2006	800149702
WT3A	7/26/2006	800239301
WT3B	7/26/2006	800239301
WT3C	7/26/2006	800238701
WT3D	7/26/2006	800238701

3.3.3 Prestressing Bed Layout

Each of the development length and transfer length members was fabricated at SPG's Winchester plant utilizing their prestressing beds. The transfer length members were created on a wall panel bed in order to allow for the use of removable formwork. The transfer length members were the only pieces cast on that bed for the day they were created.

The development length members were cast in a 430 ft long stay-in-place steel prestressing bed used to cast double tee members. One member was created by blocking the bottom two feet of a single stem of the double tee bed with wood formwork. Four members were created on each casting day, two along one stem of the double tee bed and two along the other stem. The development length members were cast along with other structural double tee members used by SPG. Figures 3.2 and 3.3 below show diagrams of the prestressing bed layouts used to cast the transfer length and development length member, respectively.

Figure 3.2 Casting Layout for Transfer Length Members

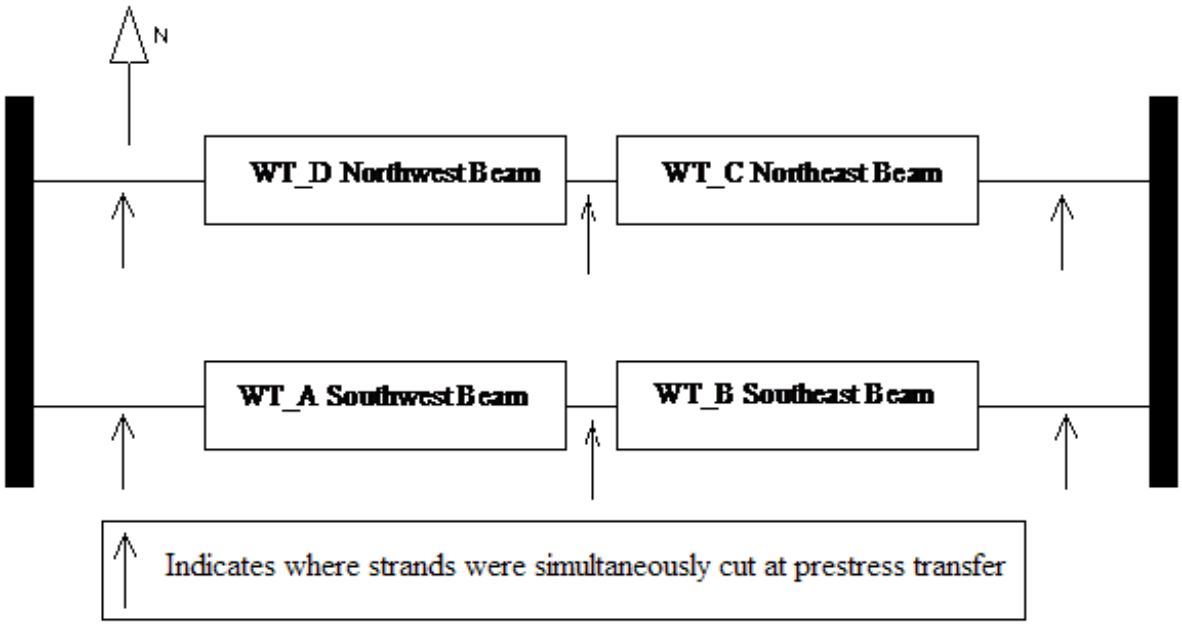

Figure 3.3 Casting Layout for Development Length Members

3.3.4 Cross Section Design

Since the forms for the development length members could not be removed, transfer length measurements could not be taken. Thus transfer length members were designed to investigate the transfer length of each concrete mix. These members were designed to mimic the stem of the development length members. A square concrete cross section was chosen, with a single strand eccentrically placed in the member. The size of the transfer length members is slightly smaller than the development length member stems. This was done to allow sufficient concrete surface strain readings to be obtained at the release of prestress. Figure 3.4 shows the cross section of the transfer length member.

The development length member design was created by an engineer within the SPG's engineering office. The choice of the cross section as a stub tee was done to facilitate the use of SPG's stay-in-place formwork. This would allow for expedient casting since the members could be created in line with other structural members. More than adequate shear reinforcement was provided. This prevented a shear failure mode from occurring which allowed the member to fail only in flexure or strand slip. Table 3.2 gives the cross sectional properties of the development length members. The transformed section properties are based on the average of the tested

values of the concrete modulus of elasticity. A cross sectional drawing of the development length member can be found in Figure 3.5.

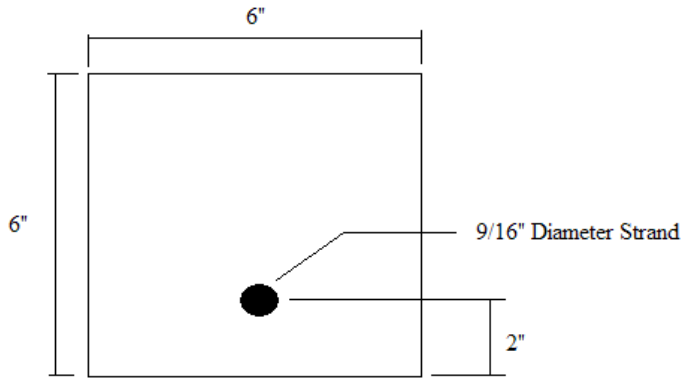

Figure 3.4 Transfer Length Member Cross Section

Table 3.2 Geometric Section Properties

Beam Name	Gross Section Properties			Transformed Section Properties			Net Section Properties		
	A_g (in.^{2})	I_g (in.^{4})	e_g (in.)	A_t (in.^{2})	I_t (in.^{4})	e_t (in.)	A_n (in.^{2})	I_n (in.^{4})	e_n (in.)
WT1A	119	2083	5.91	120	2109	5.86	119	2075	5.92
WT1B	119	2083	5.91	120	2109	5.87	119	2075	5.92
WT1C	119	2083	5.91	120	2110	5.87	119	2075	5.92
WT1D	119	2083	5.91	120	2111	5.87	119	2075	5.92
WT2A	119	2083	5.91	120	2109	5.87	119	2075	5.92
WT2B	119	2083	5.91	120	2110	5.87	119	2075	5.92
WT2C	119	2083	5.91	120	2109	5.87	119	2075	5.92
WT2D	119	2083	5.91	120	2109	5.87	119	2075	5.92
WT3A	119	2083	5.91	120	2112	5.86	119	2075	5.92
WT3B	119	2083	5.91	120	2109	5.87	119	2075	5.92
WT3C	119	2083	5.91	120	2112	5.86	119	2075	5.92
WT3D	119	2083	5.91	120	2113	5.86	119	2075	5.92

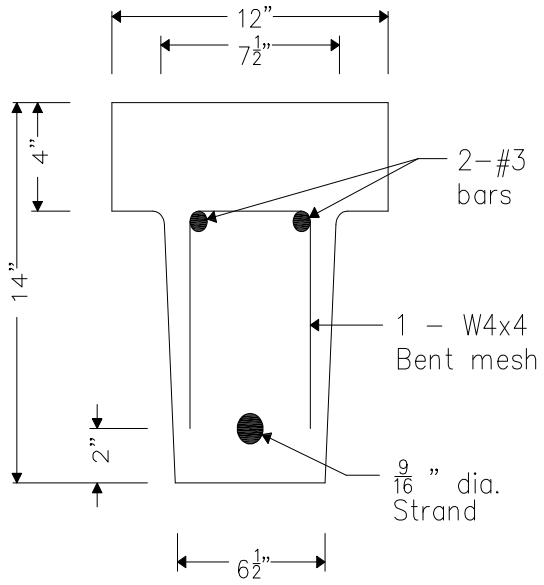

Figure 3.5 Development Length Member Cross Section

3.3.5 Details of Reinforcement

All prestressing strand was obtained by SPG from American Spring Wire (www.americanspringwire.com). All prestressing steel was grade 270 low relaxation strand. The mechanical properties of the prestressing strand were taken from mill certified testing sheets. An idealized bi-linear stress-strain curve for one strand pack is shown in Figure 3.6. A total of four different strand packs were utilized in casting the development length members. Table 3.3 gives information regarding each strand pack, including yield stress, ultimate stress, modulus of elasticity, and cross sectional area. The yield stress was determined as the stress in the steel at a steel strain of one percent.

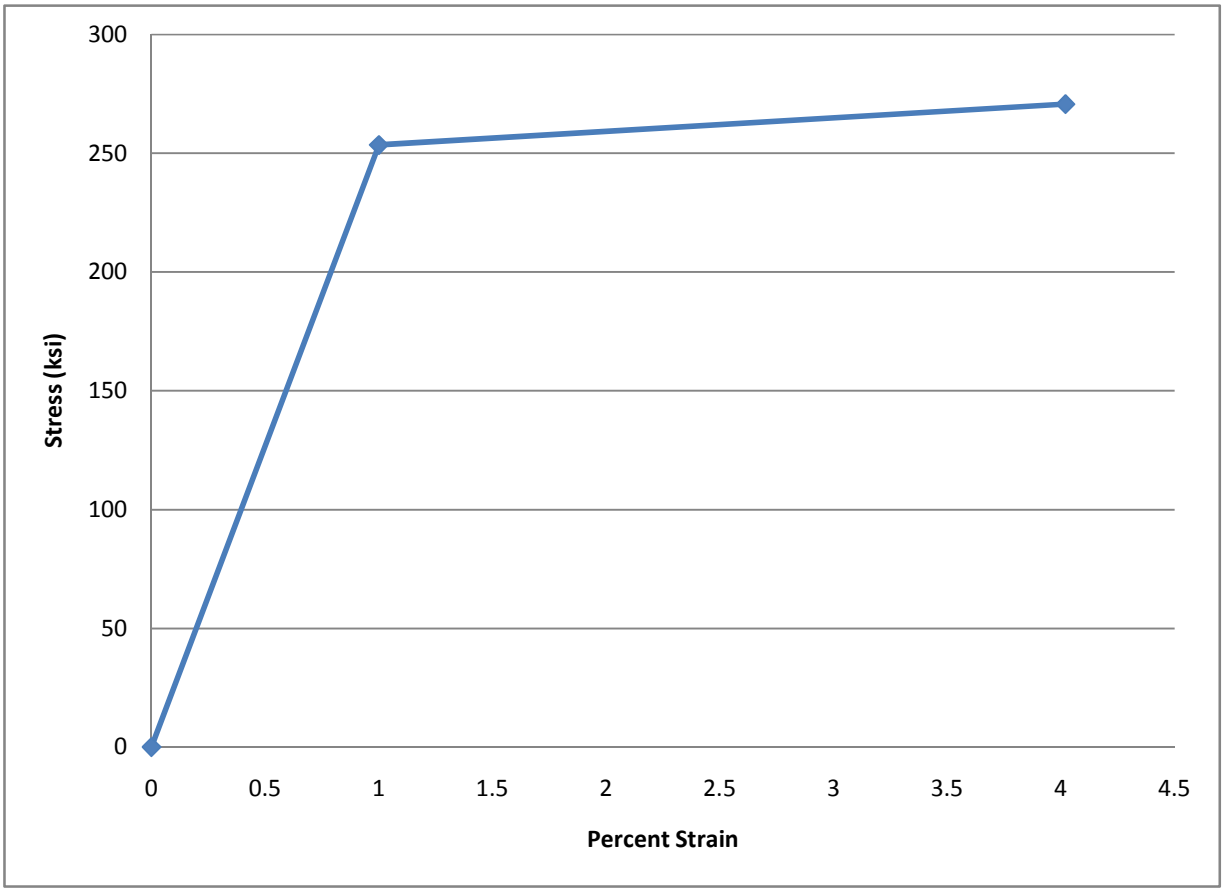

Figure 3.6 Idealized Stress Strain Curve for Strand Pack #800239301

Table 3.3 Prestressing Steel Mechanical Properties

Strand Pack #	A_{ps} (in2)	f_{py} (ksi)	f_{pu} (ksi)	E_{ps}
800205702	0.196	250	274	28940
800149702	0.196	254	275	29050
800239301	0.196	254	272	29030
800238701	0.1969	254	271	28970

Each development test beam contained one prestressing strand which provided the primary flexural reinforcement. The strand was set at an elevation of 2 in. above the member's bottom. This is considered standard industry practice and provided adequate concrete cover for the steel. The surface condition of the strand was slightly rusted. All strand packs were kept outdoors in a covered prestressing plant operation (prestressing plant has a roof but no walls). Therefore, strands were exposed to temperature fluctuations and potential moisture changes.

In addition to prestressing steel, mild reinforcement was used as the primary shear reinforcement of the development length beams. All mild reinforcement used is grade 60 steel. A W4x4 wire mesh was bent into a U-shape and placed along the member stem. This provided more shear reinforcement than code requirements and helped to ensure a flexural failure or bond failure in lieu of a shear failure. To help keep the bent wire mesh off the bottom of the form, two 3/8 in. deformed reinforcing bars were placed in the corners of the bent mesh. While the primary role of the deformed bars was to help form up the shear reinforcement, the bars did provide some extra moment capacity. Figure 3.5 shows the location of the mild steel reinforcement. Figure 3.7 is an actual picture of the in place mild reinforcement.

Figure 3.7 Development Length Member Mild Reinforcement

3.3.6 Concrete Mixture and Properties

Three concrete mix designs were utilized in the testing of transfer length and development length. All three mixes were designed to have an initial compressive strength of 3500 psi in 12 hours, and a 28 day compressive strength of 6000 psi. The concrete mixes had normal weight. Each mix was adjusted at the concrete batching plant using air entraining agents and super plasticizers. Since the amount the mixes were adjusted occurred at the batching plant, the amount of each admixture used was not known.

The first mix design was a conventional concrete mix (S1CRM). This mix has normal concrete properties, including a 6 to 8 in. slump and approximately 5% air content. The S1CRM mix was used as a control mix for a baseline comparison of the two self-consolidating concrete mixes. The properties of the three mixes are given in Table 3.4

The other concrete mix designs were self-consolidating concrete mixes (S1CCM and S1CCM2). Both had slump/flow tests results which were greater than 20 in. In addition, they both contained a smaller aggregate size than the S1CRM conventional concrete mix. This was necessary to allow the concrete mixture to flow better through the double tee form. The main difference between the two SCC mixes is the fine aggregate content. The S1CCM mix contains 100 percent manufactured sand fine aggregate. The S1CCM2 mix contains a manufactured to natural sand blend of 65 percent to 35 percent, respectively. The S1CCM2 mix is more cost effective to the SPG. Therefore, if the engineering properties are similar, the S1CCM2 will likely become the preferred SCC mix for SPG.

Table 3.4 Concrete Mix Data

Material	S1CRM (WT1 Beams)	S1CCM (WT2 Beams)	S1CCM2 (WT3 Beams)
Type I Cement (lb)	705	750	745
Coarse Agg (lb)	1750 (#57 stone)	1625 (#67 stone)	1650 (#67 stone)
Fine Agg. (lb)	1256	1340	1308
Water (gal)	30.5	34	34
Air Entraining Agent - AEA-14 (oz)	varies	varies	varies
ASTM C494 - Plastiment	varies	varies	varies
ASTM C494 - ViscoCrete 4100 (oz)	varies	varies	varies
Unit Weight (lb/ft^3)	146.9	148.1	148
Slump/Flow (in.)	8	25	21.5
Air Content (%)	4.8	5.2	5.8
W/C Ratio	0.36	0.38	0.38

3.3.7 Formwork, Strand Stressing, and Concrete Placement

Formwork for the transfer length members consisted of a wall panel prestressing bed and plywood side forms, reinforced with wooden pieces. The wall panel prestressing bed was used as the bottom of the formwork. The plywood side forms were cut to length and nailed into the wall panel bed. End panels were created by using plywood with a notch cut into the bottom to allow the strand to run through the form. The edges of the form were then caulked to prevent leakage and a foam spray was used to seal the notch around the strand. Figure 3.8 below shows the transfer length member formwork.

Figure 3.8 Transfer Length Member Formwork

The development length members utilized stay-in-place steel double tee prestressing beds for their formwork. Two foot high wood block out sections were created and placed in each double tee stem. The block-out sections were 12 ft long and placed end to end for each member. The block-outs were caulked along the steel-wood interface to prevent the concrete from leaking. A wooden end piece was created for both ends of each beam. Each end piece had a notch cut into its bottom to allow the strand to pass through the formwork. The end piece was caulked along its perimeter and a foam spray was used to seal the notch along the strand. Steel angles

were connected to the stay in place formwork in order to create the top flange of the concrete member. Figure 3.9 depicts the stay in place formwork, along with the end piece for the development length members.

Figure 3.9 Development Length Member Formwork

For the development length members, the strand used for the primary reinforcement was also the top strand for many structural double tees. All of the strands for the structural double tees were run along the 430 ft prestressing bed. Next, the stem block out formwork was placed and the final strand was run the length of the prestressing bed. The bottom strands for the structural double tees were stressed before stressing the test member's strand. Once all other strands had been stressed, the development length beam strand was fitted for stressing.

Load cells comprised of hollow aluminum cylinders equipped with full bridge strain gages were used to monitor the strand stress at the live end (live end refers to the end where the strands were jacked). The load cells were calibrated with a universal testing machine and are accurate within approximately 100 pounds. Figure 3.10 is a picture of the prestressing bed's live end. A prestressing chuck was used to provide restrain to the steel strand. Steel shims were used to distribute the prestress force evenly from the chuck to the load cell. During loading the strand stress values given by the load cells were too high. It was later discovered that the universal testing machine used to calibrate the load cells was itself improperly calibrated.

Figure 3.10 Load Cells at Live End of Prestressing Bed

Once the calibration was corrected, the measured values in the load cells were nearly identical to the values obtained from elongation hand calculations.

A hydraulic ram was used to tension each strand by pulling the strand through the abutment and chuck. Figure 3.11 depicts the use of the hydraulic ram to tension the strands. Once the design pressure was reached on the hydraulic ram, the force was released and the strand was seated in the chuck. Elongation measurements were taken to verify the stress in the steel. The load cell monitored the force in the strand while tensioning occurred. After stressing all the strands in the bed, the mild steel reinforcement was placed in each of the structural double tees. This was followed by placing the bent wire mesh and two No. 3 reinforcing bars in each of the development length members. The concrete for the structural double tees arrived first and was placed into the formwork. Once casting and vibrating of the double tees was complete, the concrete for the development length members arrived.

Figure 3.11 Hydraulic Ram Tensioning the Prestressing Strands

Before casting the development length members, slump/flow and air content tests were conducted (see Figure 3.12). After determining the air content and slump flow values, a portion of the concrete batch was used to make cylinders. The remaining concrete was then placed into the formwork. The conventional concrete mix was vibrated to consolidate the concrete and then a screed was used to level the top flange of the member. The SCC mixes did not require vibration, but a screed was used to level the top of the member. After placement, the bed was covered with a tarp and moistened to accelerate the curing process. After approximately six hours, the steel formwork began to convey heat to the concrete members by means of a heating oil pump, which also accelerated the curing process.

a)

b)

Figure 3.12 Slump/Flow Test a) Flow Spread for S1CCM b) Slump Test for S1CRM

At 12 hours after placing of the concrete, match cured cylinders were broken to determine if the bed had reached the initial compressive strength of 3500 psi. If the bed was not up to strength, another hour of curing time was added. Once the bed had reached strength, the tarps were removed from the bed and the heating pump was cut off. Strands were detensioned around the test members first. A variety of ways to detension the strands was attempted. For the S1CCM beams, bolt cutters were used to cut the strand. Torches were used to flame cut the strands for the S1CCM2 beams. The S1CRM beams were detensioned by saw cutting the strands on either end of the member at the same time. Once the development length members had been detensioned, the rest of the bed was detensioned by flame cutting each strand. After detensioning the entire bed, the development length members and the structural double tees were crane lifted from the bed and placed on the back of a flatbed truck. The members were hauled to the SPG lay down yard where they remained until being shipped to Virginia Tech.

3.4 Testing and Instrumentation

Several different tests were performed on each of the two prestressed member types. The transfer length members were only used to determine the transfer length of each concrete mix. Transfer length measurements were taken at the release of the prestress force, at 7 days after release, and at 28 days after release. This measurement was made by determining the concrete surface strains. Development lengths were determined by an iterative load testing procedure. Flexural strength was determined using the ultimate load capacity achieved during the iterative load testing procedure. Prestress losses were also measured by load testing. The following sections discuss the procedure in which these tests were performed and describe the instruments used during testing.

3.4.1 Transfer Length

The transfer length is the length of embedded strand required to develop the effective prestress force in the end of a pretensioned concrete member. Transfer lengths were determined by measuring the concrete surface strains along the centroid of the steel strand. Before release of the prestress force, the concrete surface strain is zero since there are no applied loads. After prestress force release, the concrete member compresses and surface strains are measured. As surface strains are measured from the end to the middle of the member, an increasing strain profile appears. This strain profile can be used to determine the transfer length.

3.4.1.1 DEMEC Gage and Gage Points

Concrete surface strains were measured using a DEmountable MEChanical (DEMEC) strain gage and surface mounted gage points. Manufactured by Mayes Instruments Limited of the United Kingdom (www.mayes.co.uk), the DEMEC strain gage had a gage length of 200 mm and could measure strains within an accuracy of approximately ± 5 microstrains. The DEMEC strain gage, seen in use in Figure 3.13, was a made of a metallic rod, a fixed gage point, a pivoting gage point, and the digital readout. The gage points were small metallic disks which had a small impression in the center. This impression was used to locate the gage length on the DEMEC strain gage. The gage points were placed onto the transfer length member by using a two part, quick setting epoxy. A gage point spacing of 50 mm was used along the entire length of each side of each member. Each individual strain reading was made on a gage length of 200 mm. This meant individual strain readings overlapped each other. The true strain was calculated by multiplying the measured change in strain by the pivot ratio and dividing by the gage length. The pivot lever ratio relates the actual movement in the strain readings to the measured movement of the strain readings. The pivot ratio was 0.8:1.

Figure 3.13 DEMEC Strain Gage

A gage point spacing of 50 mm was used throughout the length of the concrete member. This smaller spacing was used to capture more concrete surface strain readings, which were necessary since the member was short. Gage point readings for both sides of each end of the members were taken from the end to approximately the middle of the member, which was a distance of 60 in. For the S1CCM and S1CCM2 beams, the readings were only taken out to 52 in.

3.4.1.2 Data Collection and Transfer of Prestress

Three sets of initial DEMEC strain readings were taken before the transfer of the prestress force. The DEMEC gage was zeroed on a reference bar before each set of readings. One researcher took the readings, making certain the gage was level, while another researcher wrote the results down. If any of the readings were drastically different from any previous readings, an additional reading was taken. To transfer the prestress force, the hydraulic jack was used to slowly detension the strand. This method was used in an attempt to gradually release the prestress force, which was necessary in order not to bias any of the transfer length members with sudden prestress transfer. Immediately following prestress transfer, another set of DEMEC strain readings was taken. This information was used to determine the strain profile and transfer length. DEMEC strain readings were taken again at 7 days and 28 days after prestress release.

3.4.2 Development Length

Development length is the required length of strand embedment to develop the strand stress for flexural failure. Development length tests were conducted on each end of each beam with a goal of bracketing the development length for each type of concrete used. The development length was determined by loading each beam end at embedment lengths that varied from test to test. Determination of the development length was an iterative process. If the failure mode observed in a test was flexural, then the strand was embedded beyond its development length. If the observed failure mode was a bond failure, the development length is greater than the embedment length. By iterating the embedment length, the development length can be bracketed by test results.

3.4.2.1 Test Setup

Each of the stub double tee beams were 24 ft long. To test each end of the beam, a test span of 16 ft was established. This allowed testing of one beam end without damaging the other end (see Figures 3.14 and 3.15). A 4 in. diameter steel pin, with 5 in. of bearing contact with the

tests member, and a 4 in. diameter steel roller were used as test supports (see Figure 3.16). A hydraulic actuator was mounted to a steel frame, which was bolted to the reaction floor. This actuator applied a point load to the top of the member. To prevent local crushing, two steel plates and a thin bearing pad were used to distribute the load from the actuator across the width of the top flange. The hydraulic actuator was connected to a hand pump, which was used to apply the load to the member. Deflection of the beam was monitored directly under the point of load application by a wire pot. The wire pot was capable of accurately reading deflections as small as 0.01 in. A linear variable differential transducer (LVDT) was used to monitor the slip of the strand. This LVDT, shown in Figure 3.16 had a range of motion of approximately 0.1 in. and could record movement a small as one millionth of an inch. The LVDT was held in place by a bracket which was mounted to the end of the beam being tested. The nose of the LVDT was placed in contact with the center wire of the seven wire strand and could monitor movement of the strand relative to the beam end.

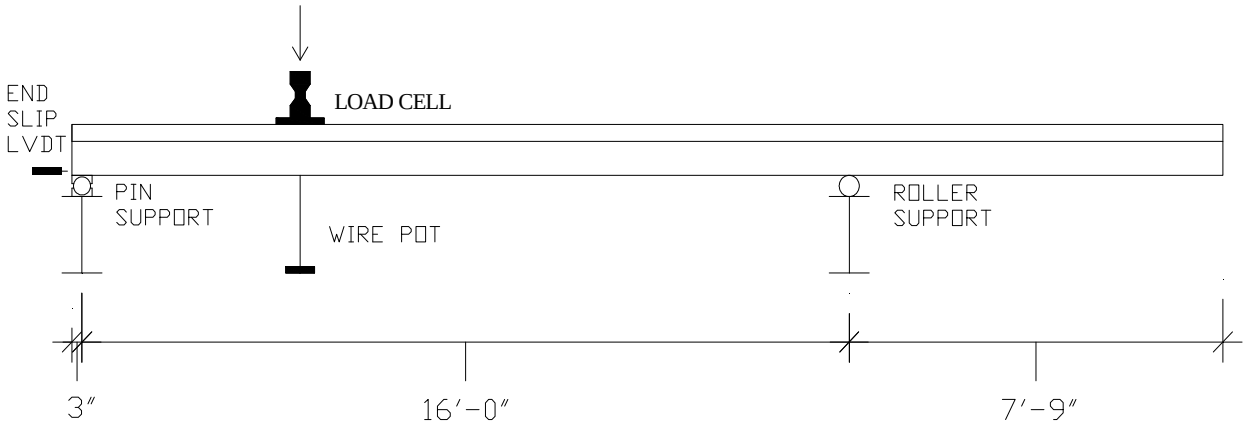

Figure 3.14 Development Length Test Schematic

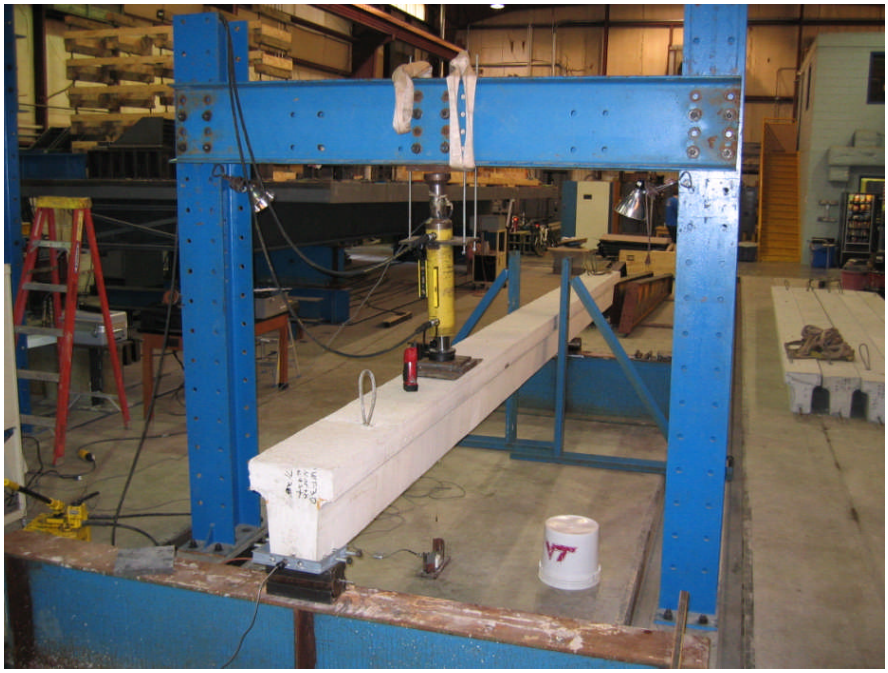

Figure 3.15 Development Length Test Setup

Figure 3.16 Pin Support and LVDT

Data for each test was collected with Vishay Measurements System 5000 scanner and accompanying Strain Smart data acquisition system software. Data was recorded at a sampling rate of one per second. All instruments were directly calibrated within the system. Each test data file was reduced into a Microsoft Excel file for analysis once the test had been completed.

3.4.2.3 Procedure

The development length portion of each test was preceded by the crack initiation and crack reopening portions of testing, which are discussed in the next section. Upon completion of the previous tests, each beam was unloaded and any unnecessary instrumentation was removed. The needed instruments were re-zeroed. The load was applied in a continuous manner until the highest load attained during the previous tests was reached, at which point the load was increased by one kip increments. After each load increase, crack growth and newly appearing cracks were marked. This process continued until either a flexural failure or a bond failure occurred. Flexural failure was observed when either the concrete crushed or completely plastic behavior was occurring (increase in deflection without increase in load). Bond failures were characterized by a sudden loss in load carrying capacity accompanied by strand slip of 0.01 in. or greater. When strand slip occurred, it was often sudden and the slip was much larger than the LVDT could measure, resulting in an “off scale” reading value reported by the LVDT.

3.4.3 Prestress Losses

Prestress losses are decreases in the strand stress which occur over time in a prestressed member. The relevant losses in this experimental project were elastic shortening, concrete creep, concrete shrinkage, and steel relaxation. Anchorage seating losses were taken into account by The Shockey Precast Group when reporting the initial stress in the steel. Prestress losses were experimentally measured in this research by crack initiation and crack reopening tests. These tests determined the effective prestress in the concrete member. The effective prestress is directly related to prestress losses. The effective prestress is the stress in the strands after prestress losses occur.

Effective prestress was experimentally determined by finding the load required to initiate cracking of the member and to reopen the same crack. These load tests, as stated in the previous section, were completed prior to the development length test. The same instrumentation used in the development length test was used in the crack initiation and crack reopening tests.

Crack initiation tests were conducted by increasing the load while visually inspecting the concrete surface for the appearance of cracks. A plot of load versus deflection was maintained in view while loading the member. As the load versus deflection curve began to deviate from the elastic range, cracks began to appear. If a crack was not visible, the load was increased incrementally until a visible crack was found. The crack was then marked on each side of the beam and on the bottom of the beam. The beam was unloaded and prepared for the crack reopening test.

Crack reopening tests were conducted by monitoring the strain across a crack as compared to the strain beside the crack while reloading the beam. The strain across the crack was measured with a crack detection gage. A crack detection gage was comprised of a bent metal bracket on which a strain gage was attached. The crack detection gage had two points of contact, which could be temporarily glued to the bottom of the beam. One crack detection gage was placed directly over the initial crack on the bottom of the beam. A second crack detection gage was placed beside the other crack detection gage. The beam was then loaded at a constant rate. While loading, a plot of the load versus strain diagram for each crack detection gage was monitored. The crack was deemed to have reopened when the two lines diverged on the load versus strain plot. The beam was then unloaded and the test was considered complete.

4. TEST RESULTS, ANALYSIS, AND DISCUSSION

4.1 Transfer Length

Concrete surface strains were measured along the ends of each side of each transfer length member before and after prestress transfer, 7 days after transfer, and 28 days after transfer. A total of three transfer lengths were determined for three time frames (prestress release, 7 days, and 28 days). Theoretical transfer lengths were determined using ACI, AASHTO, and Buckner's recommendation. Experimental results were compared against the theoretical models.

4.1.1 Material Properties

The prestress force was not transferred to the concrete members until all concrete members reached a minimum compressive strength of 3500 psi. This was the minimum concrete strength required to meet ACI stress limits at transfer (2005). Compressive strengths for the transfer length members were only obtained prior to prestress transfer. Once the compressive strengths were achieved, DEMEC gage points were affixed to the sides of each member. Table 4.1 shows the initial concrete properties for the transfer length members. The initial gage distances of the DEMEC points were measured. After measuring the initial gage distances, the prestress force was gradually transferred to the concrete members by slowly detensioning the strand with a hydraulic jack. Strain gage readings were taken after transfer of the prestress force.

Table 4.1 Initial Concrete Mix Properties

Concrete Type	Time Since Pour (Days)	Compressive Strengths at Transfer f'_{ci} (psi)	$E_{ci} = 33w_c^{1.5}f'_{ci}^{0.5}$ (ksi)
S1CRM	1	4614	3914
S1CCM	1	4650	3929
S1CCM2	1	3938	3616

4.1.2 Data Reduction and Determination of Transfer Length

DEMEC strain gage readings were taken before and after transfer of prestress force, 7 days after prestress transfer, and 28 days after prestress transfer. The difference between initial distance measurements and measurements taken after prestress transfer, multiplied by the DEMEC gauge pivot ratio of 0.8:1, and divided by the gage length of 200 mm gives the concrete

surface strain. Plotting the measured surface strain along the length of the member yields a strain profile similar to Figure 4.1. Figure 4.1 shows the initial strain reading on one side of a test member. These data points are termed the "raw" strains. Since the raw strain readings were rather jagged, a smoothing operation was undertaken to help produce a more uniform plot. A running average of three strain values was calculated since strain readings overlap three gage readings. Equation 4.1 shows the process for finding the SSP. The running average is plotted in Figure 4.1 as the "smoothed" strains.

$$\varepsilon_{SS_i} = \frac{\varepsilon_{RS,i-1} + \varepsilon_{RS,i} + \varepsilon_{RS,i+1}}{3} \qquad 4.1$$

Where:

$\varepsilon_{SS,i}$ = smoothed strain at location i

$\varepsilon_{RS,i-1}$ = raw strain prior to strain point being considered

$\varepsilon_{RS,i}$ = raw strain at location i

$\varepsilon_{RS,i+1}$ = raw strain after to strain point being considered

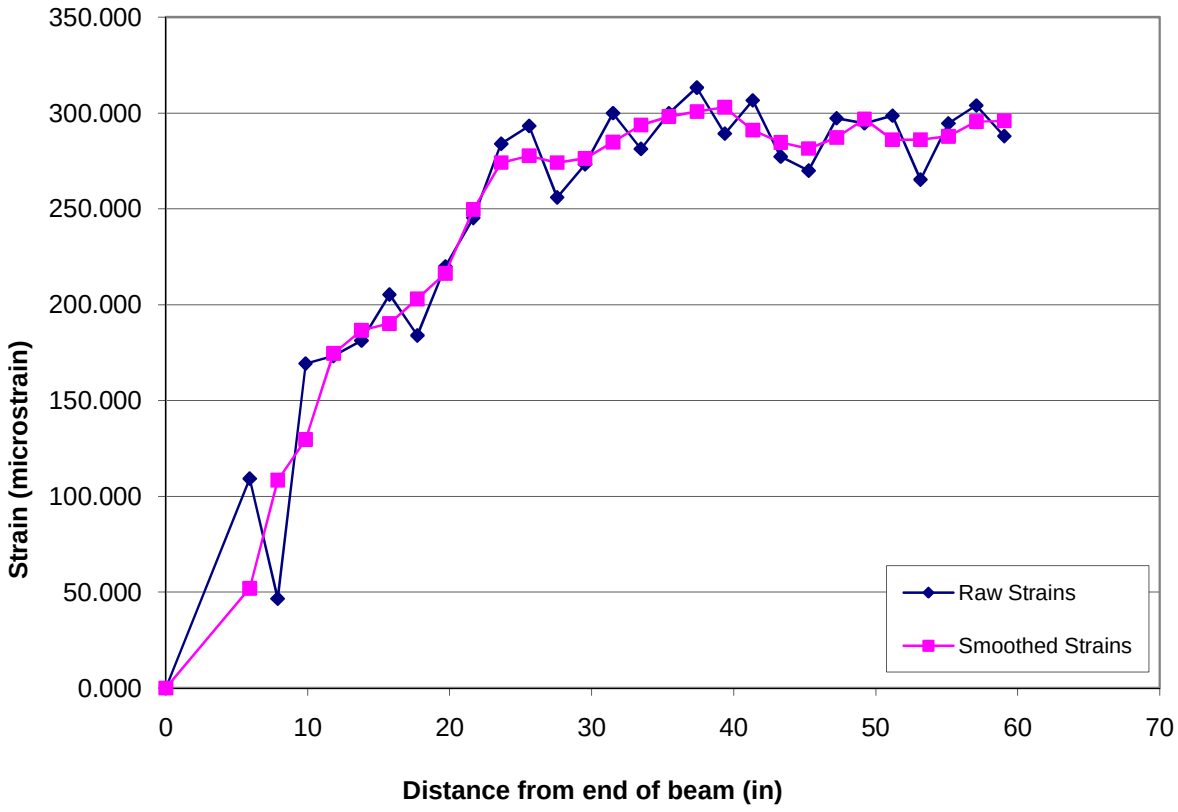

Figure 4.1 Strain Profile for S1CRM ES at Prestress Release

To further reduce the data, the smoothed strain profiles on each side at one end of a beam were averaged. This data was termed the averaged smoothed strain profile (ASSP). The ASSP for the S1CRM beam of Figure 4.1 is shown in Figure 4.2.

Additional smoothing was performed by averaging the ASSP plots for each end of a member. This plot was termed the "averaged" average smoothed strain profile (AASSP). The AASSP for the S1CRM member is shown in Figure 4.2. The AASSP for the S1CRM member at all values of measured transfer length is shown in Figure 4.3.

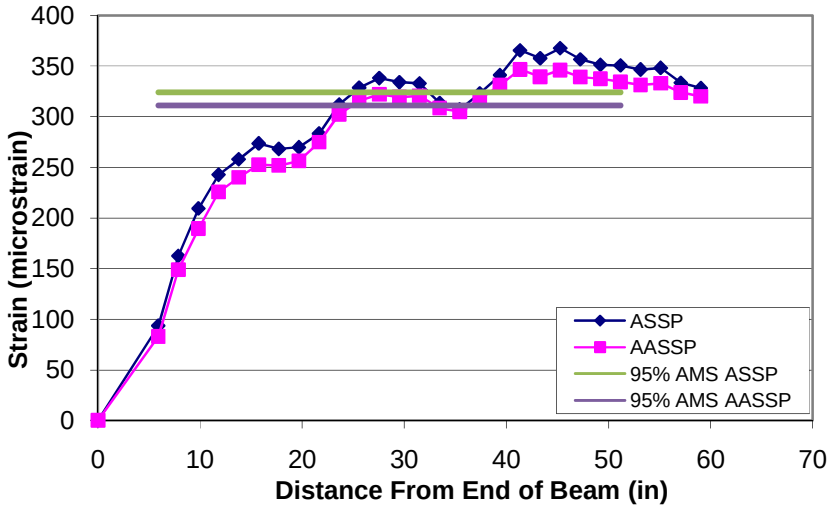

Figure 4.2 ASSP for the S1CRM North End

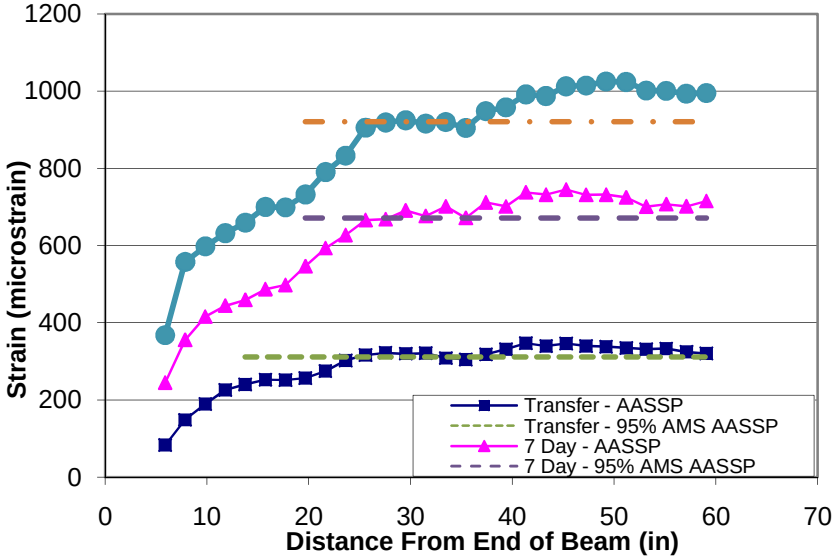

Figure 4.3 AASSP for S1CRM Member at All Measured Times

To determine the transfer length from the strain profile, the 95 percent average maximum strain (95% AMS) method was chosen. This is a generally accepted method and was used by Barnes et al. (2003) and was recommended by Buckner (1994). The procedure is outlined below.

1. The beginnig point of the strain plateau is visually identified.
2. The strain of a data points in the plateau are averaged.
3. This average value of the strain plateau is reduced by 5 percent.
4. The intersection of the strain profile and the 95 percent strain plateau is determined.
5. This intersection value indicates the transfer length.

The 95 percent average maximum strain value is plotted as a dashed line on Figure 4.3. A transfer length for both ends of each beam was determined from the ASSP, and these values were averaged to generate a transfer length for the beam. In addition, the AASSP was plotted and a transfer length was determined. Strain profiles used to determine the transfer length of all the members are located in Appendix B.

4.1.3 Transfer Length Results

Two transfer lengths were produced for each member. The first transfer length is the average of two transfer lengths determined using the ASSP profiles of each end of a member. The second transfer length was determined from the AASSP profile for each member. Tables 4.2, 4.3 and 4.4 record the transfer length data for each specimen at prestress release, 7 days after release, and 28 days after release, respectively. With the exception of the S1CRM transfer length at 28 days after prestress release, the transfer length determination using either method yields nearly the same value. From this point on, the AASSP value of the transfer length for each member will be used in discussion.

Table 4.2 Transfer Length Results at Prestress Release

Test Specimen ID	ASSP l_t (in.)	ASSP $l_{t\,(ave)}$ (in.)	AASSP l_t (in.)
S1CRM North	24.9		
S1CRM South	24.5	25	25
S1CCM North	17.7		
S1CCM South	16	17	17
S1CCM2 North	28.2		
S1CCM2 South	27	28	28

Table 4.3 Transfer Length Results 7 Days After Prestress Release

Test Specimen ID	ASSP l_t (in.)	ASSP $l_{t\,(ave)}$ (in.)	AASSP l_t (in.)
S1CRM North	27.5		
S1CRM South	25.6	27	28
S1CCM North	23		
S1CCM South	20.5	22	22
S1CCM2 North	33.5		
S1CCM2 South	34.5	34	34

Table 4.4 Transfer Length Results 28 Days After Prestress Release

Test Specimen ID	ASSP l_t (in.)	ASSP $l_{t\,(ave)}$ (in.)	AASSP l_t (in.)
S1CRM North	25.6		
S1CRM South	36.5	31	28
S1CCM North	25		
S1CCM South	26	26	26
S1CCM2 North	33		
S1CCM2 South	33.5	33	33

Results from all the transfer length measurements are summarized in Table 4.5. These measured transfer lengths are compared in Table 4.6 with the ACI and AASHTO code provisions, as well as Buckner's suggested transfer length equation, Equation 2.9. The ACI code provision for the transfer length was found in Section 11.4.4. The code stipulated transfer length is 50 strand diameters, or 28.1 in. The only measured transfer length that did not meet the ACI code provision was the 7 day and 28 day transfer length values for S1CCM2. The S1CCM2 member had a final transfer length approximately 20 percent larger than ACI code predicts. It is important to note the ACI code provision is meant to yield an average value of the transfer length. Therefore, a test result which is 20 percent longer than ACI predicts is not unusual. Next, the transfer lengths are compared with the AASHTO code stipulation of 60 strand diameters, or 33.75 in. for 9/16 in. diameter strands. All recorded transfer length measurements were less than the AASHTO code stipulation, with only the S1CCM2 mix coming close to meeting the stipulation exactly. Finally, all the transfer lengths were shorter than Buckner's suggested equation for measuring the transfer length, which had a predicted transfer length of 36.2 in. Buckner's equation is derived as an upper limit on acceptable transfer lengths. Therefore, all transfer lengths would be deemed acceptable for this theoretical stipulation.

The measured values of the transfer length did change significantly with time. Figure 4.4 represents the transfer length for each mix at the three measured times. There is a noticeable increase in transfer length for each of the three mixes from the initial transfer length measurement to the measurement taken at seven days after prestress transfer. The increase ranged from 12 to 33 percent of the initial transfer length measurement, with the conventional mix increasing the least. The overall increase in transfer length in twenty days ranged from 13 percent to 56 percent. The increase in transfer of the S1CRM and S1CCM mixes of 12 percent and 22 percent appear to be consistent with research conducted by Barnes, Grove, and Burns who found it normal to measure a 10 to 20 percent increase in transfer length over 28 days. It appears most of the change in transfer length occurred over the first seven days after prestress transfer. The S1CCM2 and S1CRM mixes did not have an increase in their transfer lengths after seven days. The S1CCM mix had an increase in its transfer length by 18 percent.

Table 4.5 Comparison of Transfer Length Values

Test Specimen ID	$l_{t,RELEASE}$ (in.)	$l_{t,7\ DAY}$ (in.)	$l_{t,28\ DAY}$ (in.)	$l_{t,7\ DAY}/l_{t,RELEASE}$	$l_{t,28\ DAY}/l_{t,RELEASE}$	$l_{t,28\ DAY}/l_{t,7\ DAY}$	Time of Test	$l_{t,S1CCM}/l_{t,S1CRM}$	$l_{t,S1CCM2}/l_{t,S1CRM}$	$l_{t,S1CCM2}/l_{t,S1CCM}$
S1CRM	25	28	28	1.13	1.12	0.99	Release	0.67	1.12	1.67
S1CCM	17	22	26	1.32	1.56	1.18	7 Day	0.78	1.21	1.54
S1CCM2	28	34	33	1.22	1.20	0.99	28 Day	0.94	1.20	1.28

Table 4.6 Measured Transfer Lengths Compared to Theoretical Values

Test Specimen ID	$l_{t,RELEASE}/l_{t,ACI}$	$l_{t,RELEASE}/l_{t,AASHTO}$	$l_{t,RELEASE}/fsi*db/3$	$l_{t,7\ DAY}/l_{t,ACI}$	$l_{t,7\ DAY}/l_{t,AASHTO}$	$l_{t,7\ DAY}/f_{si}*d_b/3$	$l_{t,28\ DAY}/l_{t,ACI}$	$l_{t,28\ DAY}/l_{t,AASHTO}$	$l_{t,28\ DAY}/fsi*db/3$
S1CRM	0.87	0.73	0.68	0.99	0.82	0.77	0.98	0.81	0.76
S1CCM	0.59	0.49	0.46	0.78	0.65	0.60	0.92	0.76	0.71
S1CCM2	0.98	0.81	0.76	1.19	0.99	0.93	1.17	0.98	0.91

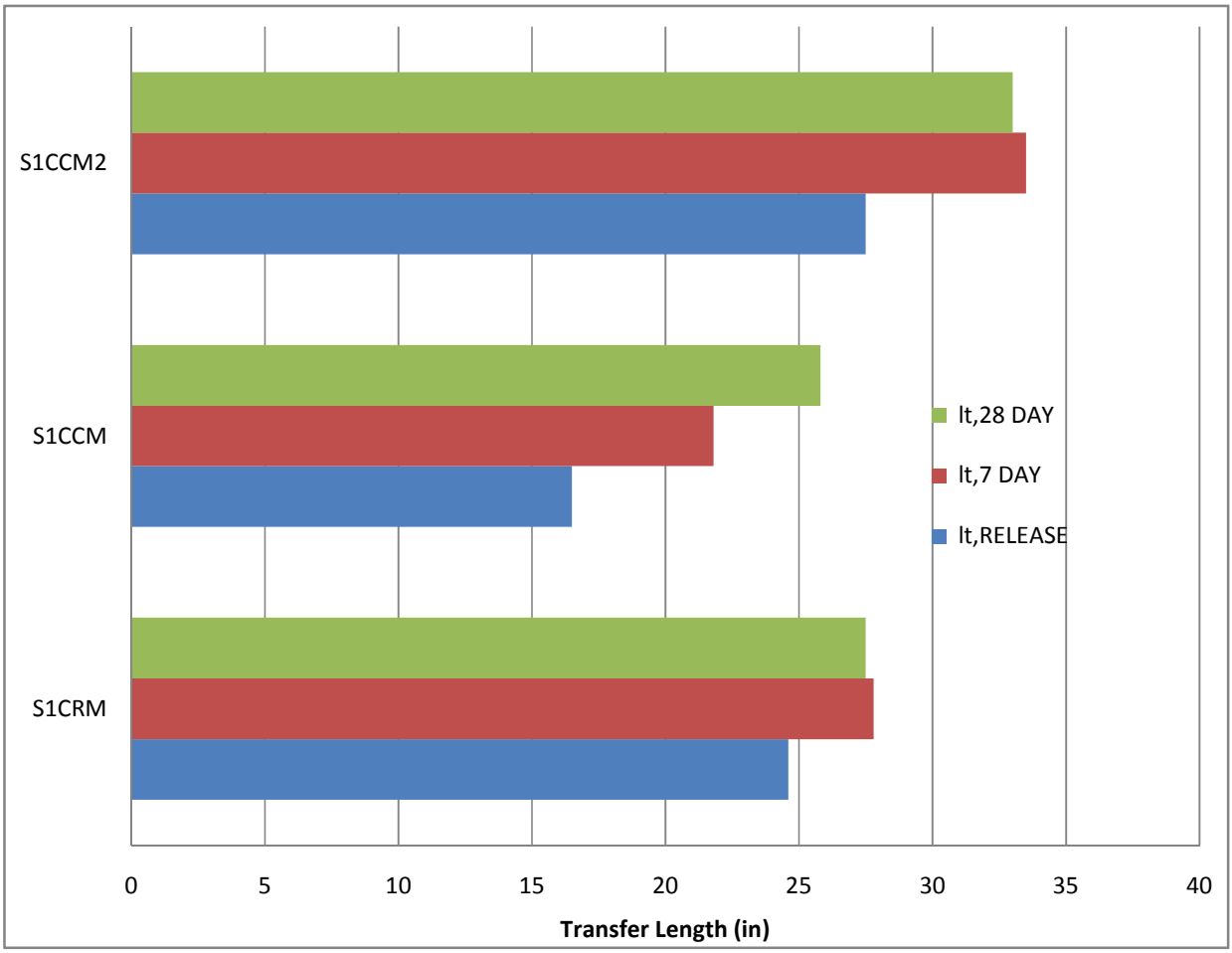

Figure 4.4 Transfer Lengths at Each Measured Time

4.1.4 Effect of Concrete Type on Transfer Length Results

The basis of this test was to compare the transfer length results of the two self-consolidating concrete mixes with the transfer length of a conventional concrete mix. Table 4.5 gives the ratio of the transfer length of each SCC mix to the conventional mix at each time step. It can be seen from the table that the transfer length for the S1CCM concrete mix was significantly shorter at prestress release than either the conventional mix or the S1CCM2 mix. However, the S1CCM mix transfer length grew considerably over the following 28 days, increasing over 50 percent of its initial transfer length. This may be a result of the location the transfer length member during release of the prestress force. The S1CCM member was the middle beam of the three beams cast. Even though the transfer was expected to be gradual, the force may have been applied more suddenly than previously expected. This would cause the end

members to absorb most of the energy from prestress force transfer and allow a much more gradual release of prestress force to the S1CCM member. This effect may explain why the transfer length measurements increase significantly at 7 and 28 days for the S1CCM member, while an increase for the S1CRM and S1CCM2 members was noted only at 7 days. The S1CCM2 mix had an initial transfer length longer than the conventional mix and remained longer than the S1CRM mix over time. This could be a result of lower concrete strength at prestress release for the S1CCM2 member as compared to the S1CRM and S1CCM.

It appears from this data that the SCC mixes performed reasonably well in comparison to the conventional concrete mix. The S1CCM mix had the lowest transfer length and the S1CCM2 mix was reasonably close to the conventional mix. It does not appear from this research study the use of self-consolidating concrete will adversely affect the transfer length of prestressing strand.

4.1.5 Bond Stresses in Transfer Length Members

The average bond stresses between the prestressing strand and the concrete required to have the measured development lengths found in Table 4.5 are listed Table 4.7. The average bond stresses were determined by rearranging Equation 2.2, found on page 11, for the average bond stress (U_t). As is expected, the bond stresses for the S1CCM concrete mix are larger than those for the S1CRM and S1CCM mixes at release. This is simply due to the fact the bond stresses are a function of the transfer length, and the transfer length for the S1CCM mix is much shorter at release than the other mixes. Just as seen in the transfer length section, the bond stresses for the S1CM and S1CRM mixes begin to converge after time. This phenomenon was explained in section 4.1.4 when discussing why the transfer length for the S1CCM mix had a large increase with time.

Table 4.7 Average Bond Stress Results for the Transfer Length Members

	Concrete Type	A_{ps} ($in.^2$)	f_{se} (ksi)	L_t (in.)	$\sum_o$ (in.)	U_t (psi)	U_t/ 400
Release Bond Stresses	S1CRM	0.18	187	25	2.36	582	1.46
	S1CCM	0.18	188	17	2.36	869	2.17
	S1CCM2	0.18	187	28	2.36	520	1.30
7 Day Bond Stresses	S1CRM	0.18	185	28	2.36	510	1.27
	S1CCM	0.18	185	22	2.36	651	1.63
	S1CCM2	0.18	185	34	2.36	422	1.06
28 Bond Stresses	S1CRM	0.18	184	28	2.36	512	1.28
	S1CCM	0.18	184	26	2.36	545	1.36
	S1CCM2	0.18	183	33	2.36	425	1.06

In the last column of Table 4.7, the calculated average bond stresses for each member is compared with the research value suggested by Hanson and Kaar. Hanson and Kaar, as explained in section 2.2.2 on page 11, suggested the average bond stress be 400 psi after completing numerous studies. The bond stresses in this research program were found to be larger than the recommended 400 psi by as little as 6 percent and as much as 117 percent. The final bond stresses for the S1CRM and the S1CCM mix were 28 percent and 36 percent larger than the 400 psi value. This could be a result of the use of 9/16 in. diameter grade 270 low relaxation prestressing strand, as opposed to the ½ in. grade 250 stress relieved strand used by Hanson and Kaar. Larger bound forces will be required when larger strand diameters and larger effective prestress values are used to yield nearly the same transfer lengths. Additionally, the transfer lengths for the S1CCM and S1CRM mixes were less than the 50 strand diameter transfer length which is derived by using Hanson and Kaar's equation. The smaller transfer length will require larger bond forces between the concrete and the prestressing strand.

4.2 Development Length

Iterative load testing was used to experimentally determine the development length of each concrete mix. Each end of each beam was load tested to capacity resulting in a total of 24 tests being performed. The development lengths for the two self-consolidating concrete mixes were bracketed from the iterative load testing procedure.

4.2.1 Material Properties

Beams were tested as early as three weeks after casting and as late as nine weeks after casting. Observations of the concrete strength gain plots in Appendix A indicate that the compressive strength of the concrete increased approximately 1500 psi after three weeks. However, strength increases were taken into account when comparing experimental values to theoretical values of flexural capacity. Before testing a new development length member, cylinder tests were performed. Two compressive cylinder tests, a splitting tensile strength test, and a modulus of elasticity test were performed at the beginning of each week of testing. Results from all cylinder tests performed are located in Appendix A.

Initial concrete material properties for the development length members are provided in Table 4.7. Average concrete material properties are provided in Table 4.8. Table 4.8 shows the mean and standard deviation of the compressive strength, the splitting tensile strength and the modulus of elasticity for each concrete type. All values of the concrete compressive strength were larger than the design strength of 6000 psi. This is due to high early strength gains in the concrete members. All concrete mixes for The Shockey Precast Group are designed to reach their 28 day compressive strength by 7 days after casting. Code provisions for the tensile strength and modulus of elasticity are also in Table 4.8. The experimental values of the tensile strength are slightly larger than code predicted values. The experimental values of the modulus of elasticity are less than the code provisions.

Table 4.8 Initial Concrete Properties for Development Length Members

Concrete Type	Time Since Pour (Hours)	Compressive Strengths f'_c (psi)	E_{ci} $[33w_c^{1.5}f'^{0.5}_{ci}]$ (ksi)
S1CRM	10.25	3580	3516
S1CCM	13	3779	3559
S1CCM2	13.5	3858	3555

Table 4.9 Final Concrete Properties for Development Length Members

Concrete Type	Average Concrete Age (days)	f'_c (psi)		f'_t (psi)			E_c (ksi)		
		Mean	Std. Dev.	Mean	Std. Dev.	$7.5f'_c{}^{0.5}$	Mean	Std. Dev.	$33w_c{}^{1.5}f'_c{}^{0.5}$
S1CRM	37	9686	531	865	26	738	5207	412	5671
S1CCM	56	10877	742	915	74	782	5736	278	6009
S1CCM2	30	9052	833	851	7	714	4480	181	5482

4.2.2 Development Length Determination

Experimental determination of the development length was completed by iterative load testing. The embedment length of the load point (distance from the point of load application to the end of the member) was varied by 6 in. increments from test to test. Points of load application were determined in order to create different types of failure modes. Short embedment lengths were used to yield a bond failure due to strand slipping. Longer embedment lengths were used to create a flexural failure mode. If a test resulted in a bond failure, the embedment length was increased for the next test setup. If a test resulted in a flexural failure mode, the embedment length was decreased for the following test. In this manner, the embedment length at which bond failure and flexural failure occur simultaneously could be bracketed. This bracketed embedment length gives a range for the development length.

4.2.3 Failure Modes

Beam deflection and strand slip were monitored and recorded in every test performed. Moment versus deflection and moment versus strand slip plots were generated in lieu of load versus deflection and load versus strand slip plots. This was done in order to compare capacity results for tests with different embedment lengths. Appendix C contains the moment versus deflection and moment versus strand slip plots for each of the tests performed.

Two distinct failure modes were observed during flexural testing of the development length members. The first mode of failure observed was a bond failure due to the strand slipping through the concrete. This failure occurred suddenly and decreased the load carrying capacity of the development length member. A total of ten bond failures occurred during testing. Figure 4.5 shows a typical moment versus deflection plot for a bond failure. Notice the sharp drop in capacity prior to reaching the 800 in.-kip level. This drop corresponds to the slipping of the

strand through the concrete member. Figure 4.6 shows the plot of the bending moment versus strand slip for Figure 4.5. As can be seen in the figure, the strand slip is essentially zero until reaching the bending moment capacity, which creates a larger stress than the bond between the strand and concrete can handle. This causes the strand to slip nearly instantaneously past the 0.01 in. general bond failure criteria. In fact, the slip is so large that the LVDT is no longer in contact with the strand after slip occurs, as can be seen in Figure 4.7. Since only one strand was used for flexural capacity, bond failure results in the ultimate failure of the member, whereas members with multiple strands may continue to take additional load until the remaining strands slip or the member fails in flexural.

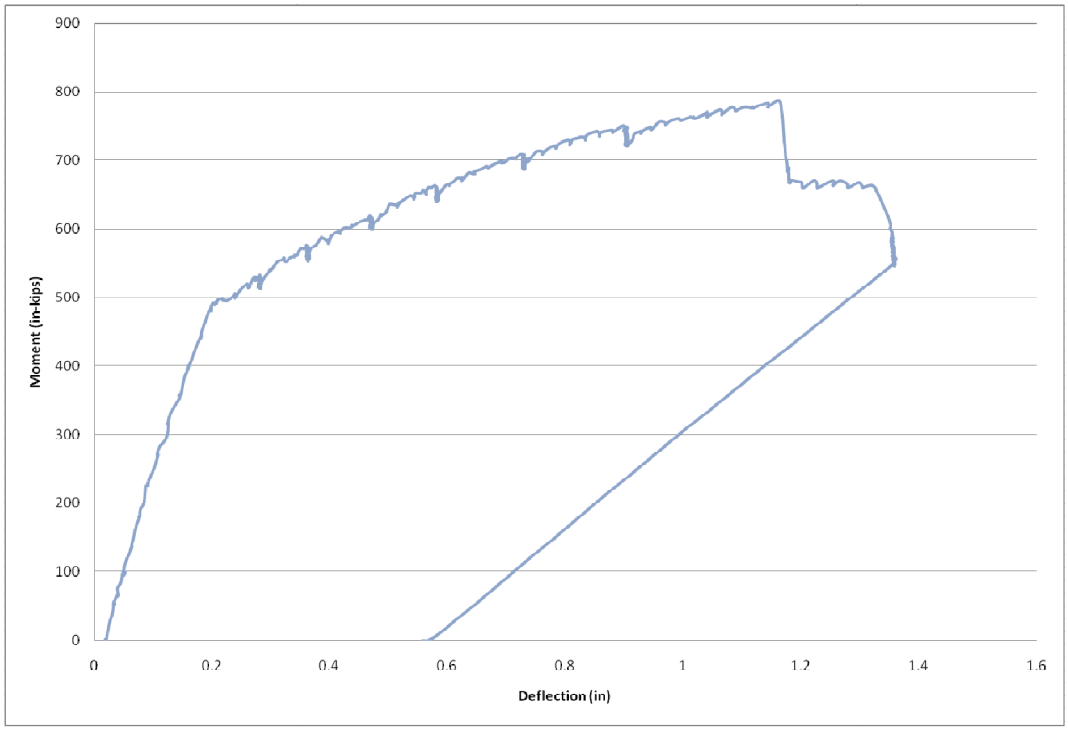

Figure 4.5 Moment versus Deflction for WT2B WE

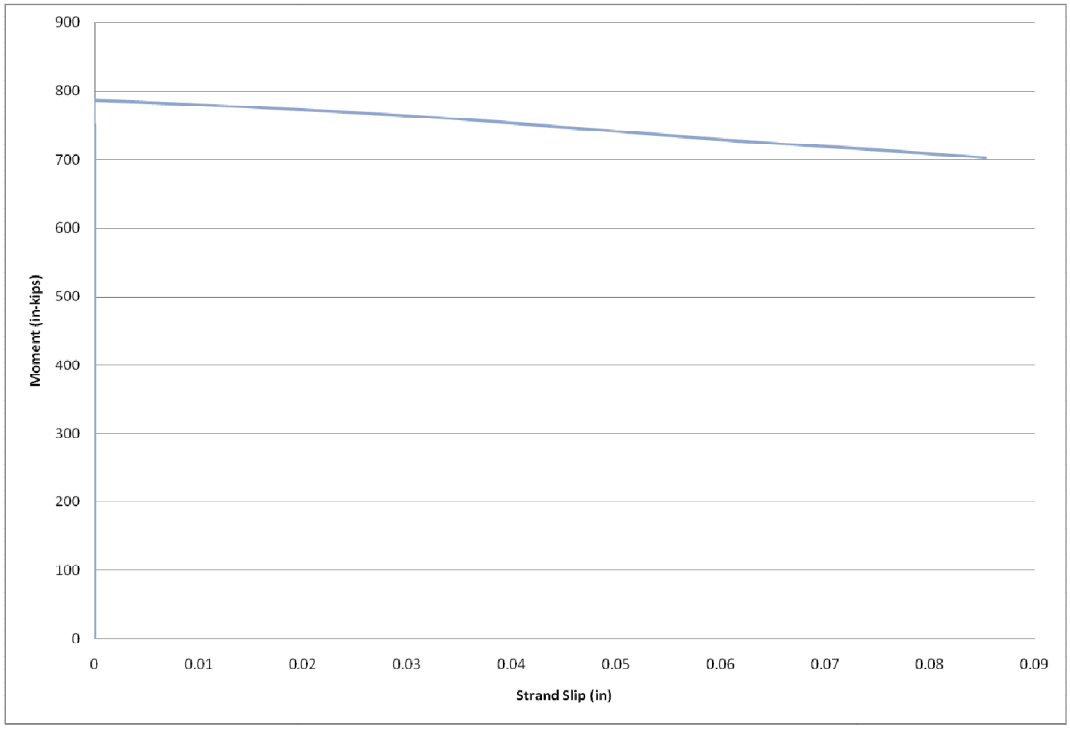

Figure 4.6 Moment versus Strand Slip for WT2B WE

Figure 4.7 Loss of Contact Between LVDT and Strand Due to Strand Slip

The other failure mode experienced in testing was flexural failure. This failure was characterized by crushing of the concrete near the point of load application, and by plastic behavior of the member. A total of fourteen flexural failures occurred during testing. Figure 4.8 shows a typical moment versus deflection plot for a flexural failure. As can be seen, there are three regions in the moment versus deflection plot. The first is an elastic region, which is bounded by the point of zero moment and the cracking moment. Once cracking occurred, the slope of the curve decreased and an elastic-plastic yielding region began. This region ends as the member reached its ultimate capacity and began to deform plastically without an increase in the applied moment. This strength plateau could continue for a longer period than shown in this figure if load was continuously applied. However, the member would begin to significantly deteriorate as its deflection increased. This would make removing the member from the test setup difficult. Therefore, the test was stopped and the member was unloaded prior to realizing the member's full ductility.

A representative plot of the moment versus strand slip for a flexural failure is given in Figure 4.9. The strand slip behavior of a flexural failure is essentially the same as that of a bond failure up to the point where the strand slips. The LVDT measurement drifts around an initial value and the strand moves very slightly into the member. Since the bond length is long enough,

the strand does not slip, and the flexural stress in the strand required for ultimate flexural capacity is reached.

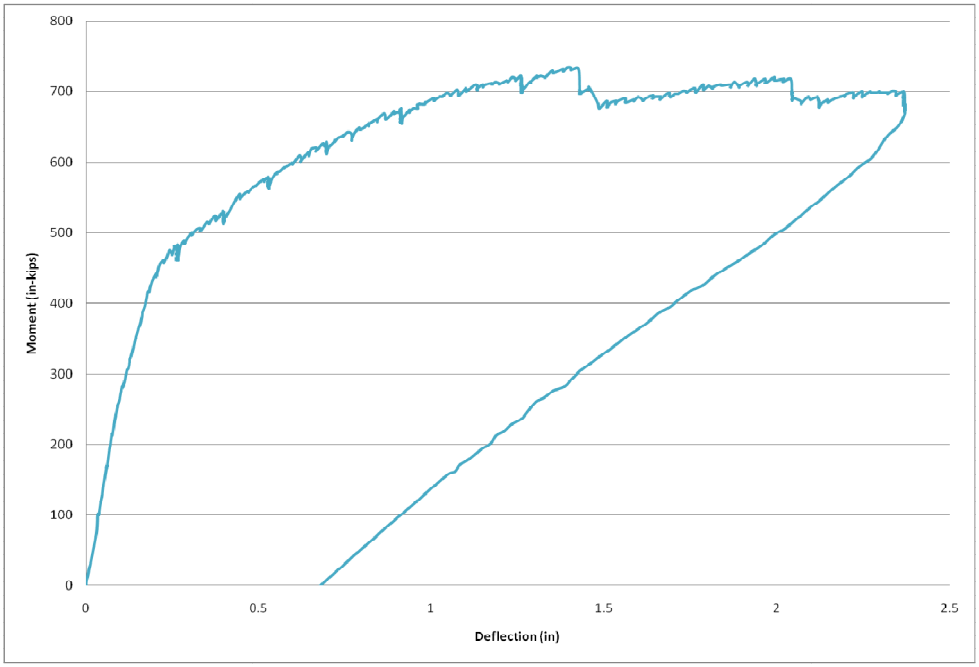

Figure 4.8 Moment versus Deflection for WT2C WE

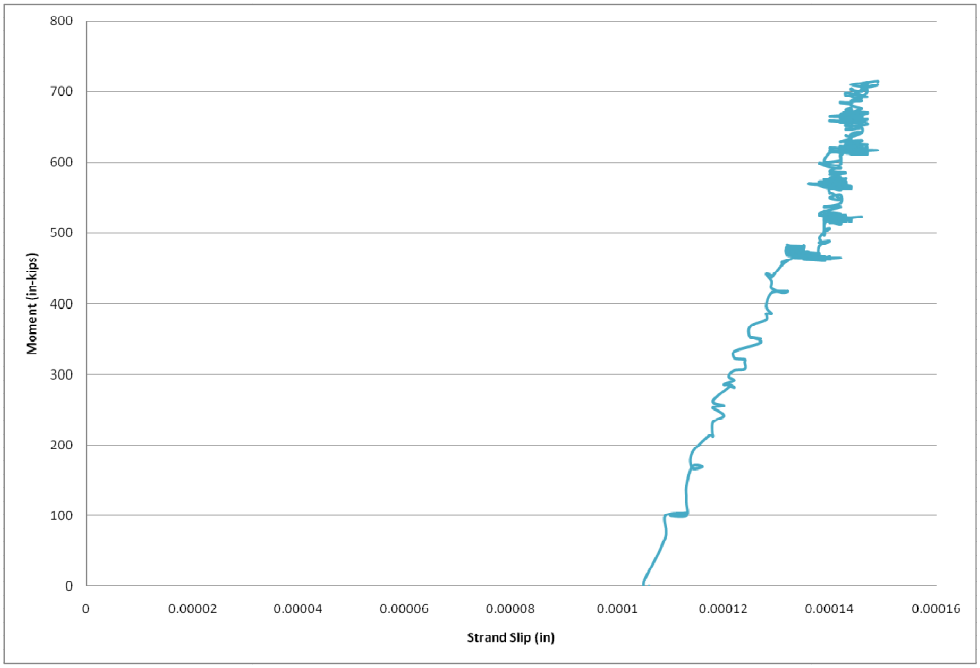

Figure 4.9 Moment vs. Strand Slip for WT2C WE

4.2.4 Crack Patterns

Beams were loaded in increments of 1 kip during the development length tests. After each load increment, beams were visually inspected for cracks. Any visible crack was marked with a permanent marker, along with the load at which it attained its present length. The observed cracking pattern was typical of flexural members. The first cracks began near the load application point, on the bottom of the beam. As the load increased, the first crack propagated directly up the member, towards the load. The initial crack began to branch out as it neared the load application point, and it continued to propagate towards the load point until either strand slippage or concrete crushing occurred. New cracks formed at regular intervals along the beam length as load was increased. The new cracks began as vertical flexural cracks and remained vertical until almost reaching the top flange. Then, the cracks began to curl towards the load. Often these cracks branched out once reaching the flange, similar to the initial crack behavior. There was no discernable difference between cracking behavior of the self-consolidating concrete members and the conventional concrete members. Figures 4.10 and 4.11 depict the flexural crack patterns.

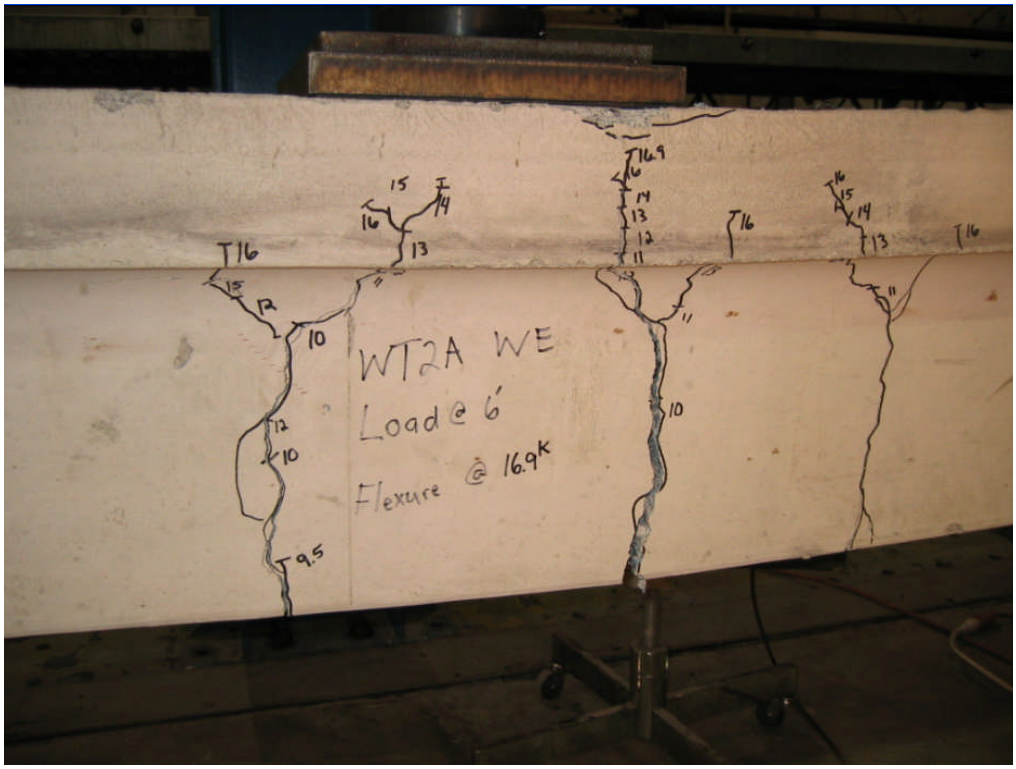

Figure 4.10 Close Up of Cracking Pattern for WT2A WE

Figure 4.11 Cracking Pattern for WT2A WE

4.2.5 Development Length Results

The results from the development length test are tabulated in Table 4.10. The data is grouped into three categories, one for each of the concrete mixes. The self-weight bending moment was included in the calculations. The tested embedment length for each member is provided, in addition to the strength of the concrete at the time of testing. The maximum bending moment is compared to the theoretical moment strength using f_{ps} calculated with ACI's equation 18-3 (equation 2.17).

The development length of each type of concrete was determined by bracketing an embedment length with flexural failure at a longer length, and bond failure at a shorter length. The embedment lengths for which flexural failures occurred are listed as the upper bound development length for each concrete mix in Table 4.11. ACI and AASHTO code calculated values for the development length are given as well. The effective prestress force used in the development length determination was calculated using the AASHTO models for determining effective prestress. This and other theoretical loss models will be discussed in Section 4.3.

A development length value was not determined for the conventional concrete mix (S1CRM). This was due to the inability to achieve repeatable results at the same embedment length. The first three tested embedment length for the S1CRM mix were 75 in., 87 in., and 93in. A strand slip/bond failure occurred at each of the embedment length locations. A 99 in. embedment length (midspan loading) was then attempted and produced a flexural failure. Each of the embedment lengths mentioned before were then retested and in each case a flexural failure ensued. Table 4.12 shows the non repeating tests data for the S1CRM members. There was no repeatability in the data to conclusively determine a development length. Interestingly, for the S1CRM mix the flexural failure members cast along one strand while the bond failure members were cast along another strand. The members which failed in flexure were cast along the South strand, whereas the members which failed by strand slip were cast along the North strand (refer to Figure 3.3 on page 35 for casting layout). Therefore, it is apparent the bond between the strand and the concrete for the bond failure members was poor compared to the concrete/strand bond of the other strands. Possible reasons for this poor bond quality include a greasy or new strand. Another possibility is inadequate vibration. Whatever the cause, the bond between the strand and the concrete for the North strand line of the S1CRM members was much weaker than the bond between the strand and concrete on the South strand line.

Table 4.10 Development Length Testing Results

Beam ID	Concrete ID	f'_c (ksi)	Tested Embedment Length (in.)	Maximum $M_{APPLIED}$ (in.-kips)	M_{ACI} (in.-kips)	$M_{APPLIED}/M_{ACI}$	Observed Failure Mode
WT1D EE	S1CRM	9.07	75	703	701	1.00	Strand Slip
WT1A EE		10.5	75	834	707	1.18	Flexure
WT1D WE		9.07	87	793	701	1.13	Strand Slip
WT1B WE		10.3	87	793	706	1.12	Flexure
WT1C WE		9.71	93	787	704	1.12	Strand Slip
WT1B EE		10.3	93	883	706	1.25	Flexure
WT1A WE		10.5	99	800	707	1.13	Flexure
WT1C EE		9.71	99	857	704	1.22	Flexure
WT2B WE	S1CCM	10.1	63	780	709	1.10	Strand Slip
WT2D EE		10.6	63	768	713	1.08	Strand Slip
WT2A EE		10.4	69	761	711	1.07	Strand Slip
WT2D WE		10.6	69	774	713	1.08	Strand Slip
WT2A WE		10.4	75	807	711	1.13	Flexure
WT2B EE		10.1	75	766	709	1.08	Flexure
WT2C EE		10.5	99	800	713	1.12	Flexure
WT2C WE		10.5	99	776	713	1.09	Flexure
WT3A EE	S1CCM2	8.75	63	673	698	0.96	Strand Slip
WT3D WE		8.44	63	685	697	0.98	Strand Slip
WT3C EE		8.75	69	739	699	1.06	Strand Slip
WT3A WE		8.75	69	756	698	1.08	Flexure
WT3C WE		8.75	75	771	699	1.10	Flexure
WT3D EE		8.44	75	802	697	1.15	Flexure
WT3B EE		10.5	99	742	706	1.05	Flexure
WT3B WE		10.5	99	819	706	1.16	Flexure

Table 4.11 Development Length Comparison

Member	Type of Concrete	f_{ps} (ksi)	f_{se} (ksi)	$l_{d,ACI/AASHTO}$ (in.)	$l_{d,TEST}$ Upper Bound (in.)	$l_{d,TEST}/l_{d,ACI/AASHTO}$
WT1	S1CRM	264	151	92	N/A	N/A
WT2	S1CCM	268	150	94	75	0.80
WT3	S1CCM2	263	154	90	75	0.83

Table 4.12 Effect of Casting Location on Failure Type Observed in S1CRM Beams

Beam ID	Concrete ID	Casting Location	Tested Embedment Length (in.)	Observed Failure Mode
WT1D EE	S1CRM	Northwest	75	Strand Slip
WT1D WE		Northwest	87	Strand Slip
WT1C WE		Northeast	93	Strand Slip
WT1A EE		Southwest	75	Flexure
WT1B WE		Southeast	87	Flexure
WT1B EE		Southeast	93	Flexure

The development length results for the two self-consolidating concrete mixes are much shorter than the theoretical values predicted by ACI and AASHTO. Based on the effective prestress values used to calculate the code development length, the S1CCM mix and the S1CCM2 mix had 20 percent and 17 percent shorter development lengths than code predictions, respectively. It is possible the flexural bond length of the self-consolidating concrete is much shorter than traditional models. Transfer length testing indicated a transfer length for the SCC mixes which is very close to code prediction models. The transfer length testing performed in this study used a hydraulic jack to slowly detension the strand. This resulted in a gradual transfer of prestress force from the strand to the concrete. In typical practice, a more sudden transfer of prestress force is used. In casting the development length members, a sudden prestress release method was used to save time on unloading the prestressing bed and to simulate realistic transfer of prestress force. This would tend to cause a longer transfer length than gradual release. Therefore, if the transfer lengths are longer than code predicted values, but the development length is much shorter than the code predicted values, the flexural bond length must be significantly shorter than code predictions. This notion has been seen in research done by Girgis and Tuan on the bond strength of SCC.

4.2.6 Flexural Strength

The flexural strength of each individual test can be found in Table 4.10. It can be seen that in all but two cases, the flexural strength of the concrete members exceeded the ACI predicted member design strength. The two cases which did not meet ACI predicted values were a result of a strand slip failure, and the capacities were within 4 percent of the predicted design strength.

Table 4.13 further breaks down the moment capacities by averaging the moment capacities of each type of member. The table breaks down the capacities listed in Table 4.9 into capacities from flexure only, capacities from strand slip/bond failure only, and all capacities. It can be seen that the average nominal strength for flexural failures are at least 11 percent greater than ACI predicted values. The conventional concrete mix is actually 18 percent greater than the predicted value. From this data, it appears the SCC mixes have a slightly lower flexural strength than the conventional concrete mixes when considering flexural failures, but the SCC members still have nominal moment capacities in excess of predicted strengths.

Table 4.13 Flexural Capacity Comparison

Beam ID	Concrete ID	Average Maximum $M_{APPLIED}$ (in.-kips)	Average M_{ACI} (in.-kips)	Average $M_{APPLIED}/M_{ACI}$
WT1 (Flexure Failure)	S1CRM	833	706	1.18
WT1 (Bond Failure)		7601	702	1.08
WT1 (All Failures)		806	704	1.14
WT2 (Flexure Failure)	S1CCM2	787	711	1.11
WT2 (Bond Failure)		771	712	1.08
WT2 (All Failures)		779	712	1.09
WT3 (Flexure Failure)	S1CCM2	778	702	1.11
WT3 (Bond Failure)		699	698	1.00
WT2(All Failures)		748	700	1.07

When bond failures are analyzed exclusively, the S1CCM self-consolidating concrete mix and the S1CRM conventional concrete mix had flexural capacities which were, on average, eight percent larger than the predicted values. The S1CCM2 self-consolidating mix met exactly the predicted ACI flexural capacity value. The reduced bending moment strength for the

S1CCM2 mix for bond failure members may be a result of earlier testing of the WT3 members than the WT2 and WT1 members. The majority of the WT3 members were tested between 21 and 35 days after pour, whereas the remaining of the tests were performed after 35 days.

Looking at all flexural failures, it is seen that the average values of the flexural capacities for all the concrete mixes surpass the code predicted values. Once again, the conventional concrete members had the highest flexural strength as compared to the self-consolidating members. The two SCC mixes were much closer in capacity to the S1CRM mix when all flexural strengths are considered. This data shows that the SCC mixes are better than code predicted values, and are comparable in strength to the conventional concrete mix.

Looking at each of the moment versus deflection plots of Appendix C shows the ductility of each concrete mix to be reasonably comparable. The development length members were very lightly reinforced, having a reinforcement ratio of 0.35 percent. A low value of the reinforcement ratio tends to lead to members which exhibit very ductile behavior. This was the case with this experimental study. A more conclusive evaluation of the ductility properties of SCC compared to conventional concrete should be done with larger reinforcement ratios and section shapes used more commonly in structural design practice.

4.2.7 Cracking Moments

Table 4.14 shows a comparison of the cracking moments actually recorded during testing and the theoretical values determined with the sixth edition PCI Design Handbook. Two theoretical cracking moments were determined. The first one used an average value of the measured split cylinder tests. The second theoretical cracking moment used the modulus of rupture found in the ACI code, which is $7.5\sqrt{f'_c}$, where f'_c was the measured compressive strength of the cylinders from cylinder testing during the week the beam was tested. From Table 4.14 it can be seen that each concrete mix on average had a cracking moment less than the predicted cracking moment. In fact, all measured cracking moments were below the theoretical cracking moments. The cracking moment recorded for the conventional concrete mix is the furthest from the predicted values with 83 percent of the f_t cracking moment and 88 percent of the f_r cracking moment.

Each SCC mix had an experimental cracking moment below the theoretical cracking moment using the spit tensile strength. The S1CCM mix reached 88 percent of the f_t theoretical cracking moment, while the S1CCM2achieved 86 percent of the f_t theoretical cracking moment,

on average. Both SCC mixes achieved 92 percent of the f_r theoretical cracking moment, on average. The range of values for the SCC mixes was from 7 to 16 percent below the f_t cracking moment and from 3 to 13 percent below the f_r cracking moments. This data does not seem to fit the theoretical models for the cracking moment. Additionally, it appears the theoretical cracking moments using the split tensile strength of the concrete is between 4 and 7 percent larger than cracking moments using the code predicted modulus of rupture, on average.

Table 4.14 Comparison of Experimental and Theoretical Cracking Moments

Beam ID	Experimental Cracking Moment (in-kips)	PCI Cracking Moment Using Tested f_t (in-kips)	PCI Cracking Moment Using $f_r = 7.5*(f'_c)^{0.5}$ (in-kips)	$M_{cr\text{-}EXPERIMENTAL}/M_{cr\text{-}PCI,ft}$	$M_{cr\text{-}EXPERIMENTAL}/M_{cr\text{-}PCI,fr}$	$M_{cr\text{-}PCI,ft}/M_{cr\text{-}PCI,fr}$
WT1A EE	338	461	441	0.73	0.76	1.05
WT1A WE	360	461	441	0.78	0.82	1.05
WT1B EE	383	461	439	0.83	0.87	1.05
WT1B WE	402	461	439	0.87	0.92	1.05
WT1C EE	384	461	433	0.83	0.89	1.07
WT1C WE	430	461	433	0.93	0.99	1.07
WT1D EE	383	461	427	0.83	0.90	1.08
WT1D WE	378	461	427	0.82	0.89	1.08
Average	382	461	435	0.83	0.88	1.06
WT2A EE	416	459	441	0.90	0.94	1.04
WT2A WE	428	459	441	0.93	0.97	1.04
WT2B EE	405	459	438	0.88	0.92	1.05
WT2B WE	392	459	438	0.85	0.89	1.05
WT2C EE	408	459	442	0.89	0.92	1.04
WT2C WE	408	459	442	0.89	0.92	1.04
WT2D EE	388	459	443	0.84	0.88	1.04
WT2D WE	390	459	443	0.85	0.88	1.04
Average	404	459	441	0.88	0.92	1.04
WT3A EE	396	454	421	0.87	0.94	1.08
WT3A WE	390	454	421	0.86	0.93	1.08
WT3B EE	384	454	439	0.85	0.87	1.03
WT3B WE	384	454	439	0.85	0.87	1.03
WT3C EE	381	454	421	0.84	0.90	1.08
WT3C WE	410	454	421	0.90	0.97	1.08
WT3D EE	387	454	418	0.85	0.93	1.09
WT3D WE	384	454	418	0.84	0.92	1.09
Average	389	454	425	0.86	0.92	1.07

The values of the measured cracking moments will be useful in experimentally determining the effective prestress. The next section will discuss the use of the cracking moments to arrive at an effective prestress value.

4.3 Prestress Losses

The effective prestress was theoretically predicted and experimentally determined for twelve prestressed concrete beams. As was explained previously, the effective prestress is directly related to the prestress losses. Theoretical values of prestress losses were estimated using three prestress loss models. The three prestress loss models are the PCI Design Handbook model, a 1975 PCI prestress loss model, and an AASHTO model. Experimental determination of prestress loss was obtained by two methods; crack initiation and crack reopening.

4.3.1 Theoretical Prestress Loss Models

Prestress losses were theoretically predicted using three different models. The first model is a lump sum model used to determine the final design prestress losses expected for a pretensioned precast concrete member. The other two models are time step models which determine losses throughout the lifetime of the member. Time step models are effective since they address the dependence of one cause of prestress loss with another. Several assumptions are implemented in the use of these models. These assumptions are outlined below.

The first assumption is that the material properties and concrete strengths are known prior to using the prestress loss models. The prestress losses calculated in this study are not calculated using design values of concrete strength or steel strand ultimate strength. The theoretical loss models utilize the actual values of the strand ultimate strength, both initial and final concrete strengths, and measured values of the concrete modulus of elasticity. Also, the jacking force is the actual force used, not the design jacking force.

Strands were tensioned approximately six hours before the concrete was poured into the development length member forms. Placing of the concrete for the structural double tees cast with the development length members began approximately 4 hours after tensioning of the strand. Anchorage and seating losses were taken into account by stressing the strand past initial required stress and allowing the seating losses to counteract this overstressing. This meant the initial force in the strand was the specified initial force. Relative humidity was monitored with electronic sensing data. The average value of the relative humidity (75 percent) was used in the required calculations.

4.3.1.1 PCI Design Handbook

Estimations for prestress losses in the Sixth Edition PCI Design Handbook are based on a report sponsored by a joint committee, ACI-ASCE Committee 423, Prestressed Concrete. The report offers equations for determining prestress losses due to elastic shortening, concrete creep, concrete shrinkage, and steel relaxation. The PCI Design Handbook recommends the use of these prestress loss equations for practical design applications. The handbook suggests the use of another loss model if the structural application is unusual. One particularly interesting aspect of this loss model is its lack of a time function for determination of creep strains. The accuracy of this model will be compared with the accuracy of the other prestress loss models employed in this study.

Elastic shortening losses are calculated by Equation 4.2.

$$ES = K_{es} E_{ps} f_{cir} / E_{ci} \qquad 4.2$$

Where:

ES = losses due to elastic shortening (ksi)

K_{es} = 1.0 for pretensioned members

E_{ps} = modulus of elasticity of prestressing tendons (ksi)

E_{ci} = modulus of elasticity of concrete at time prestress is applied (ksi)

F_{cir} = net compressive stress in concrete at center of gravity of prestressing force immediately after the prestress has been applied to the concrete, given by Equation 4.3 below

$$f_{cir} = K_{cir}\left(\frac{P_i}{A_g} + \frac{P_i e^2}{I_g}\right) - \frac{M_g e}{I_g} \qquad 4.3$$

Where:

K_{cir} = 0.9 for pretensioned members

P_i = initial prestress force after anchorage seating loss (kips)

e = eccentricity of center of gravity of tendons with respect to center of gravity of concrete at the cross section considered (in.)

A_g = area of gross concrete section at the cross section considered ($in.^2$)

I_g = moment of inertia of gross concrete section at the cross section considered ($in.^4$)

M_g = bending moment due to dead weight of prestressed member and any other permanent loads in place at time of prestressing (in.-kips)

Creep losses are calculated according to Equation 4.4.

$$CR = K_{cr}\left(E_{ps} / E_c\right)\left(f_{cir} - f_{cds}\right) \quad 4.4$$

Where:

CR = losses due to creep of concrete (ksi)

K_{cr} = 2.0 for normal weight concrete

E_c = modulus of elasticity of concrete at 28 days

f_{cds} = stress in concrete at center of gravity of prestressing force due to all superimposed permanent dead loads that are applied to the member after it has been prestressed; given by Equation 4.5 below (ksi)

$$f_{cds} = M_{sd}(e) / I_g \quad 4.5$$

Where:

M_{sd} = moment due to all superimposed permanent dead and sustained loads applied after prestressing (in.-kip)

Shrinkage losses are given Equation 4.6 below.

$$SH = \left(8.2 \times 10^{-6}\right) K_{sh} E_{ps} \left(1 - 0.6V / S\right)\left(100 - R.H.\right) \quad 4.6$$

Where:

SH = losses due to shrinkage

K_{sh} = 1.0 for pretensioned members

V/S = volume-to-surface ratio (in.)

R.H. = average ambient relative humidity (%)

Losses due to steel relaxation are calculated by using Equation 4.7.

$$RE = \left[K_{re} - J\left(SH + CR + ES\right)\right]C \qquad 4.7$$

Where:

RE = losses due to relaxation of the tendon (ksi)

K_{re} and J are available from Table 4.15 and C is taken from Table 4.16

Table 4.15 Values of K_{re} and J

Type of Tendon	K_{re}	J
270 Grade stress-relieved strand or wire	20	0.15
250 Grade stress-relieved strand or wire	18.5	0.14
240 or 235 Grade stress-relieved wire	17.6	0.13
270 Grade low-relaxation strand	5	0.040
250 Grade low-relaxation wire	4.63	0.037
240 or 235 Grade low-relaxation wire	4.4	0.035
145 or 160 Grade stress relieved bar	6	0.05

Table 4.16 Values of C

f_{pi}/f_{pu}	Stress-relieved strand or wire	Stress-relieved bar or low-relaxation strand or wire
0.80		1.28
0.79		1.22
0.78		1.16
0.77		1.11
0.76		1.05
0.75	1.45	1.00
0.74	1.36	0.95
0.73	1.27	0.90
0.72	1.18	0.85
0.71	1.09	0.80
0.70	1.00	0.75
0.69	0.94	0.70
0.68	0.89	0.66
0.67	0.83	0.61
0.66	0.78	0.57
0.65	0.73	0.53
0.64	0.68	0.49
0.63	0.63	0.45
0.62	0.58	0.41
0.61	0.53	0.37
0.60	0.49	0.33

The Sixth Edition PCI Handbook model was used to predict the prestress losses in each beam. The results of the theoretical predictions are shown in Table 4.17. The effective prestress value is the initial prestress value minus the losses due to elastic shortening, creep, and shrinkage of the concrete, and relaxation of the steel prestressing strand. The last column of Table 4.15 shows the effective prestress for a particular beam.

Table 4.17 Sixth Edition PCI Design Handbook Theoretical Values of Effective Prestress

Beam Name	End Time (days)	ES (ksi)	CR (ksi)	SH (ksi)	RE (ksi)	f_{pe} (ksi)	f_{pe} (ksi)
WT1A EE	56	6.36	9.58	5.14	2.20	150	150
WT1A WE	61	6.36	9.58	5.14	2.20	150	
WT1B EE	46	6.36	9.58	5.14	2.20	150	150
WT1B WE	47	6.36	9.58	5.14	2.20	150	
WT1C EE	34	6.34	9.56	5.13	2.20	149	149
WT1C WE	33	6.34	9.56	5.13	2.20	149	
WT1D EE	28	6.34	9.56	5.13	2.20	149	149
WT1D WE	32	6.34	9.56	5.13	2.20	149	
WT2A EE	44	6.24	8.76	5.12	2.22	151	151
WT2A WE	47	6.24	8.76	5.12	2.22	151	
WT2B EE	42	6.24	8.76	5.12	2.22	151	151
WT2B WE	42	6.24	8.76	5.12	2.22	151	
WT2C EE	65	6.27	8.79	5.14	2.22	151	151
WT2C WE	65	6.27	8.79	5.14	2.22	151	
WT2D EE	56	6.27	8.79	5.14	2.22	151	151
WT2D WE	51	6.27	8.79	5.14	2.22	151	
WT3A EE	25	6.29	10.94	5.14	2.18	149	149
WT3A WE	27	6.29	10.94	5.14	2.18	149	
WT3B EE	65	6.29	10.94	5.14	2.18	149	149
WT3B WE	65	6.29	10.94	5.14	2.18	149	
WT3C EE	22	6.27	10.92	5.13	2.18	148	148
WT3C WE	23	6.27	10.92	5.13	2.18	148	
WT3D EE	21	6.27	10.92	5.13	2.18	148	148
WT3D WE	20	6.27	10.92	5.13	2.18	148	

4.3.2.1 1975 PCI Recommendations for Prestress Losses

Recommendations from the PCI Committee on Prestress Losses were used in this study to determine the effective prestress in the development length members (PCI 1975). This method, while over thirty years old, is still recognized by ACI as an acceptable method for determining prestress losses. PCI recommends the use of at least four time steps for calculating prestress losses. Only the second time step is applicable in this study. The second time step is from transfer of prestress to application of load other than the members self weight. This time step was considered to begin once transfer of the prestress force occurred and ended at the beginning of the load testing procedure.

Elastic shortening losses are calculated by Equation 4.8.

$$ES = f_{cr}\frac{E_s}{E_{ci}} \tag{4.8}$$

Where:

ES = elastic shortening loss (ksi)

f_{cr} = concrete stress at centroid of prestressing steel just after transfer (ksi)

E_s = modulus of elasticity of prestressing strand (ksi)

E_{ci} = initial modulus of elasticity of concrete (ksi)

Creep losses were calculated according to Equation 4.9.

$$CR = (UCR)(SCF)(MCF)(PCR)(f_c) \tag{4.9}$$

Where:

CR = creep loss (ksi)

UCR = $63 - 20E_c/10^6$ (E_c is the concrete modulus of elasticity in psi)

PCR = $AUC_{\text{end of step}} - AUC_{\text{beginning of step}}$

MCF = 1.0 for accelerated cured members

f_c = net concrete stress at centroid of prestressing strand at beginning of time step (ksi)

SCF and AUC are available in Table 4.18 and Table 4.19.

Table 4.18 PCI Creep Factors for Member Size and Shape

Volume to Surface Ratio (in.)	SCF
1	1.05
2	0.96
3	0.87
4	0.77
5	0.68
>5	0.68

Table 4.19 PCI Creep Factors for Time

Time After Prestress (days)	AUC
1	0.08
2	0.15
5	0.18
7	0.23
10	0.24
20	0.30
30	0.35
60	0.45
90	0.51
180	0.61
365	0.74
End of Service	1.00

Shrinkage losses were calculated using Equation 4.10.

$$SH = (USH)(PSH)(SSF) \qquad 4.10$$

Where:

SH = shrinkage loss (ksi)

USH = $27{,}000 - 3000E_c/10^6 \geq 12{,}000$ (units of USH and E_c are in psi)

PSH = $AUS_{\text{end of step}} - AUS_{\text{beginning of step}}$

SSF and AUS are presented in Table 4.20 and Table 4.21

Table 4.20 PCI Shrinkage Factors for Member Size and Shape

Time After Prestress (days)	AUC
1	0.08
2	0.15
5	0.18
7	0.23
10	0.24
20	0.30
30	0.35
60	0.45
90	0.51
180	0.61
365	0.74
End of Service	1.00

Table 4.21 Shrinkage Factors for Time

Time After Prestress (days)	AUS
1	0.08
2	0.15
5	0.20
7	0.22
10	0.27
20	0.36
30	0.42
60	0.55
90	0.62
180	0.68
365	0.86
End of Service	1.00

Relaxation losses in the steel strand are calculated by Equation 4.11.

$$RET = \frac{f_{st}}{45}\log\left(\frac{24t_{end}}{24t_{begin}}\right)\left(\frac{f_{st}}{f_{py}} - 0.55\right) \qquad 4.11$$

$$\left(\frac{f_{st}}{f_{py}} - 0.55\right) \geq 0.05$$

Where:

RET = steel relaxation loss (ksi)

f_{st} = stress in prestressing steel at beginning of time step (ksi)

t_{end} = time at end of time step (days)

t_{begin} = time at beginning of time step (days)

f_{py} = yield stress of prestressing steel (ksi)

The 1975 PCI model was used to predict the prestress losses in each beam. The results of the theoretical predictions are shown in Table 4.22. The initial prestress is the stress in the concrete just after prestress transfer, or the jacking stress subtracted by the prestress losses due to elastic shortening. The steel relaxation losses in the steel and the creep and shrinkage losses in the concrete are calculated from the time of prestress transfer to the time of loading. The second column of the chart shows the number of days from prestress transfer to loading.

Table 4.22 1975 PCI Recommended Prestress Loss Predictions

Beam Name	End Time (days)	f_{pj} (ksi)	ES (ksi)	f_{pi} (ksi)	RET (ksi)	SH (ksi)	CR (ksi)	f_{pe} (ksi)	f_{pe} (ksi)
WT1A EE	56	173	7.06	166	0.68	5.06	3.01	158	157
WT1A WE	61	173	7.06	166	0.69	5.27	3.14	157	
WT1B EE	46	173	7.06	166	0.65	4.57	2.73	158	158
WT1B WE	47	173	7.06	166	0.65	4.63	2.76	158	
WT1C EE	34	173	7.05	166	0.58	3.99	2.39	159	159
WT1C WE	33	173	7.05	166	0.58	3.94	2.36	159	
WT1D EE	28	173	7.05	166	0.55	3.66	2.19	159	159
WT1D WE	32	173	7.05	166	0.57	3.90	2.34	159	
WT2A EE	44	173	6.93	166	0.69	4.48	2.67	158	158
WT2A WE	47	173	6.93	166	0.70	4.63	2.75	158	
WT2B EE	42	173	6.93	166	0.68	4.38	2.61	158	158
WT2B WE	42	173	6.93	166	0.68	4.38	2.61	158	
WT2C EE	65	173	6.96	166	0.70	5.38	3.20	157	157
WT2C WE	65	173	6.96	166	0.70	5.38	3.20	157	
WT2D EE	56	173	6.96	166	0.67	5.06	3.01	157	157
WT2D WE	51	173	6.96	166	0.66	4.82	2.86	158	
WT3A EE	25	173	6.98	166	0.55	3.86	2.07	160	160
WT3A WE	27	173	6.98	166	0.56	4.01	2.15	160	
WT3B EE	65	173	6.98	166	0.71	6.00	3.21	157	157
WT3B WE	65	173	6.98	166	0.71	6.00	3.21	157	
WT3C EE	22	173	6.97	166	0.51	3.64	1.94	160	160
WT3C WE	23	173	6.97	166	0.52	3.71	1.98	159	
WT3D EE	21	173	6.97	166	0.50	3.56	1.90	160	160
WT3D WE	20	173	6.97	166	0.50	3.49	1.86	160	

4.3.1.3 AASHTO Recommendation for Prestress Losses

Finally, prestress losses were calculated according to the refined method of *AASHTO LRFD Bridge Design Specifications* (AASHTO 2006). Prestress Losses were divided into initial losses due to elastic shortening, and long term losses due to creep and shrinkage of the concrete, and relaxation of the steel strand. Article 5.9.5.2.3a was used to determine the elastic shortening losses (similar to 1975 PCI method). Article 5.9.5.4.2 was used to calculate the long term losses between prestress transfer and the time of loading.

Articles 5.4.2.3.2 and 5.4.2.3.3 were used to estimates of creep and shrinkage of the concrete. The creep coefficient was determined by Equation 4.12.

$$\psi(t,t_i) = 1.9 k_{vs} k_{hc} k_f k_{td} t^{-0.118} \qquad 4.12$$

Where:

ψ = creep coefficient

k_{vs} = 1.45 – 0.13*(volume to surface ratio) $\geq$ 0.0

k_{hc} = 1.56 – 0.008*(relative humidity)

k_f = 5/(1+f'$_{ci}$)(is the initial concrete compressive strength in ksi)

k_{td} = t/(61 – 4*f'$_{ci}$ + t)

t = time between prestress transfer and load testing (days)

t_i = age of concrete at prestress transfer (days)

The shrinkage strain was determined by equation 4.13.

$$\varepsilon_{sh} = k_{vs} k_{hs} k_f k_{td} \left(480 \times 10^{-6}\right) \qquad 4.13$$

Where:

ε_{sh} = shrinkage strain

k_{sh} = 2.0 -0.014*(relative humidity)

The relative humidity was assumed to be 75 percent since this is the average daily value given at the Shockey Precast Plant. The factors k_{vs}, k_f, and k_{td}, were common to both the creep and shrinkage equations. The time used in the k_{td} term was taken as the time between the transfer of prestress and beginning of load testing. The transformed section coefficient is given by equation

4.14. This term is necessary to take into account long term creep and shrinkage losses. A ten year time value was used to evaluate the transformed section coefficient.

$$K_{id} = \frac{1}{1 + \frac{E_p}{E_{ci}} \frac{A_{ps}}{A_g} \left(1 + \frac{A_g e_g^{\,2}}{I_g} \right) \left[1 + 0.7\psi\left(t_f, t_i\right) \right]} \qquad 4.14$$

Where:

K_{id} = transformed section coefficient for time between transfer and deck placement

E_p = modulus of elasticity of prestressing strand (ksi)

E_{ci} = initial modulus of elasticity of the concrete (ksi)

A_{ps} = area of prestressing steel (in.^{2})

A_g = gross section area (in.^{2})

e_g = gross section strand eccentricity (in.)

I_g = gross section moment of inertia (in.^{4})

$\psi_b(t_f,t_i)$ = creep coefficient at final time

Articles 5.9.5.4.2a, 5.9.5.4.2b, and 5.9.5.4.2c were used to calculate time dependent prestress losses due to shrinkage of concrete, creep of concrete, and relaxation of the steel strand, respectively. Equation 4.15 was used to determine the shrinkage losses.

$$\Delta f_{pSR} = \varepsilon_{bid} E_p K_{id} \qquad 4.15$$

Where:

Δf_{pSR} = prestress loss due to shrinkage (ksi)

ε_{bid} = concrete shrinkage strain in beam between end of cure and testing

E_p = modulus of elasticity of prestressing strand (ksi)

K_{id} = transformed section coefficient for time between transfer and load testing

Creep losses were calculated by Equation 4.16.

$$\Delta f_{pCR} = \frac{E_p}{E_{ci}} f_{cgp} \psi_b (t_d, t_i) K_{id} \qquad 4.16$$

Where:

Δf_{pCR} = prestress loss due to creep (ksi)

E_p = modulus of elasticity (ksi)

E_{ci} = initial modulus of elasticity of concrete (ksi)

f_{cgp} = concrete stress at centroid of prestressing strands just after transfer (ksi)

$\psi_b(t_d,t_i)$ = creep coefficient for time between and load testing

K_{id} = transformed section coefficient for time between transfer and loading

Finally, steel relaxation losses were computed with Equation 4.17.

$$\Delta f_{pR1} = \frac{f_{pi}}{K_L} \left(\frac{f_{pt}}{f_{py}} - 0.55 \right) \qquad 4.17$$

Where:

Δf_{pR1} = prestress loss due to relaxation (ksi)

f_{pt} = stress in prestressing strands just after transfer (ksi)

K_L = 30 for low relaxation strands

f_{py} = yield stress of prestressing strands (ksi)

The AASHTO refined method of estimating prestress losses, outlined above, was used to determine the prestress losses in each development length member. The results are shown in Table 4.23.

Table 4.23 AASHTO Prestress Loss Predictions

Beam Name	End Time (days)	f_{pj} (ksi)	Δf_{pES}	f_{pi}	Δf_{pR1}	Δf_{pSR}	Δf_{pCR}	f_{pe} (ksi)	f_{pe} (ksi)
WT1A EE	56	173	7.06	166	0.77	8.18	8.64	149	148
WT1A WE	61	173	7.06	166	0.77	8.50	8.98	148	
WT1B EE	46	173	7.06	166	0.77	7.45	7.87	150	150
WT1B WE	47	173	7.06	166	0.77	7.53	7.95	150	
WT1C EE	34	173	7.05	166	0.76	6.31	6.66	152	152
WT1C WE	33	173	7.05	166	0.76	6.20	6.55	152	
WT1D EE	28	173	7.05	166	0.76	5.61	5.93	153	153
WT1D WE	32	173	7.05	166	0.76	6.09	6.43	152	
WT2A EE	44	173	6.93	166	0.81	7.05	7.33	151	151
WT2A WE	47	173	6.93	166	0.81	7.28	7.58	150	
WT2B EE	42	173	6.93	166	0.81	6.88	7.16	151	151
WT2B WE	42	173	6.93	166	0.81	6.88	7.16	151	
WT2C EE	65	173	6.96	166	0.76	8.47	8.81	148	148
WT2C WE	65	173	6.96	166	0.76	8.47	8.81	148	
WT2D EE	56	173	6.96	166	0.76	7.94	8.26	149	149
WT2D WE	51	173	6.96	166	0.76	7.60	7.91	150	
WT3A EE	25	173	6.98	166	0.77	5.04	5.26	155	155
WT3A WE	27	173	6.98	166	0.77	5.29	5.52	155	
WT3B EE	65	173	6.98	166	0.77	8.36	8.73	149	149
WT3B WE	65	173	6.98	166	0.77	8.36	8.73	149	
WT3C EE	22	173	6.97	166	0.76	4.62	4.82	156	155
WT3C WE	23	173	6.97	166	0.76	4.76	4.97	155	
WT3D EE	21	173	6.97	166	0.76	4.47	4.67	156	156
WT3D WE	20	173	6.97	166	0.76	4.33	4.52	156	

4.3.2 Experimental Measurements of Prestress Losses

Prestress losses were measured experimentally for both ends of each beam during the development length testing. Two methods were used to determine the effective prestress in each beam. Crack initiation and crack reopening tests were performed to determine the effective prestress. Using basic mechanics principles, the effective prestress in each beam was calculated.

4.3.2.1 Experimental Measurement of Effective Prestress by Crack Initiation Tests

Effective prestress of each beam at the time of loading was determined by crack initiation testing. This test was performed by loading a member until observed cracking occurred in the bottom of the member. The initiation of a crack in the concrete is a result of the stress in the concrete exceeding its tensile strength. Basic theory of mechanics allows the back calculation of the effective prestress by Equation 4.18.

$$f_{pe} = \left(\frac{1}{\frac{A_{ps}}{A_g} + \frac{A_{ps} e_g y_g}{I_g}} \right) \left(\frac{M_o y_t}{I_t} + \frac{M_{applied} y_t}{I_t} - f_t \right) \qquad 4.18$$

Where:

f_{pe} = effective prestress (ksi)

A_{ps} = cross sectional area of prestressing strands (in.^{2})

A_g = gross section area (in.^{2})

e_g = gross section strand eccentricity (in.)

y_g = distance from gross section centroid to location of strain measurements (in.)

I_g = gross section moment of inertia (in.^{4})

y_t = distance from transformed section centroid to location of strain measurement (in.)

I_t =transformed section moment of inertia (in.^{4})

M_o = self weight moment (in.-kip)

$M_{applied}$ = applied moment at crack initiation (in.-kip)

f_t = tensile strength of concrete from split cylinder tests (ksi)

The tensile strength of the concrete used in these calculations was found by averaging the results for all the split cylinder tests for each type of concrete. Average values of the concrete tensile strength are found in Table 4.8. Additionally, a change in the experimentally measured concrete tensile strength of just 50 psi will result in an 8.5 ksi difference in the measured effective prestress. This is a significant difference for a small change in the measured concrete tensile strength. More split cylinder tests performed throughout a research program could help to increase the accuracy of the crack initiation testing. A more accurate value of the concrete tensile strength for Equation 4.18 would be given by experimental modulus of rupture tests. Moduli of rupture tests accurately simulate the tensile stress gradient present in bending. Therefore, the values obtained in this test are more effective in determining the actual tensile strength of concrete in bending. The tensile strength of these tests are also higher than the tensile strength observed in split cylinder tests. If modulus of rupture values were used instead split cylinder values, the experimentally determined effective prestress values would be lower.

Crack initiation was detected by visual observation of the test member after each increment of load was applied. Load was applied continuously up to a predetermined value calculated to be less than the cracking moment. The member was visually examined for any signs of cracking. If no cracks had appeared, an additional load of one kip was added to the member. While loading the member, a plot of load versus deflection was monitored. The load versus deflection plot begins as a linear elastic straight line from zero until it reaches the cracking moment. Once the cracking moment is approached, the slope of the load versus deflection plot begins to decrease. This indicates cracking is occurring in the beam. Therefore, monitoring the load versus deflection plot aided in determining the initiation of cracking. Once cracks were observed, the crack was traced with a permanent marker on the bottom and sides of the beam. The load was recorded and the beam was unloaded.

Results of the crack initiation testing are presented in Table 4.24. The applied cracking load in the table is the load at which cracking was first observed. The applied moment is the moment created by the applied load at initiation of cracking. Two separate load tests were performed on each beam. Therefore, the effective prestress in the beam is the average of the effective prestress determined for each end of the beam. The difference in effective prestress values for either end of a beam varied from no difference in one beam to nearly 30 ksi in another beam, with a relatively even distribution of differences between.

Table 4.24 Experimental Values of Effective Prestress for Crack Initiation

Beam Name	$P_{applied}$ (k)	$M_{applied}$ (in.-k)	f_{pe} (ksi)	$f_{pe,average}$ (ksi)
WT1A EE	7.5	338	99	106
WT1A WE	7.4	360	113	
WT1B EE	8.0	383	127	133
WT1B WE	8.5	402	139	
WT1C EE	8.0	384	128	143
WT1C WE	9.0	430	157	
WT1D EE	8.5	383	127	125
WT1D WE	8.0	378	124	
WT2A EE	9.6	416	150	154
WT2A WE	9.5	428	157	
WT2B EE	9.0	405	143	139
WT2B WE	9.5	392	135	
WT2C EE	8.5	408	145	145
WT2C WE	8.5	408	145	
WT2D EE	9.4	388	132	133
WT2D WE	9.0	390	134	
WT3A EE	9.6	396	139	137
WT3A WE	9.0	390	135	
WT3B EE	8.0	384	132	132
WT3B WE	8.0	384	132	
WT3C EE	8.8	381	129	138
WT3C WE	9.1	410	147	
WT3D EE	8.6	387	133	132
WT3D WE	9.3	384	131	

4.3.2.2 Experimental Measurement of Effective Prestress by Crack Reopening Tests

Effective prestress was also measured by crack reopening tests. The beams discussed in the crack initiation tests were fitted with strain gages, one situated across the crack, the other beside the crack. These beams were then reloaded until the observed crack reopened. The stress in the bottom of the beam was assumed to be zero at the onset of crack reopening. Equation 4.18 was used to determine the effective prestress. The applied moment for this calculation is the moment required to reopen the crack. The tensile strength of the concrete was zero since the bottom of the beam was already cracked.

Crack detection gauges were used to determine when the crack reopened. Discussion of the crack detection gauges is provided in section 3.4.3. Load versus strain for each crack detection gauge was monitored during the reloading of each member. As the crack reopened, the strain in the crack detection gauge placed across the crack began to deviate from the crack detection gauge attached beside the crack. Determining the load at which the two crack detection gauge strain measurements deviated was assumed to be the load at which the cracks reopened. An example of a crack reopening plot is provided in Figure 4.12. Crack reopening plots for all tests are provided in Appendix D.

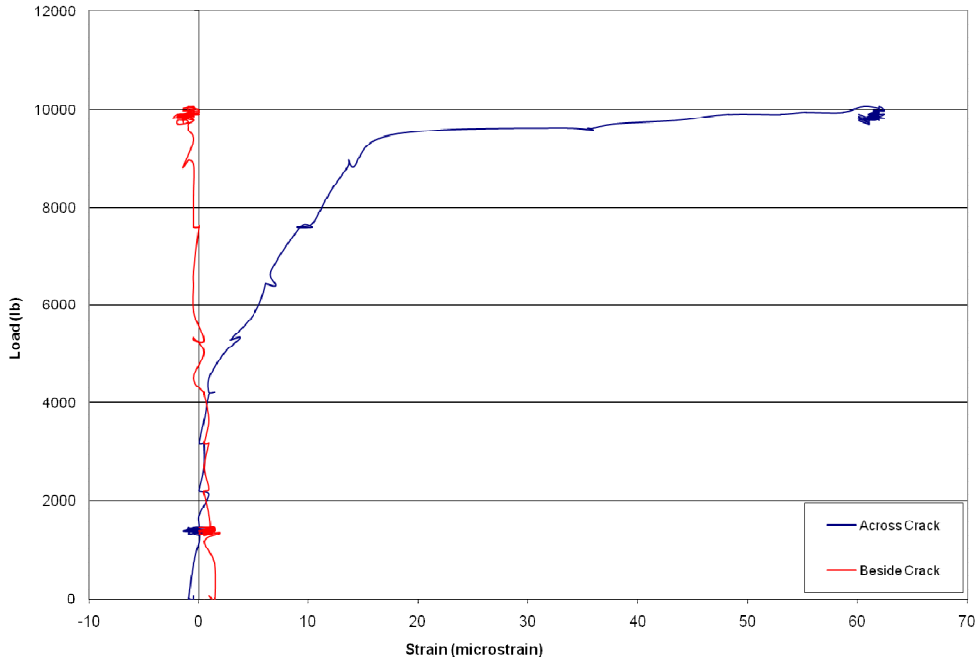

Figure 4.12 Crack Reopening Plot for WT2D WE

Results from crack reopening tests are shown in Table 4.25. The results for the effective prestress at opposite ends of a beam ranged from 0 to 58 ksi. This is a significant dispersion of results. The point at which the two plots diverge was difficult to determine in a few cases. A 0.5 kip misinterpretation of the divergence point could lead to 10 ksi change in the measured effective prestress. This is a significant change in effective prestress for a small change in load and could result in inaccuracies in the data presented.

Table 4.25 Experimental Values of Effective Prestress for Crack Re-opening

Beam Name	$P_{applied}$ (k)	$M_{applied}$ (in.-k)	f_{pe} (ksi)	$f_{pe,average}$ (ksi)
WT1A EE	3.0	135	114	141
WT1A WE	4.6	221	168	
WT1B EE	4.0	191	150	149
WT1B WE	4.0	189	148	
WT1C EE	4.4	211	162	153
WT1C WE	3.8	182	143	
WT1D EE	4.1	185	145	154
WT1D WE	4.5	213	163	
WT2A EE	4.3	186	146	159
WT2A WE	5.0	225	171	
WT2B EE	4.7	212	162	159
WT2B WE	4.9	202	156	
WT2C EE	4.2	202	156	156
WT2C WE	4.2	202	156	
WT2D EE	4.5	186	146	149
WT2D WE	4.5	195	152	
WT3A EE	4.0	227	172	159
WT3A WE	3.0	187	147	
WT3B EE	3.0	274	202	173
WT3B WE	2.0	183	144	
WT3C EE	3.0	187	147	159
WT3C WE	3.3	225	171	
WT3D EE	3.0	204	157	156
WT3D WE	3.5	199	154	

4.3.3 Comparison and Discussion of Prestress Loss Methods

The predictions made by the three theoretical models are relatively close to each other, with a variation in predicted values no greater than 10 ksi. The Sixth Edition PCI Design Handbook predicted the largest prestress losses, while the 1975 PCI recommended prestress loss model predicted the least amount of prestress loss. The larger amount of losses predicted in the handbook model can be expected since there was no allowance for time dependence. The model seemed to assume an average amount of creep occurred. The AASHTO prestress loss model predicted values near the handbook design model, although the values were more dispersed, as were the values of the 1975 PCI model. This is due to the ability of the 1975 PCI model and the AASHTO model to take into account the time dependency of creep.

The two experimental prestress loss determination model values are significantly different from each other. The crack initiation method predicted that losses which averaged 15 percent greater than the crack reopening method. Thus the effective prestress was determined to be 15 percent, on average, less for crack initiation tests than for crack reopening tests. The difference between the two measurements ranged from a 3 percent difference to a 33 percent difference between the two methods. This is a large difference in the experimental measurements of effective prestress force. Comparisons of the two experimental methods with the theoretical values are provided in Table 4.26.

The three theoretical prestress models are compared to the two experimental prestress models in Table 4.24. The values in Table 4.26 are presented as the ratio of the experimental loss prediction to the theoretical loss prediction. The crack initiation experimental measurement is seen to be consistently lower than all three prestress models. The crack initiation method ranges from 85 to 90 percent of the theoretical prestress models. In only three tests did the effective prestress for the crack initiation range less than 20 percent of the predicted values. However, these low values only brought the average value down 2 percent in each model. Therefore, it appears the crack initiation generally underestimates the effective prestress in the member. Crack reopening test data generally fit the theoretical prestress models well. With the exception of a few low and high values from individual beam end tests, all the data for each individual effective prestress test was within 10 percent of the model prediction. When all the effective prestress ratios are averaged, the percent difference between an individual theoretical model and the crack reopening value is between -1 and 4 percent. This is a very good correlation

for experimental data predicting prestress losses. Therefore, given a large enough body of data, the crack reopening test can accurately predict the effective prestress of a prestressed concrete beam.

Table 4.26 Summary of Prestress Losses

Beam Name	Crack Initiation			Crack Reopening		
	$f_{pe,Experimental}/f_{pe,PCI\ Handbook}$ (ksi)	$f_{pe,Experimental}/f_{pe,PCI\ 1975}$ (ksi)	$f_{pe,Experimental}/f_{pe,AASHTO}$ (ksi)	$f_{pe,Experimental}/f_{pe,PCI\ Handbook}$ (ksi)	$f_{pe,Experimental}/f_{pe,PCI\ 1975}$ (ksi)	$f_{pe,Experimental}/f_{pe,AASHTO}$ (ksi)
WT1A EE	0.66	0.63	0.66	0.76	0.73	0.77
WT1A WE	0.75	0.72	0.76	1.12	1.07	1.14
WT1B EE	0.85	0.80	0.85	1.00	0.95	1.00
WT1B WE	0.93	0.88	0.93	0.99	0.94	0.99
WT1C EE	0.86	0.81	0.84	1.08	1.02	1.07
WT1C WE	1.05	0.99	1.03	0.96	0.91	0.94
WT1D EE	0.85	0.80	0.83	0.97	0.91	0.95
WT1D WE	0.83	0.78	0.81	1.09	1.03	1.07
WT2A EE	1.00	0.95	0.99	0.97	0.93	0.97
WT2A WE	1.04	1.00	1.05	1.13	1.08	1.14
WT2B EE	0.95	0.91	0.95	1.08	1.03	1.07
WT2B WE	0.89	0.85	0.89	1.04	0.99	1.03
WT2C EE	0.96	0.93	0.98	1.04	1.00	1.06
WT2C WE	0.96	0.93	0.98	1.04	1.00	1.06
WT2D EE	0.88	0.84	0.89	0.97	0.93	0.98
WT2D WE	0.89	0.85	0.89	1.01	0.97	1.02
WT3A EE	0.93	0.87	0.89	1.15	1.08	1.11
WT3A WE	0.90	0.84	0.87	0.99	0.92	0.95
WT3B EE	0.88	0.84	0.89	1.36	1.29	1.36
WT3B WE	0.88	0.84	0.89	0.97	0.92	0.97
WT3C EE	0.87	0.81	0.83	0.99	0.92	0.94
WT3C WE	0.99	0.92	0.95	1.15	1.07	1.10
WT3D EE	0.90	0.83	0.85	1.06	0.99	1.01
WT3D WE	0.88	0.82	0.84	1.04	0.96	0.99
Average Ratio	0.90	0.85	0.89	1.04	0.99	1.03

4.3.4 Effect of Concrete Type on Prestress Loss Calculations

The concrete type appears to have an effect on the amount of prestress losses experimentally determined. Table 4.27 show the average effective prestress values determined by crack initiation and crack reopening for each concrete mix type, with the WT3B excluded from the S1CCM2 crack re-opening values since its effective prestress was measured larger than the initial prestress. The effective prestress for the S1CCM concrete mix appears to have 12 percent less prestress loss than the S1CRM mix for the crack initiation testing. The S1CCM2 mix has 6 percent fewer prestress losses than the S1CRM for the crack initiation testing. This trend is also seen in the crack reopening determined measurements. The S1CCM and S1CCM2 crack re-opening values are 4 and 6 percent larger than the S1CRM mix, respectively. The higher values of the effective prestress for the SCC mixes tend to show a lower creep and shrinkage effect in SCC mixes. To evaluate this observation further, the change in concrete surface strains for the transfer length members over time are investigated.

Table 4.27 Average Effective Prestress Comparison between Each Concrete Mix

Concrete Type	Initial Prestress (ksi)	Effective Prestress (ksi)		Effective Prestress Comparison		
		Initiation	Crack Re-opening		Initiation	Crack Re-opening
S1CRM	166	127	149	$f_{pe,S1CCM}/f_{pe,S1CRM}$	1.12	1.04
S1CCM	166	143	156	$f_{pe,S1CCM2}/f_{pe,S1CRM}$	1.06	1.06
S1CCM2	166	135	158	$f_{pe,S1CCM}/f_{pe,S1CCM2}$	1.06	0.99

The measured values of the concrete surface strains of the transfer length members at each time step were plotted versus the length of the member. Figure 4.12 shows a typical plot for the time variation of the concrete surface strain in the transfer length members. As was discussed in section 4.1.2, the average maximum strain (AMS) value, or the average value of the strain plateau, is required in order to find the transfer length. Analyzing the time variance of the AMS will give an indication of the increase in the strain by creep and shrinkage effects for each concrete mix. Table 4.28 shows the AMS values used in determining the transfer length for each concrete mix. The release AMS value will represent the initial elastic shortening strain of the

concrete member. Increases in the concrete surface strains at 7 days and 28 days are due to creep and shrinkage in the concrete and prestressing strand relaxation. Since the same prestressing strand was in each concrete member, only the creep and shrinkage characteristics of each concrete should vary.

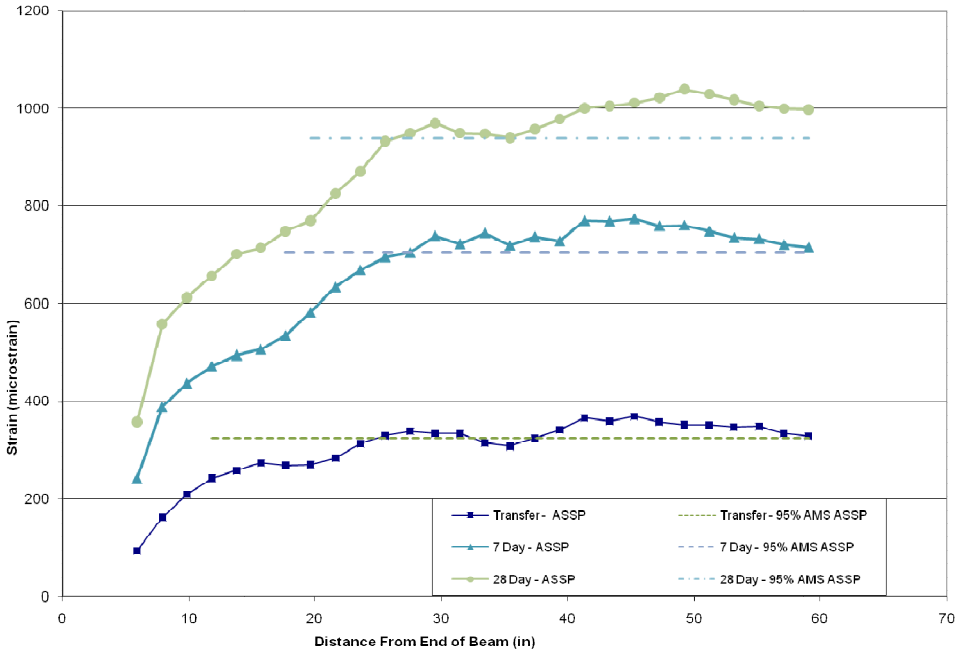

Figure 4.12 Typical Transfer Length Determination Plot for the Three Times Investigated

Table 4.28 Comparison of AMS Values with Time and Concrete Type

Concrete Type	$AMS_{7\ Day}/AMS_{Release}$	$AMS_{28\ Day}/AMS_{7\ Day}$	$AMS_{28\ Day}/AMS_{Release}$		S1CCM/ S1CRM	S1CCM2/ S1CRM	S1CCM/ S1CCM2
S1CRM	2.16	1.37	2.96	$AMS_{7\ Day}/AMS_{Release}$	1.12	0.97	1.15
S1CCM	2.41	1.44	3.47	$AMS_{28\ Day}/AMS_{7\ Day}$	1.05	1.04	1.01
S1CCM2	2.10	1.43	3.00	$AMS_{28\ Day}/AMS_{Release}$	1.17	1.01	1.16

As can be seen in Table 4.28, the S1CCM mix has the largest change in concrete strain with a 28 day AMS value nearly 3.5 times the release AMS value. The S1CRM and S1CCM 28 day AMS values are both approximately 3 times greater than the release AMS values.

Comparing the change in AMS values with the concrete types, it is seen in the transfer length testing that the S1CCM mix seems to have greater increases in strain than the S1CRM or the S1CCM2 mixes. This tends to show greater creep and shrinkage in the S1CCM mix than the other mixes. This contradicts the development length effective prestress loss measured value trend, which shows the S1CRM mix having more losses due to creep and shrinkage than the SCC mixes. Again, as was discussed in the section on transfer length comparison, the S1CCM member may not have been subjected as suddenly to the initial prestress force at release as the S1CRM and S1CCM2 member. The S1CCM2 member may have received the least gradual release of the three transfer length members. This could explain why there is such a large increase in the AMS value for the S1CCM mix. If the prestress force was not released as suddenly for the S1CCM member, then the change in strain may be greater over time, as is seen in the results.

It can be seen that there is no correlation between the development length prestress losses due to creep and shrinkage and the transfer length change in AMS for this research program. However, there is only one transfer length member for each mix, and therefore there may not be enough data present to truly present a correlation in either case. Therefore, the 24 development length tests are more reliable in comparing creep and shrinkage losses than the transfer length tests. It can then be gleamed from the development length test that creep and shrinkage losses for the two SCC mixes in this research are not larger than the conventional concrete mix.

5. SUMMARY, CONCLUSIONS, AND RECOMMENDATIONS

5.1 Summary

Three square prismatic transfer length members were cast and tested at the Winchester, VA plant of The Shockey Precast Group. In addition, twelve stud tee development length beams were cast at Shockey's precast plant and shipped to the Virginia Tech Structures and Materials Laboratory for testing. This research was conducted to evaluate the engineering properties of two potential self-consolidating concrete mixes and compare their properties to a current SPG conventional mix. This thesis pertains to the research performed for the Shockey Precast Group. The transfer and development length of self-consolidating concrete was investigated and compared to a conventional concrete mix. Additionally, prestress losses were experimentally measured and compared to theoretical models.

Transfer and development length members made of two separate SCC mixes and one conventional mix were tested. Transfer lengths were determined by measuring the concrete surface strain at the steel centroid before and after prestress release, 7 days after prestress release, and 28 days after prestress release. The change in the concrete surface strain was used to determine the transfer length at each time interval. The effect of time on transfer length was monitored for each mix. Development lengths were found from iterative load testing at each end of each beam. Flexural strengths of each mix were examined by comparing the ultimate moments each beam was able to attain with the ACI prediction of the ultimate moment.

Prestress losses were experimentally determined by flexural testing with crack initiation and crack reopening tests. The effective prestress in each beam was calculated by determining the load at which initial cracking occurs and by determining the load at which the initial crack will reopen. The measured values of the effective prestress were compared with three theoretical prestress loss models, the sixth edition PCI Handbook model, the 1975 PCI Committee on Prestress Losses model, and the AASTHO model.

5.2 Conclusions

Transfer lengths were measured for both ends of each transfer length test member. The following conclusions were drawn from limited testing of the transfer length tests:

1. All initial transfer lengths for each concrete mix were less than ACI and AASHTO code minimums.

2. The transfer lengths of each mix increased with time. The amount of increase with time varied amongst mixes. The conventional mix had the least change in transfer length, with only a 13 percent increase over the testing period. The S1CCM2 mix had a 20 percent increase over the 28 days and the S1CCM mix had a 56 percent increase in the transfer length.
3. Only one mix, the S1CCM2 mix, eventually surpassed the ACI code predicted value of the transfer length by approximately 20 percent. Since the ACI transfer length equation is based on finding an average transfer length value for all present data, a transfer length value 20 percent above the code predicted value is not uncommon. All three mixes had final transfer lengths below the AASHTO code prediction, which shows that the transfer length of each mix may be acceptable.
4. Measurement of concrete surface strains and the use of the 95 percent average maximum strain plateau method were effective means of determining the transfer length.

Development length results were determined from iterative load testing. A total of 24 tests were performed, with 8 tests completed on each mix type. The following conclusions have been drawn from these tests:

1. The self-consolidating concrete mixes each had development lengths well below ACI and AASHTO predicted values.
2. The SCC mixes had development lengths approximately 20 percent less than ACI and AASHTO predictions. This large difference in tested and predicted values suggests the SCC mixes have excellent bonding characteristics with 9/16 in. diameter strands. Additionally, the shorter development length may be due to a short flexural bond length.
3. A comparison of development lengths for the SCC mixes and for a conventional mix could not be made. The conventional concrete mix did not have repeating test results and thus a “developed” length was not bracketed.

The flexural strength of each mix was experimentally determined during the iterative load testing procedure. The results of flexural load testing are summarized below:

1. Twenty-two of twenty-four load tests reached loads which exceeded the predicted capacity of the members. The only two tests which did not reach the predicted

capacity failed in strand slippage and were within four percent of the predicted values.

2. The conventional concrete mix was able to sustain the largest bending moments, having an average flexural capacity 14 percent larger than code predicted values.
3. Each self-consolidating concrete mix had an average flexural capacity which exceeded or met the predicted values, even when a strand bond failure occurred.
4. The SCC concrete mixes had slightly less strength than the conventional concrete mix. However, the difference was not significant and all mix types had average strength values greater than the ACI model predicted.

Prestress losses were measured experimentally and compared to three separate theoretical models. The following conclusions were drawn from prestress loss predictions and measurements:

1. The values predicted by each of the three theoretical models were very similar. This was an interesting finding since the sixth edition PCI design Handbook does not take the time from prestress release to loading into account, while the other two models do.
2. The prestress loss values measured by the crack initiation tests were typically 10 to 15 percent more than the theoretical models.
3. Crack reopening measurements of the effective prestress were very close to the values obtained from the three theoretical models. The difference between measured values and calculated values ranged from one percent below to four percent above. This suggests crack reopening tests are a valid means to determine the effective prestress in a pretensioned concrete member.
4. The conventional concrete mix experienced greater prestress losses than both SCC mixes experienced. This trend may indicate less creep and shrinkage losses for SCC than for the conventional concrete. Comparing this notion to the change in concrete surface strains at the time steps in the transfer length members did not show the same correlation between creep and shrinkage losses and concrete mix type. However, since there were only three transfer length members, one for each concrete mix, the prestress losses determined in the development length testing are

more reliable than the transfer length testing results. Therefore, it appears to be less creep and shrinkage losses in SCC mixes than in the conventional concrete mix

5.3 Recommendations for Further Research

Little research has been done to measure the transfer length and development length of self-consolidating pretensioned concrete members. The test results from this project indicate the bonding properties of SCC with prestressing strand are comparable to the bonding characteristics of conventional concrete. However, this research was limited to two particular SCC mixes and one conventional mix. Further research is necessary to evaluate these properties in a larger variety of SCC mix designs.

Additionally, the cross sections used in these tests were relatively small compared to structural members used in traditional practice. The stub tee cross section is not a typical structural cross section. Further research should be done to evaluate the transfer length, development length, flexural strength, and ductility characteristics of SCC with scale structural members used in practice.

Experimental measurements of prestress losses by crack reopening tests seemed to give reliable results. Further research should be done to confirm the ability of crack reopening tests to affectively predict prestress losses.

REFERENCES

American Association of State and Highway Transportation Officials (AASHTO). (2006). *AASHTO LRFD Bridge Design Specifications*, Third Edition, Washington, D.C.

American Concrete Institute (ACI). (2005). *Building Code Requirements for Structural Concrete and Commentary*, Committee 318, Farmington Hills, Michigan.

Baran, E., Shield, C.K., & French, C.E. (2005) "A Comparison of Methods for Experimentally Determining Prestress Losses in Pretensioned Prestressed Concrete Girders." *Ned H. Burns Symposium on Historic Innovations in Prestressed Concrete,* American Concrete Institute, Farmington Hills, Michigan.

Barnes, R. W., Grove, J. W., & Burns, N. H. (2003) "Experimental Assessment of Factors Affecting Transfer Length." *ACI Structural Journal*, 100(6), 740-748.

Buckner, C. D. (1995). "A Review of Strand Development Length for Pretensioned Concrete Members." *PCI Journal*, 40(2), 84-105.

Chan, Y., Chen, Y., & Liu, Y. (2003). "Effect of Consolidation on Bond of Reinforcement in Concrete of Different Workabilities." *ACI Materials Journal,* 100 (4), 294-301.

Druta, C. (2003). "Tensile Strength and Bonding Characteristics of Self-Compacting Concrete." M.S. Thesis, Louisiana State University and Agricultural and Mechanical College, Baton Rouge, Louisiana.

Girgis, A. M., & Tuan, C. Y. (2005). "Bond Strength and Transfer Length of Pretensioned Bridge Girders Cast With Self-Consolidating Concrete." *PCI Journal*, 50(6), 72-87.

Hamilton, H. R., Labonte, T., &Ansley, M.H. (2005) "Behavior of Pretensioned Type II AASHTO Girders Constructed with Self-Consolidating Concrete." *Ned H. Burns Symposium on Historic Innovations in Prestressed Concrete,* American Concrete Institute, Farmington Hills, Michigan.

Hodges, H. T. (2006). "Top Strand Effect and Evaluation of Effective Prestress in Prestressed Concrete Beams." M.S. Thesis, Virginia Polytechnic Institute and State University, Blacksburg, Virginia.

Nassar, A. J. (2002). "Investigation of Transfer Length, Development Length, Flexural Strength, and Prestress Loss Trend in Fully Bonded High Strength Lightweight Prestressed Girders." M.S. Thesis, Virginia Polytechnic Institute and State University, Blacksburg, Virginia.

Natio, C. J., Parent, G., & Brunn, G. (2006). "Performance of Bulb-Tee Girders Made with Self-Consolidating Concrete." *PCI Journal*, 51(6), 72-85.

Nilson, A. H. (1987). *Design of Prestressed Concrete*, Second Edition, John Wiley & Sons, New York.

Martin, L. D. & Perry, C.J., Editors. (2004) *PCI Design Handbook: Precast and Prestressed Concrete.* 6th Edition, Chicago.

Precast/Prestressed Concrete Institute (PCI) Committee on Prestressed Losses (1975). "Recommendation for Estimating Prestress Losses." *PCI Journal*, 20(4), 43-75.

Russel, B. W., & Burns, N. H. (1996). "Measured Transferred Lengths of 0.5 and 0.6 in. Strands in Pretensioned Concrete." *PCI Journal*, 41(5), 44-65.

Schindler, A. K. et al. (2007). "Properties of Self-Consolidating Concrete for Prestressed Members." *ACI Materials Journal*, 104(1), 53-61.

Shahawy, M. (2001). "A Critical Evaluation of the AASHTO Provisions for Strand Development Length of Prestressed Concrete Members." *PCI Journal*, 46(4), 94-117.

Tabatabai, H., & Dickson, T. J. (1993). "The History of the Prestressing Strand Development Length Equation." *PCI Journal*, 38(6), 64-75.

APPENDIX A Concrete Material Test Data

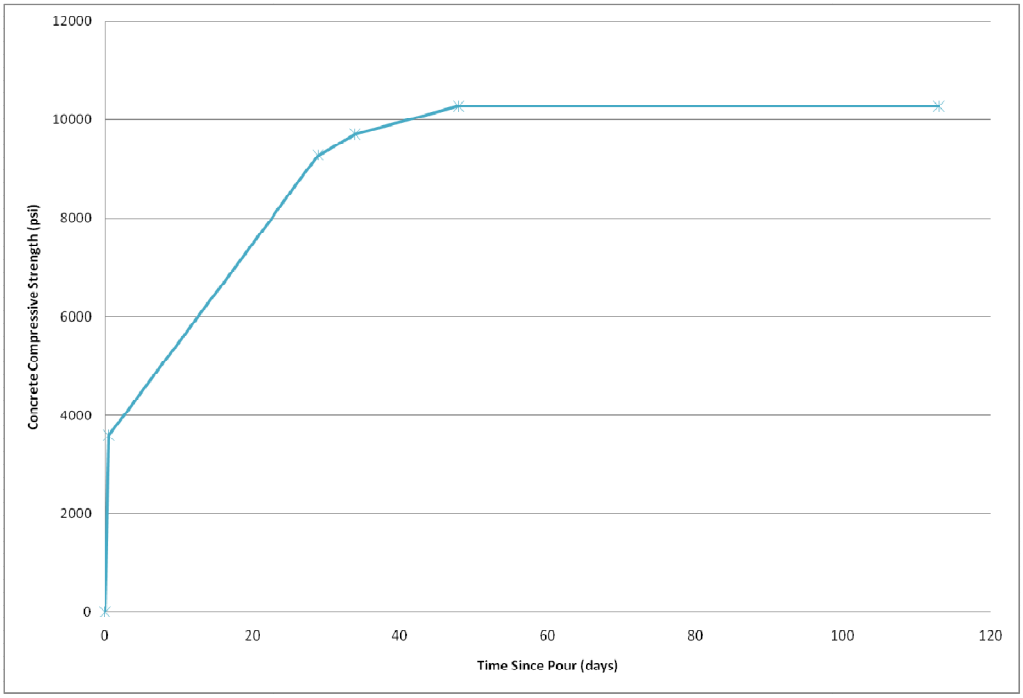

Figure A.1 S1CRM Concrete Strength Gain

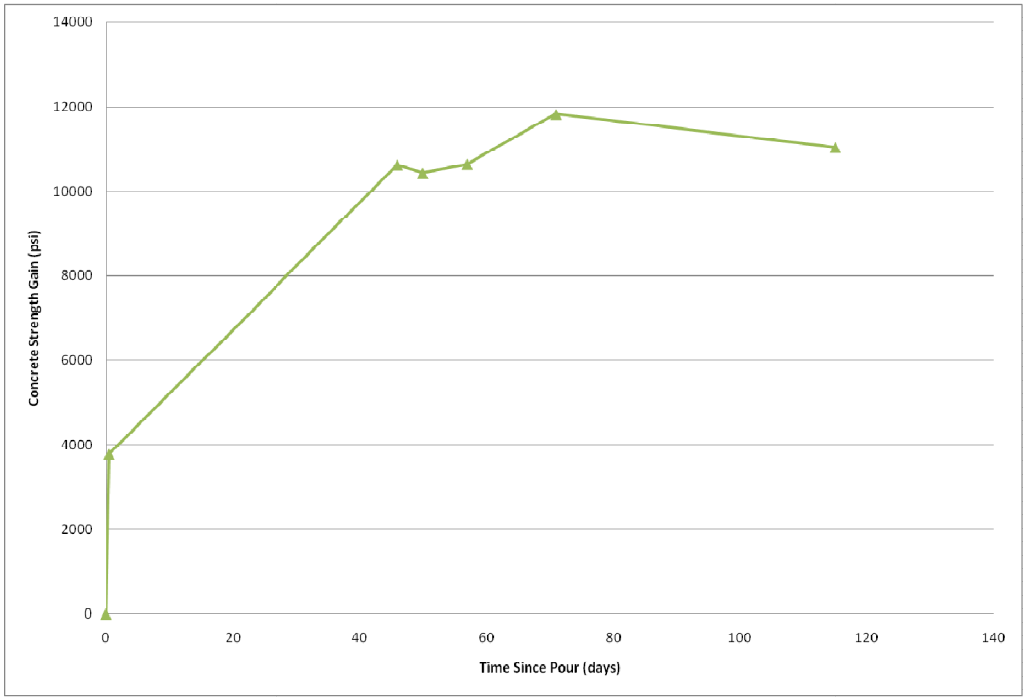

Figure A.2 S1CCM Concrete Strength Gain

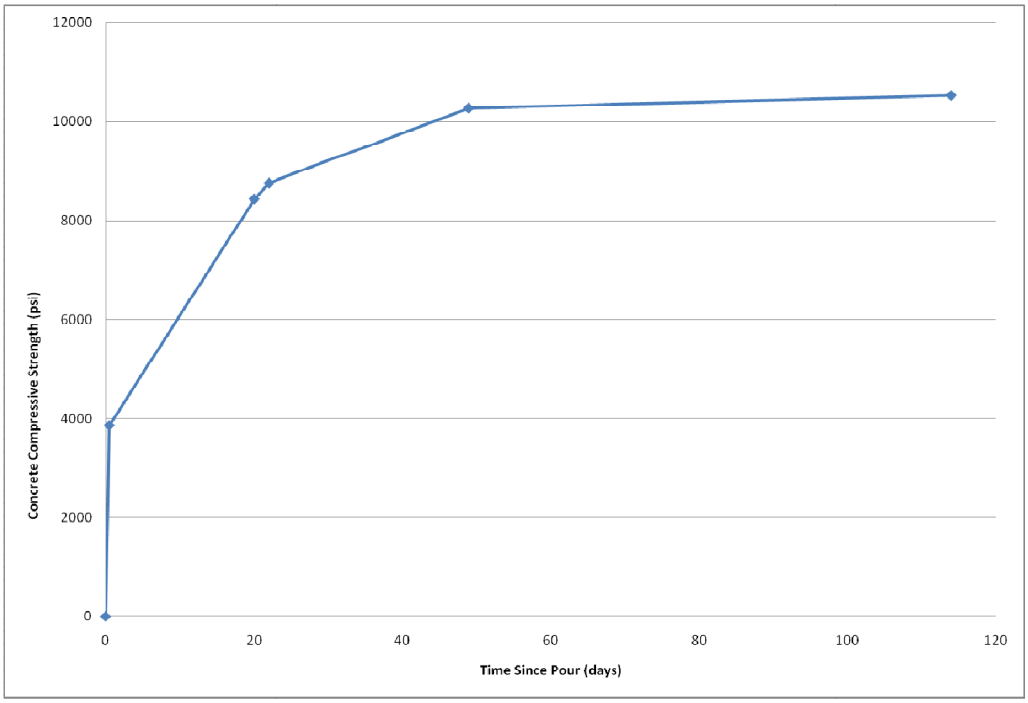

Figure A.3 S1CCM2 Concrete Strength Gain

Table A.1 Initial Concrete Cylinder Test Results

Date:	Concrete Type	Compressive Strength f'c (psi)
7/27/2006	S1CRM	3580
7/25/2006	S1CCM	3779
7/26/2006	S1CCM2	3858

Table A.2 Final Concrete Cylinder Test Results for S1CRM

Time		Compressive Strengths	Split Tensile Strengths	Modulus of Elasticity
Date:	Days	f'_c (psi)	f_t (psi)	E_c (ksi)
8/25/2006	29	9,708	895	5677
8/25/2006		8,992		
8/25/2006		9,151		
8/30/2006	34	9,549	846	5034
8/30/2006		9,868		
9/13/2006	48	10,584	855	4910
9/13/2006		9,947		
11/27/2006	113	10,265	895	5115

Table A.3 Final Concrete Cylinder Test Results for S1CCM

Time		Compressive Strengths	Split Tensile Strengths	Modulus of Elasticity
Date:	Days	f'_c (psi)	f_t (psi)	E_c (ksi)
9/4/2006	46	11,141	836	5,347
9/4/2006		10,106		
9/8/2006	50	10,345	895	5,964
9/8/2006		10,504		
9/15/2006	57	10,345	915	5,731
9/15/2006		10,942		
9/29/2006	71	11,220	1,015	5,903
9/29/2006		12,414		
11/17/2006	115	10,902	895	5,229
11/17/2006		10,504		
11/17/2006		11,698		

Table A.4 Final Concrete Cylinder Test Results for S1CCM2

Time		Compressive Strengths	Split Tensile Strengths	Modulus of Elasticity
Date:	Days	f'_c (psi)	f_t (psi)	E_c (ksi)
8/15/2006	20	8,435		
8/17/2006	22	8,913	846	4352
8/17/2006		8,594		
9/13/2006	49	10,265	855	4608
11/17/2006	114	10,186	826	4661
11/17/2006		10,504		
11/17/2006		10,345		
11/17/2006		10,663		
11/17/2006		10,504		
11/17/2006		10,902		

APPENDIX B Strain Profiles for Transfer Length

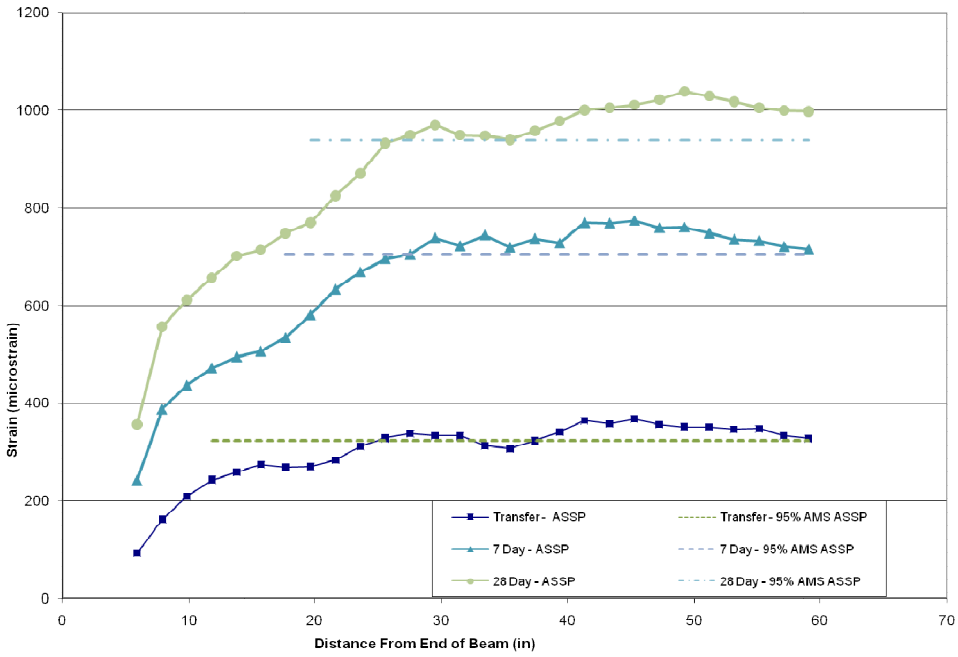

Figure B.1 Strain Profile for S1CRM (North End)

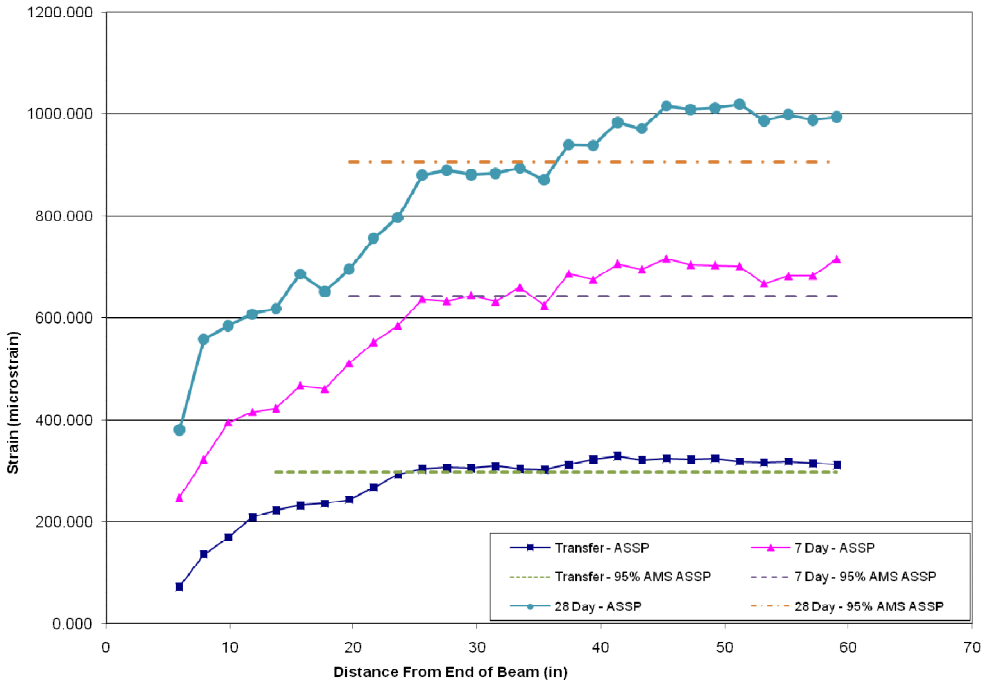

Figure B.2 Strain Profile for S1CRM (South End)

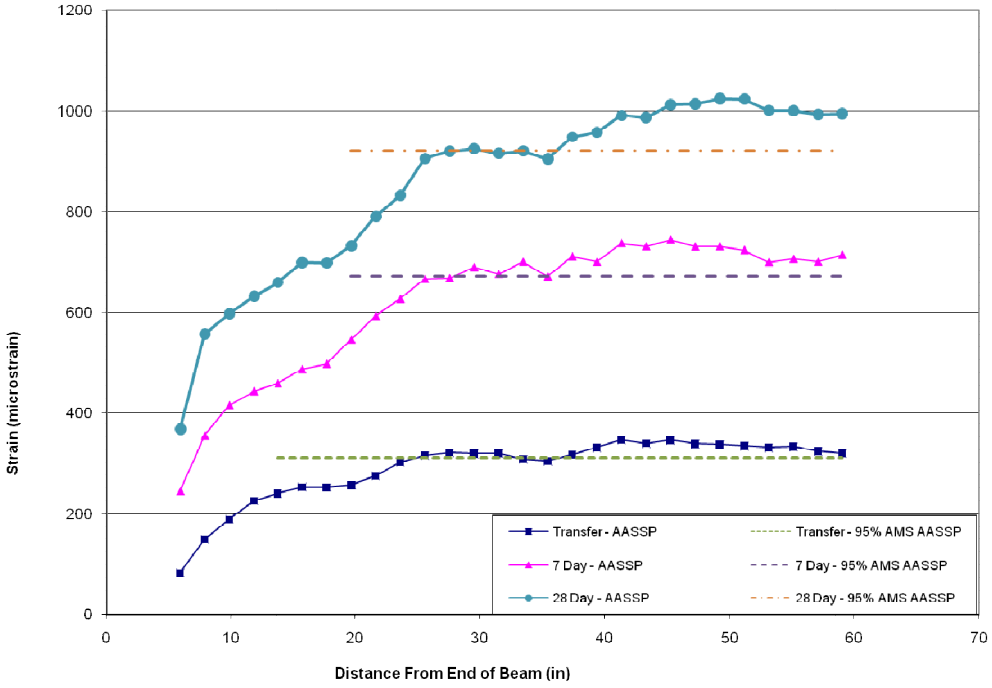

Figure B.3 Strain Profile for S1CRM (AASSP)

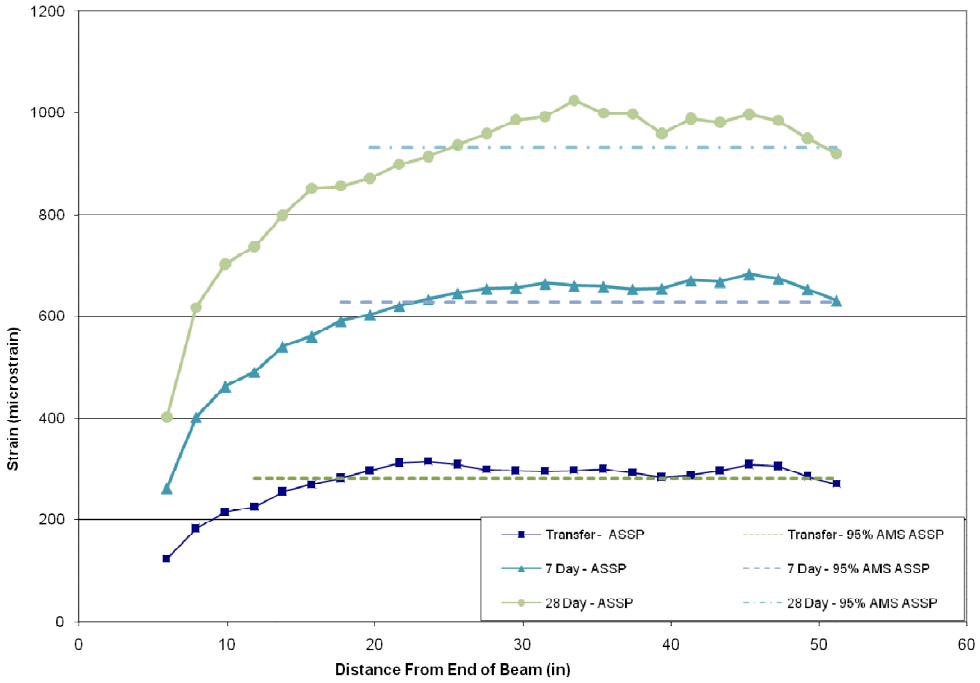

Figure B.4 Strain Profile for S1CCM (North End)

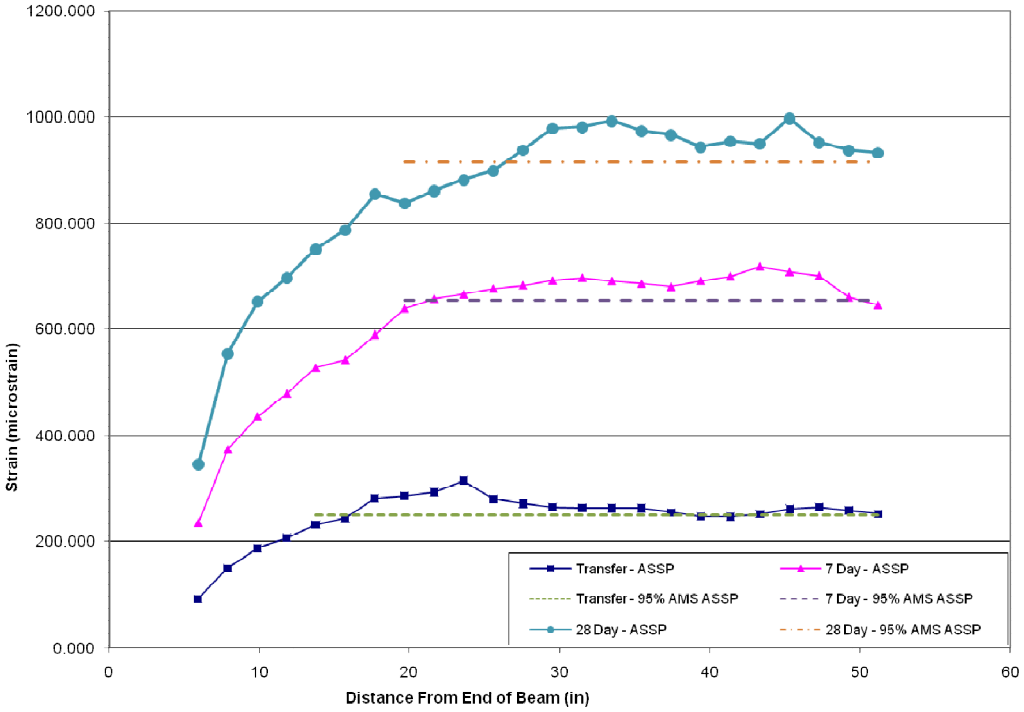

Figure B.5 Strain Profile for S1CCM (South End)

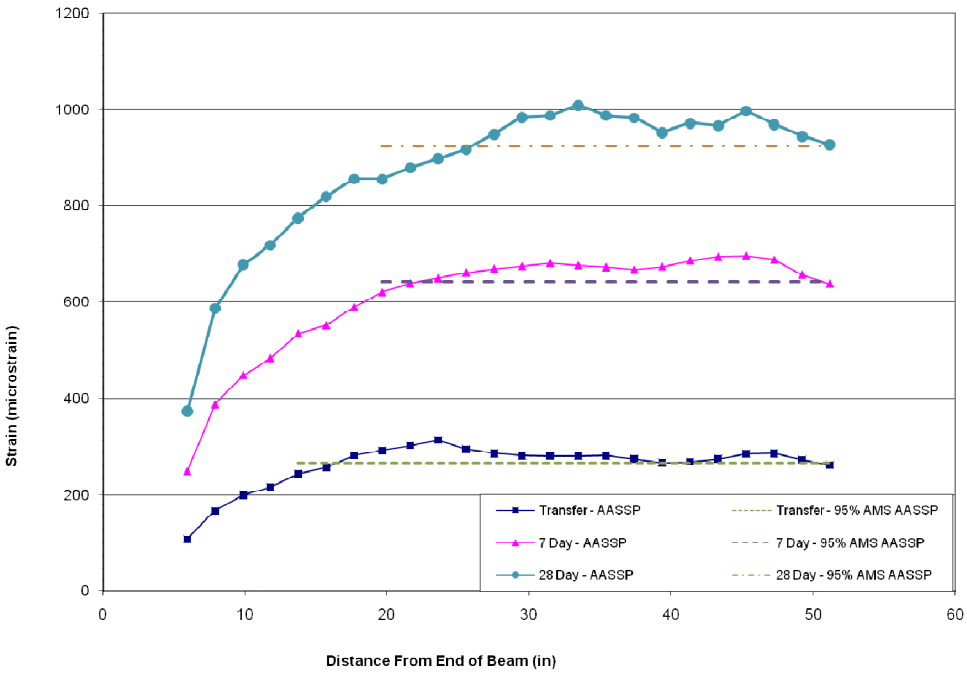

Figure B.6 Strain Profile for S1CCM (AASSP)

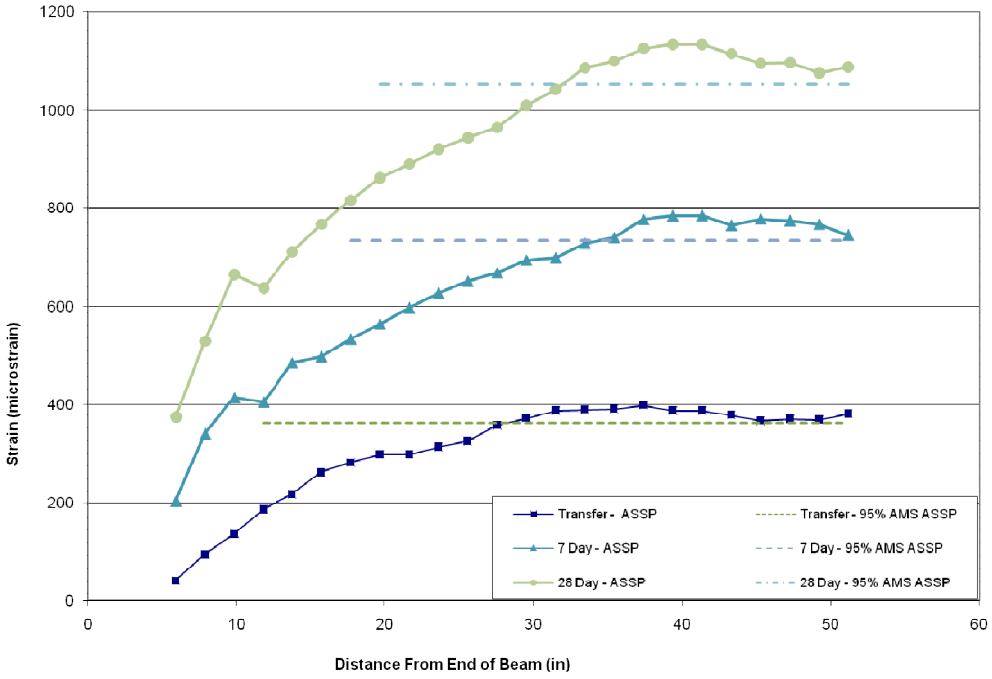

Figure B.7 Strain Profile for S1CCM2 (North End)

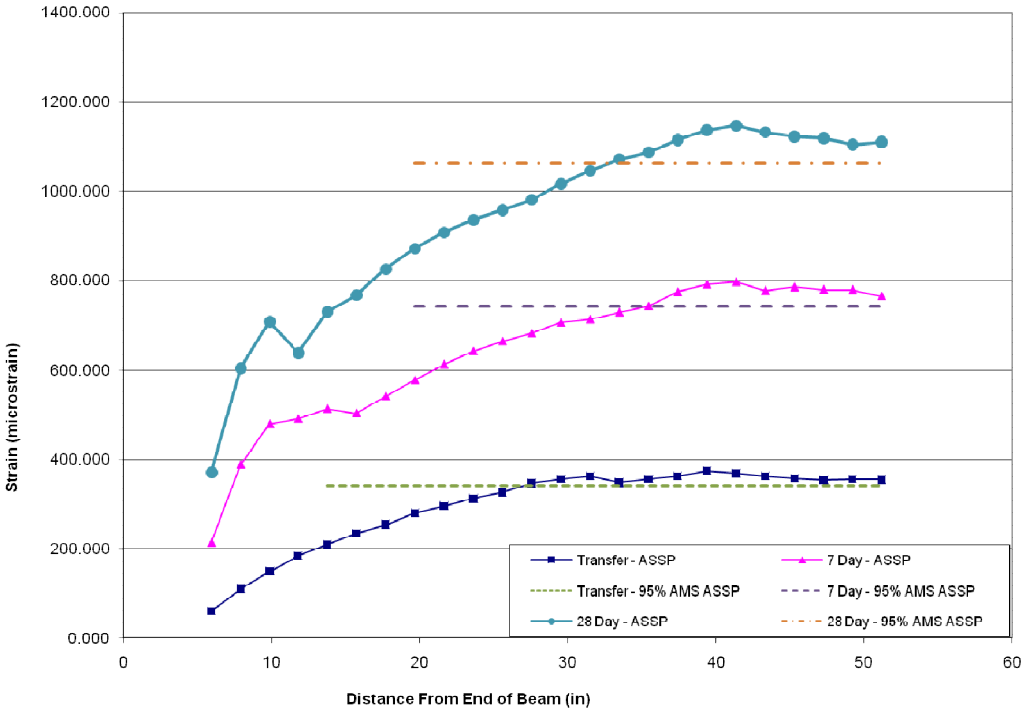

Figure B.8 Strain Profile for S1CCM2 (South End)

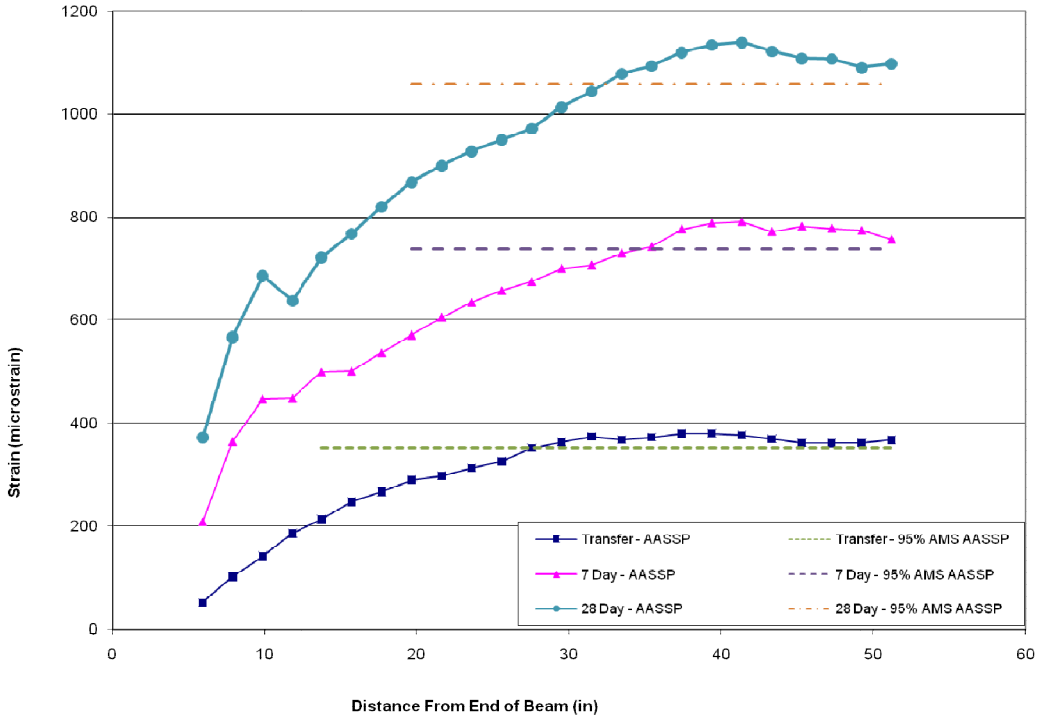

Figure B.9 Strain Profile for S1CCM2 (AASSP)

APPENDIX C Moment vs. Deflection and Moment vs. Strand Slip Plots

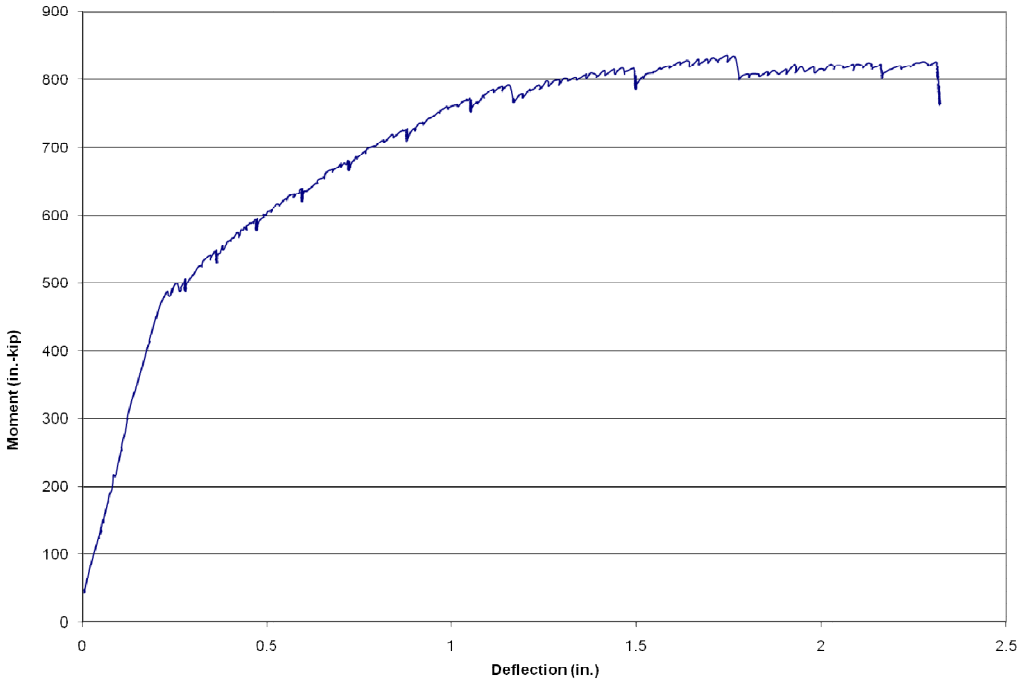

Figure C.1 Moment vs. Deflection for WT1A EE

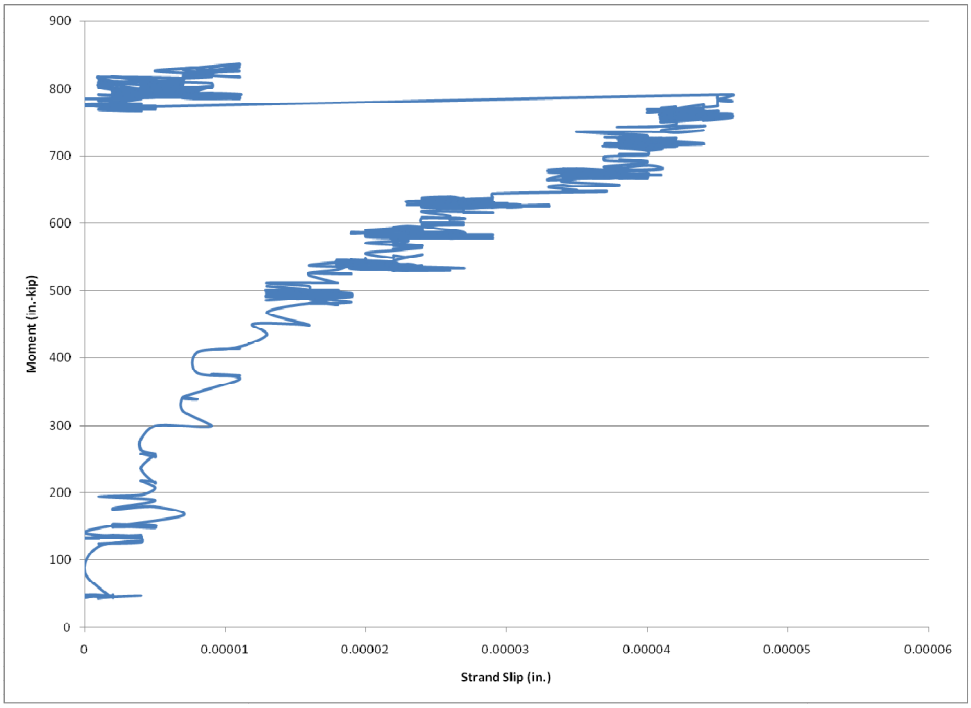

Figure C.2 Moment vs. Strand Slip for WT1A EE

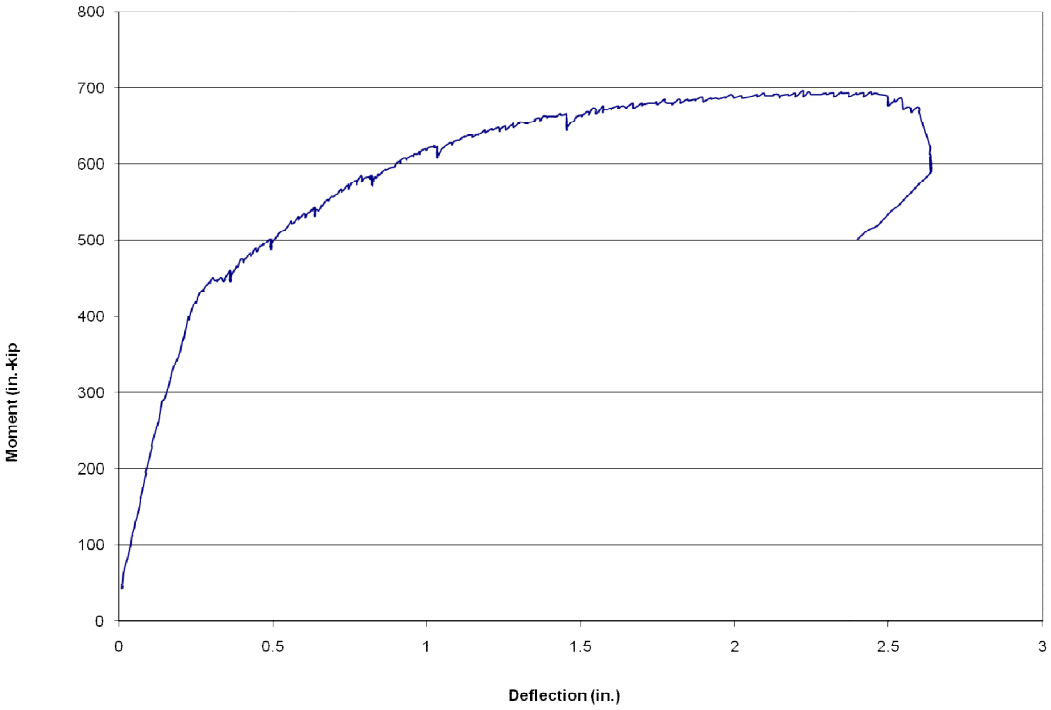

Figure C.3 Moment vs. Deflection for WT1A WE

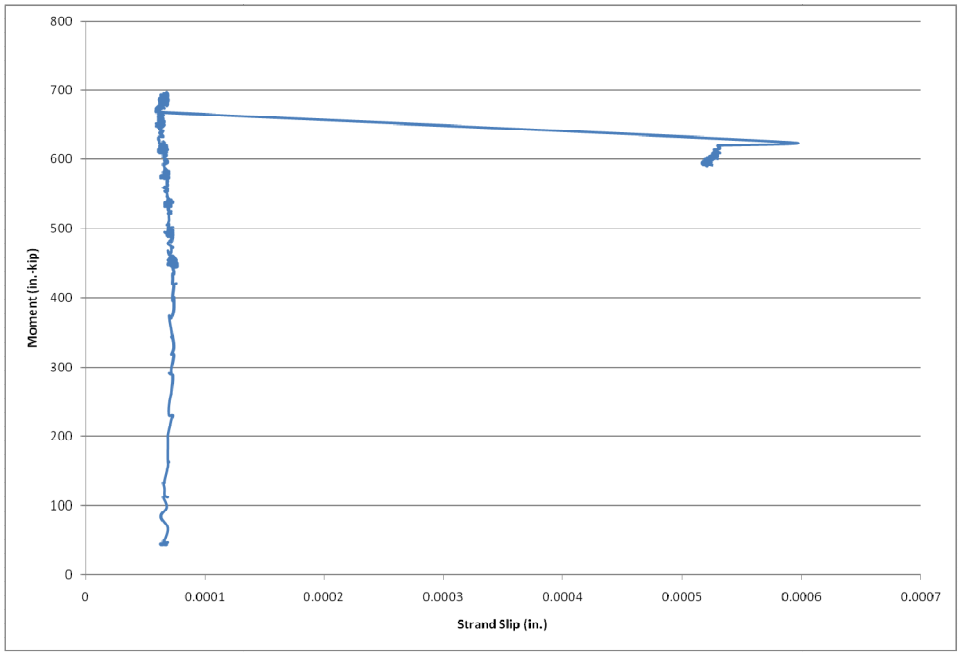

Figure C.4 Moment vs. Strand Slip for WT1A WE

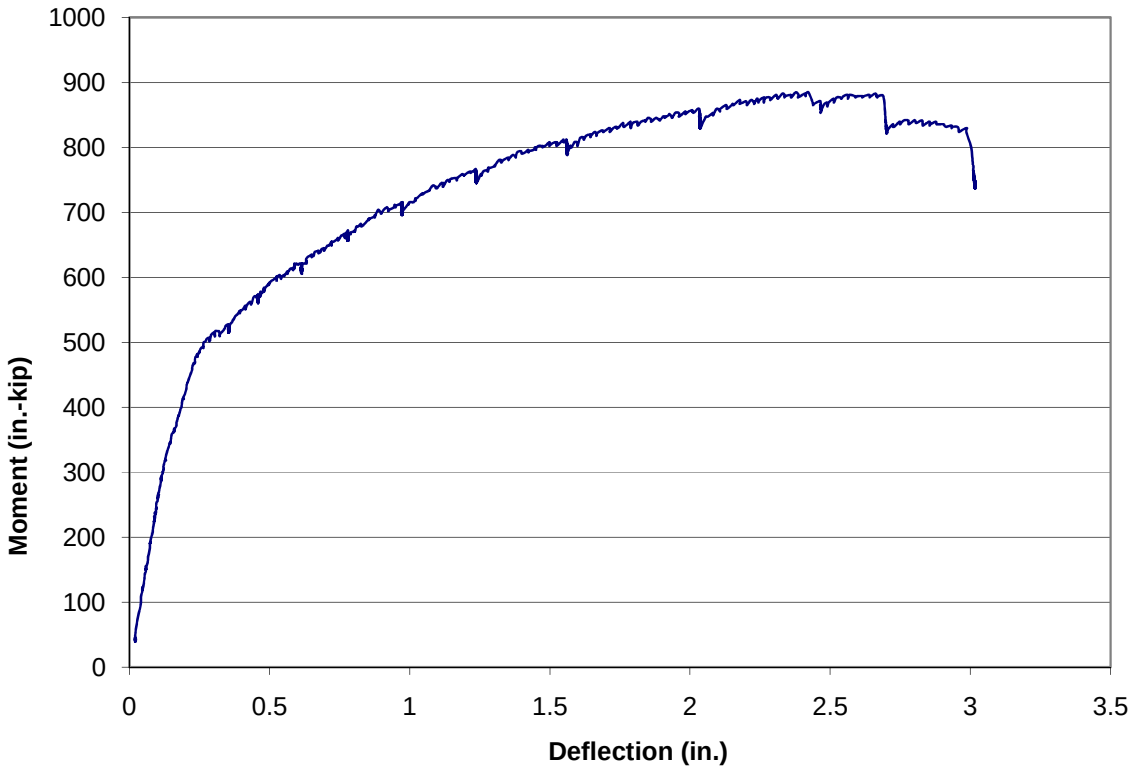

Figure C.5 Moment vs. Deflection for WT1B EE

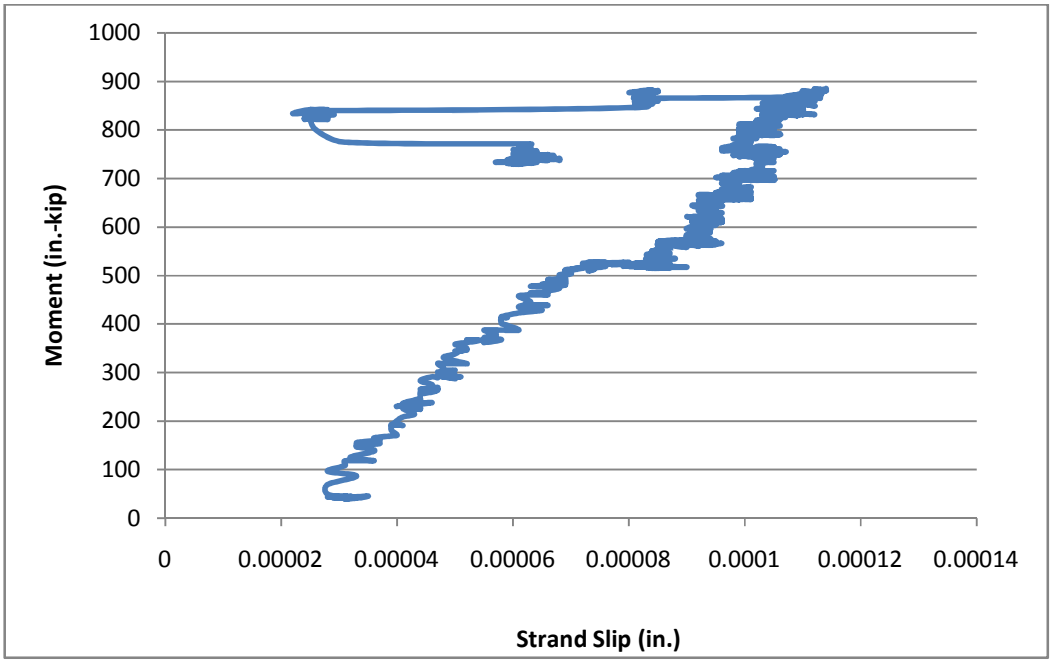

Figure C.6 Moment vs. Strand Slip for WT1B EE

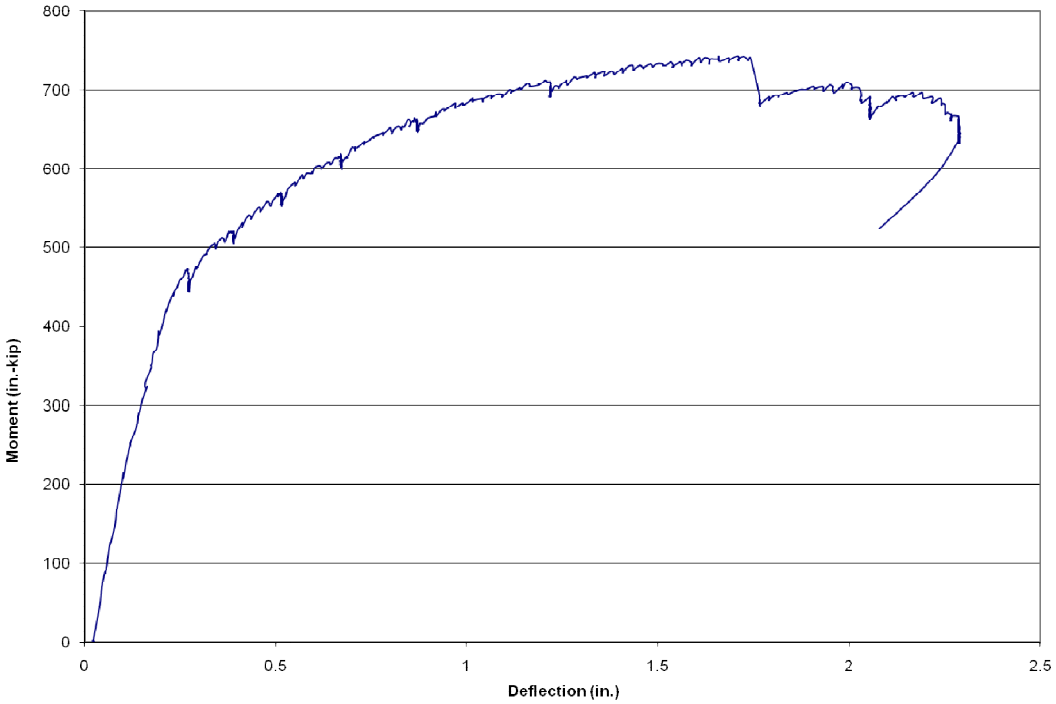

Figure C.7 Moment vs. Deflection for WT1B WE

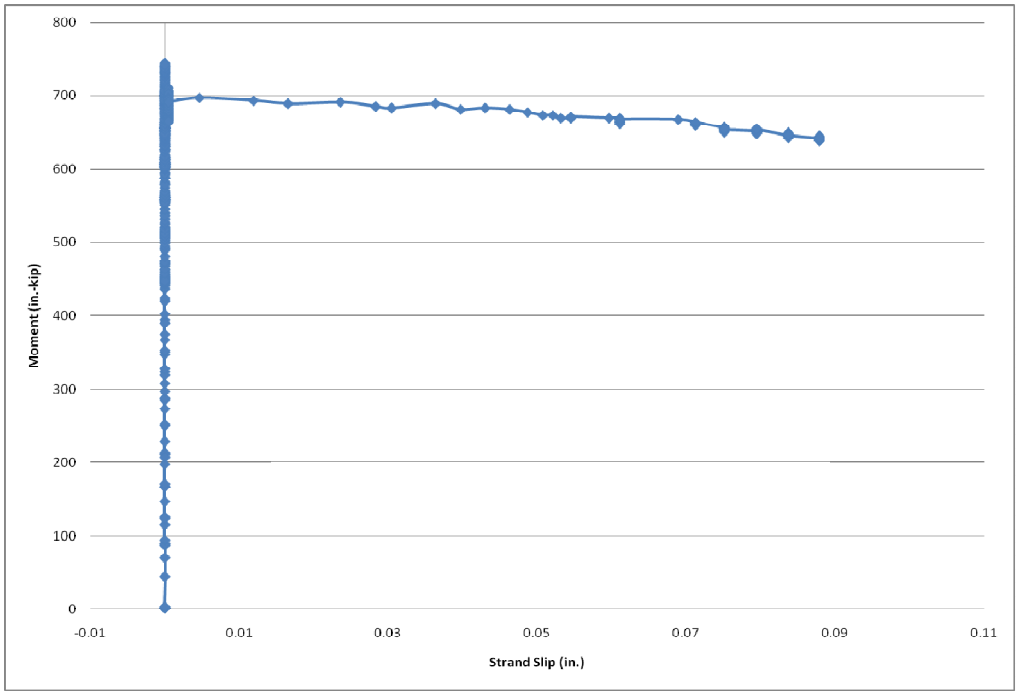

Figure C.8 Moment vs. Strand Slip for WT1B WE

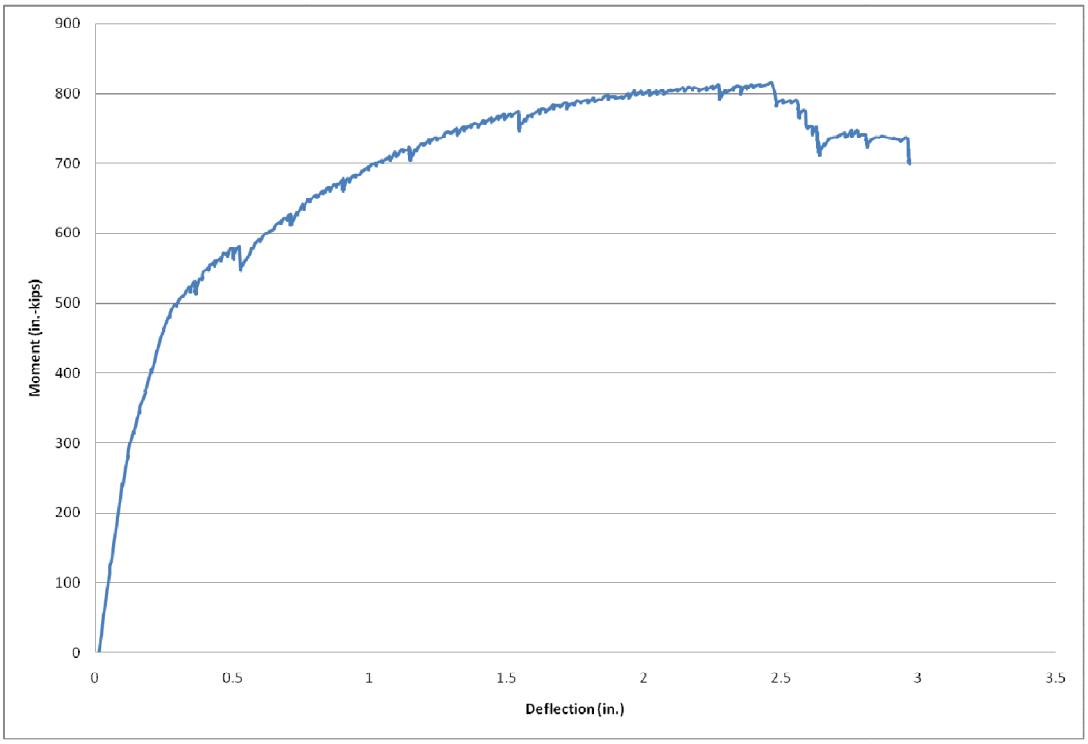

Figure C.9 Moment vs. Deflection for WT1C EE

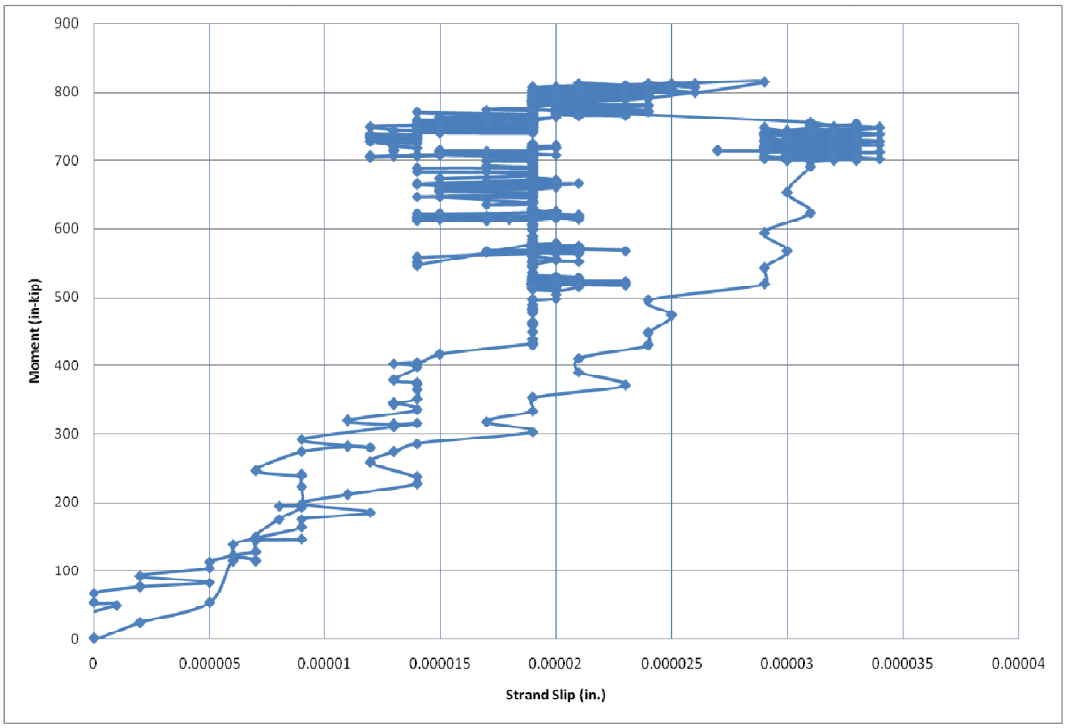

Figure C.10 Moment vs. Strand Slip for WT1C EE

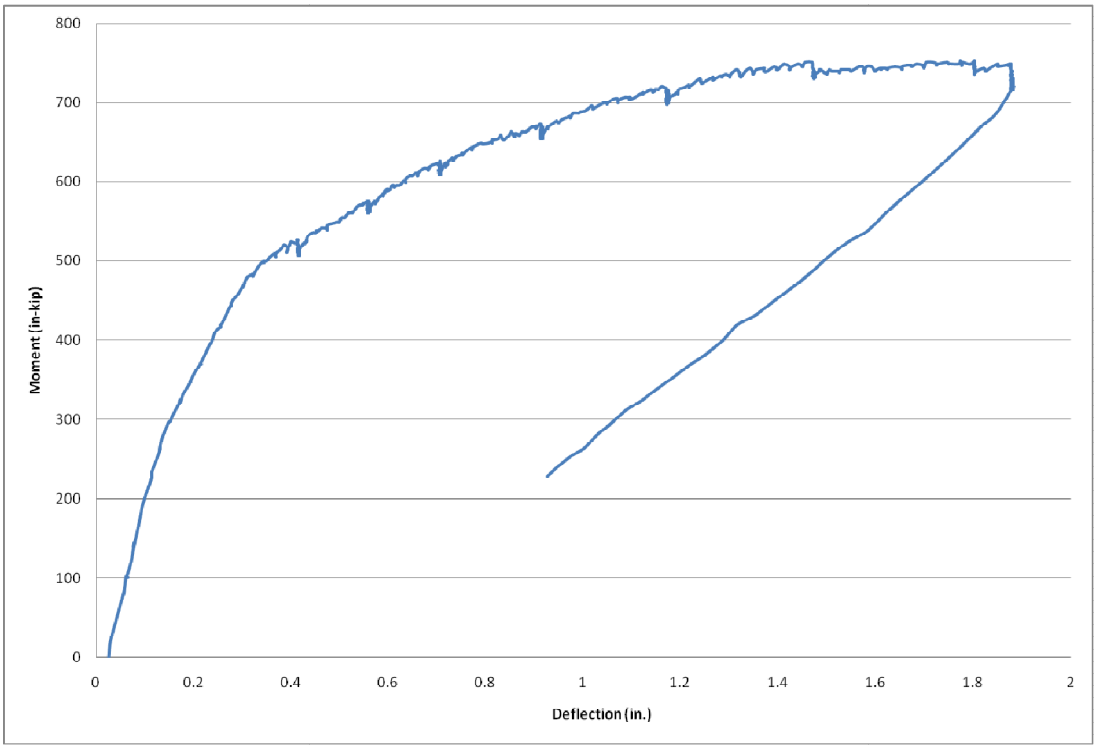

Figure C.11 Moment vs. Deflection for WT1C WE

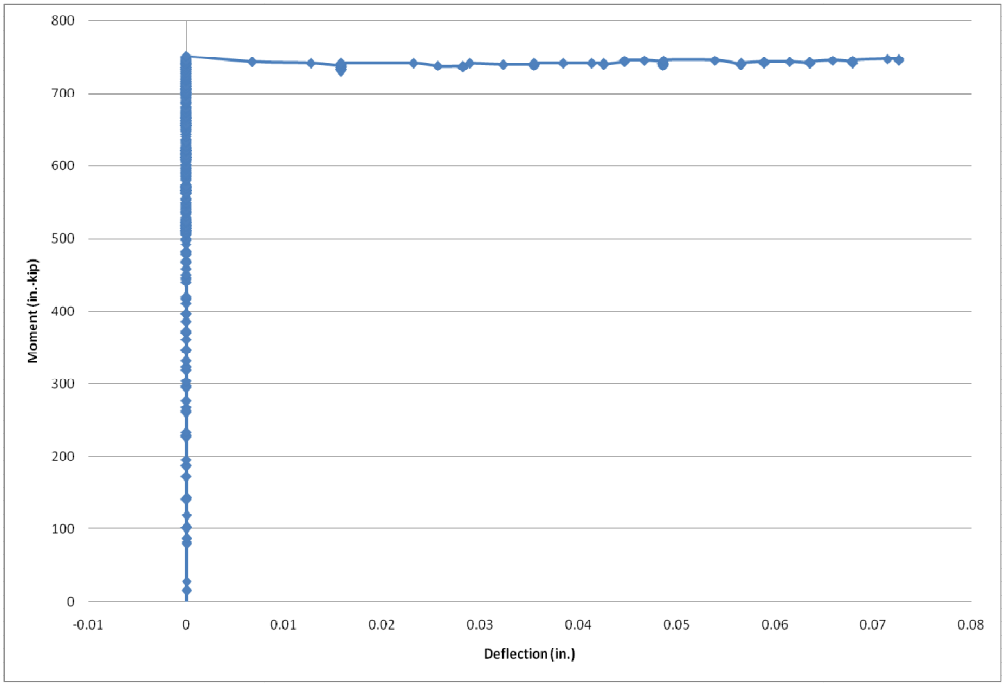

Figure C.12 Moment vs. Strand Slip for WT1C WE

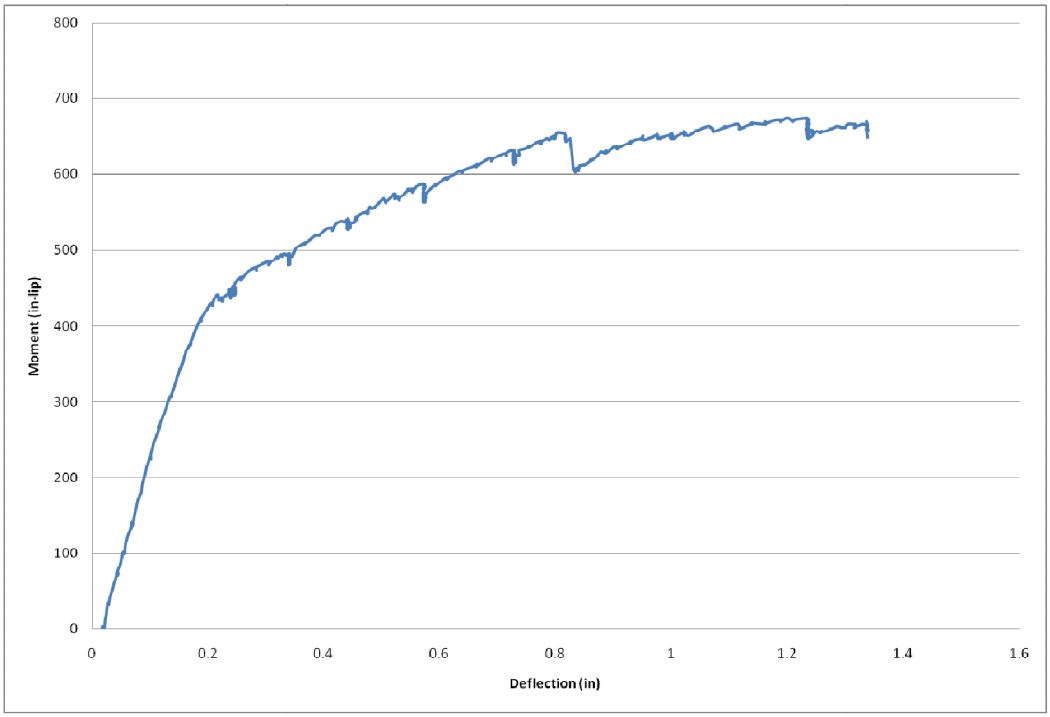

Figure C.13 Moment vs. Deflection for WT1D EE

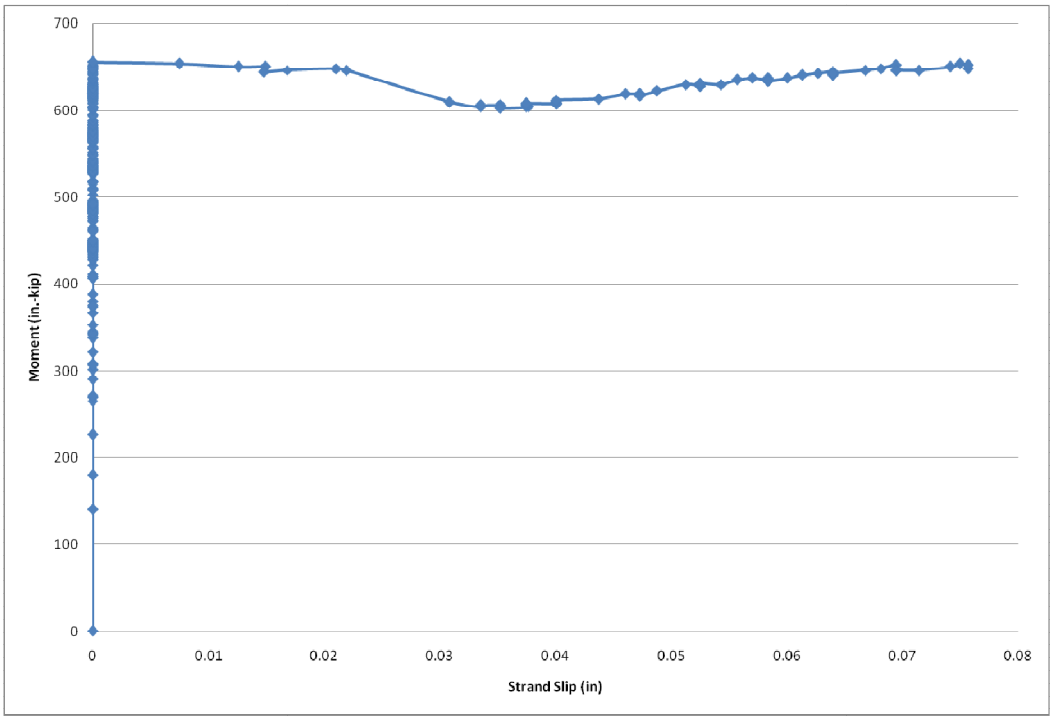

Figure C.14 Moment vs. Strand Slip for WT1D EE

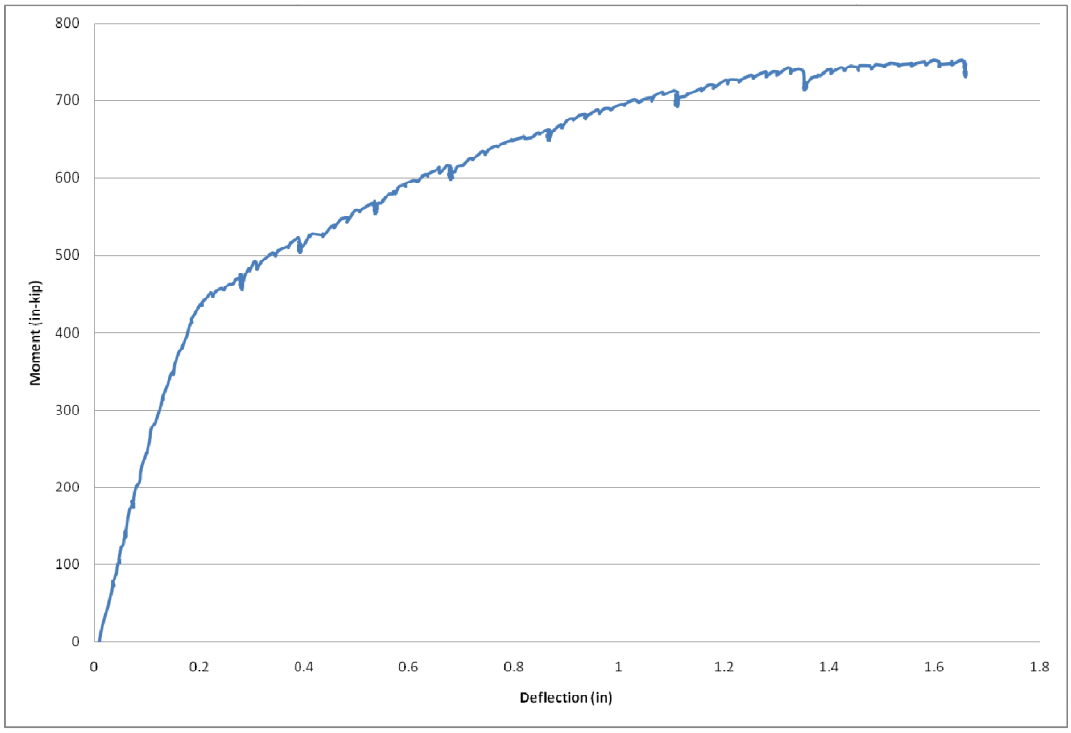

Figure C.15 Moment vs. Deflection for WT1D WE

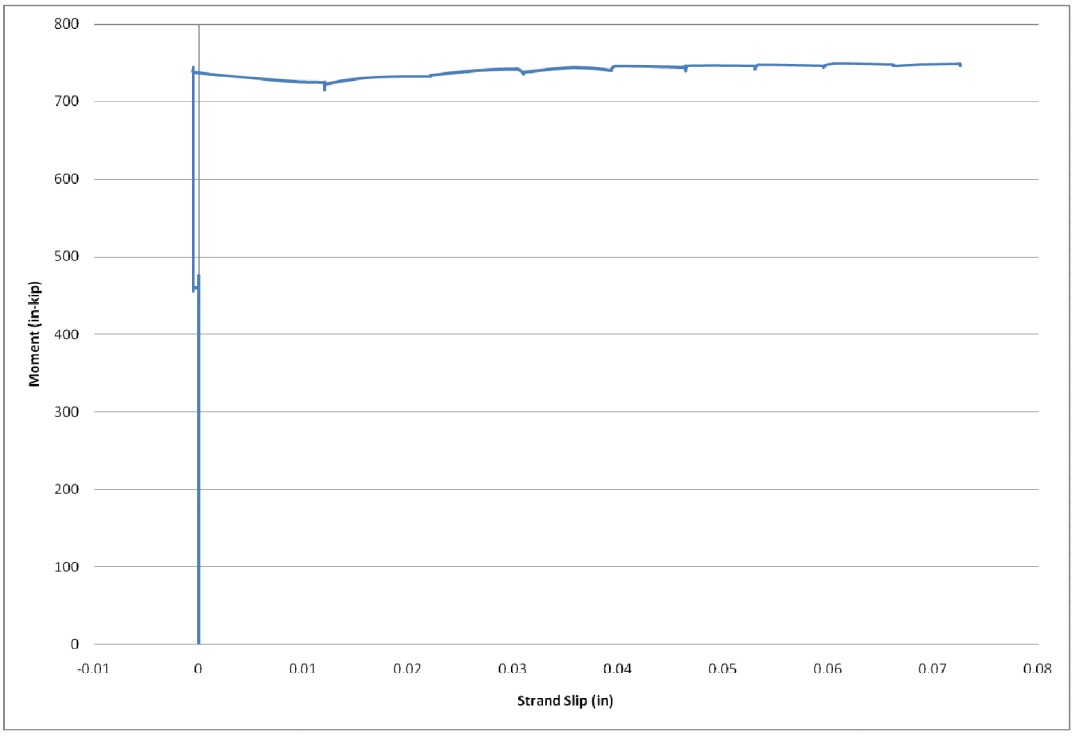

Figure C.16 Moment vs. Strand Slip for WT1D WE

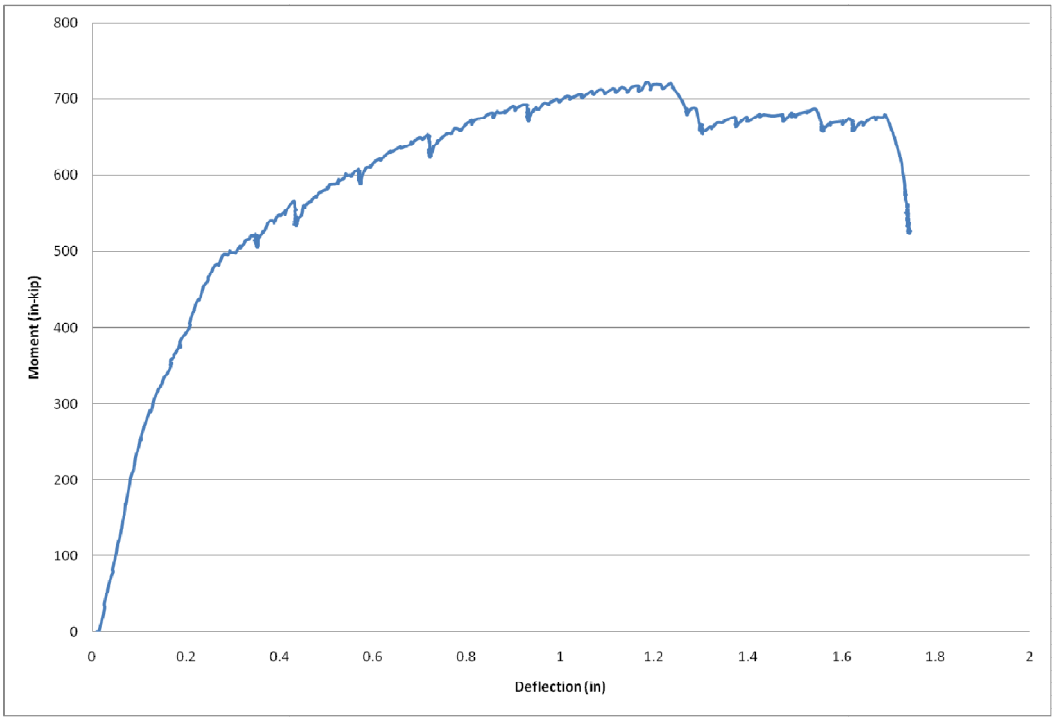

Figure C.17 Moment vs. Deflection for WT2A EE

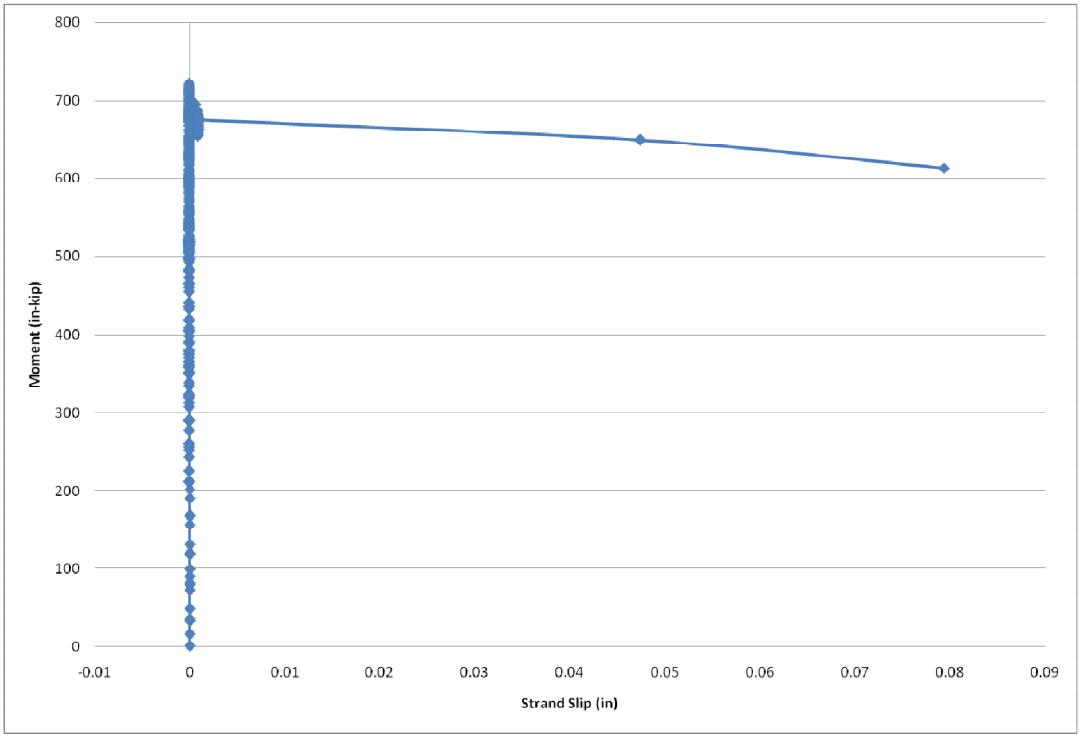

Figure C.18 Moment vs. Strand Slip for WT2A EE

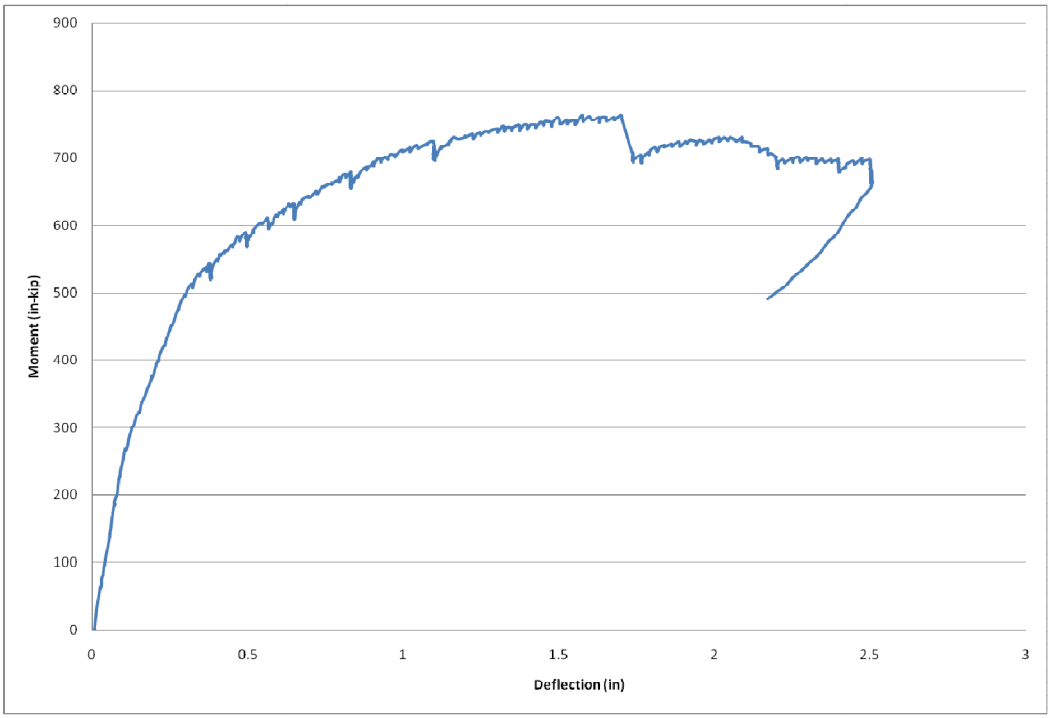

Figure C.19 Moment vs. Deflection for WT2A WE

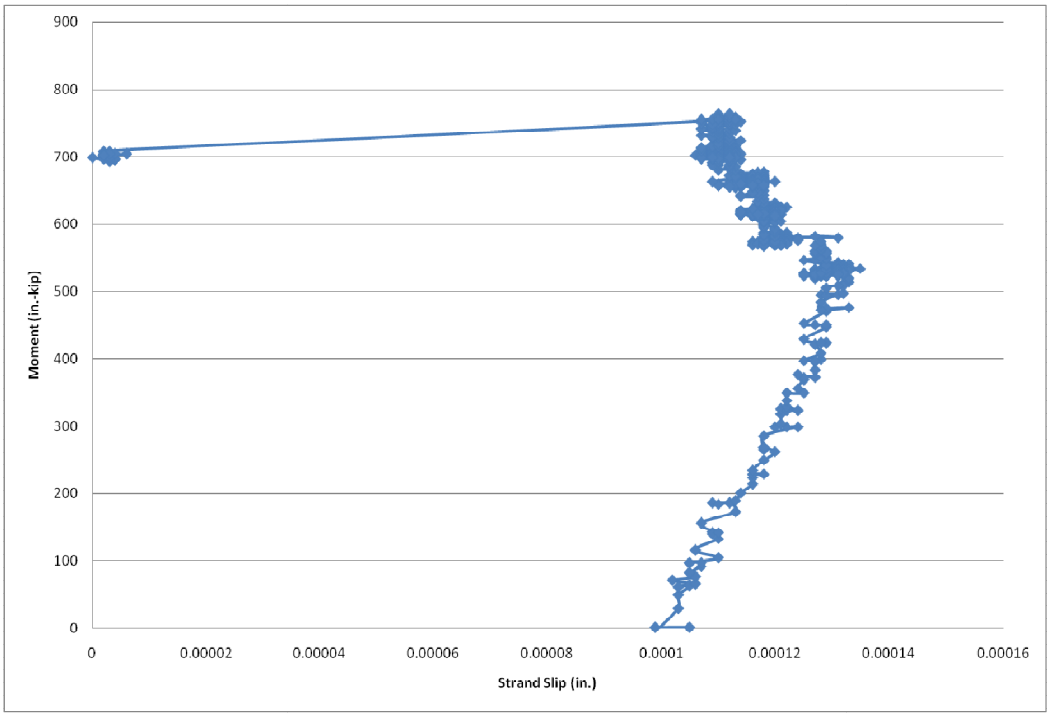

Figure C.20 Moment vs. Strand Slip for WT2A WE

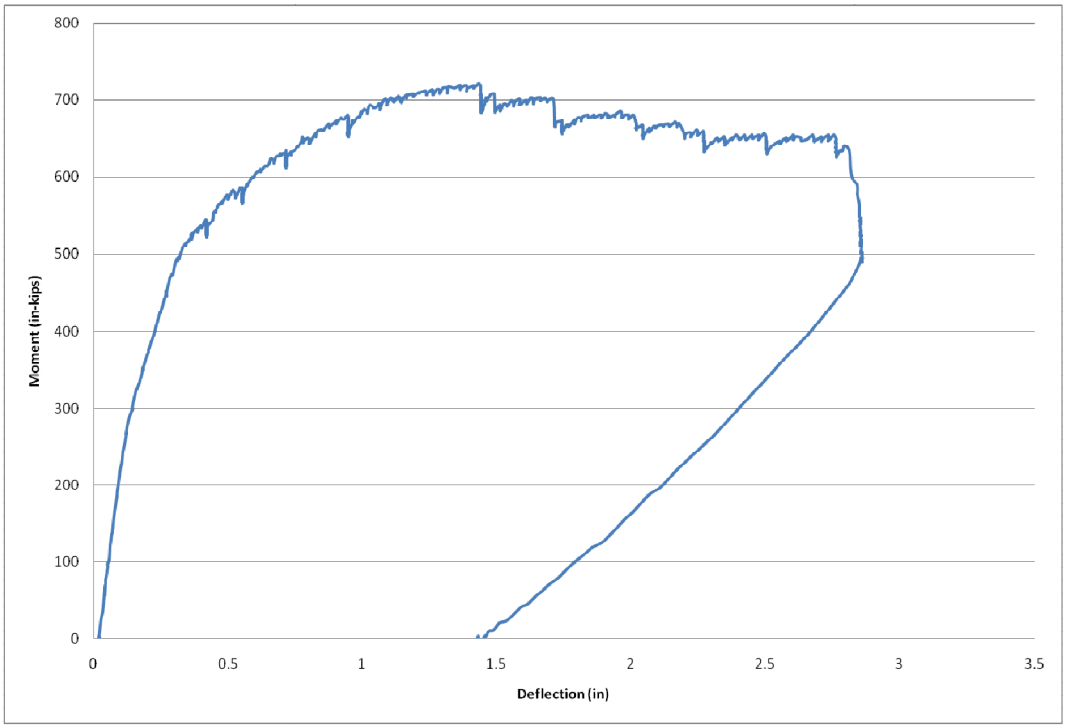

Figure C.21 Moment vs. Deflection for WT2B EE

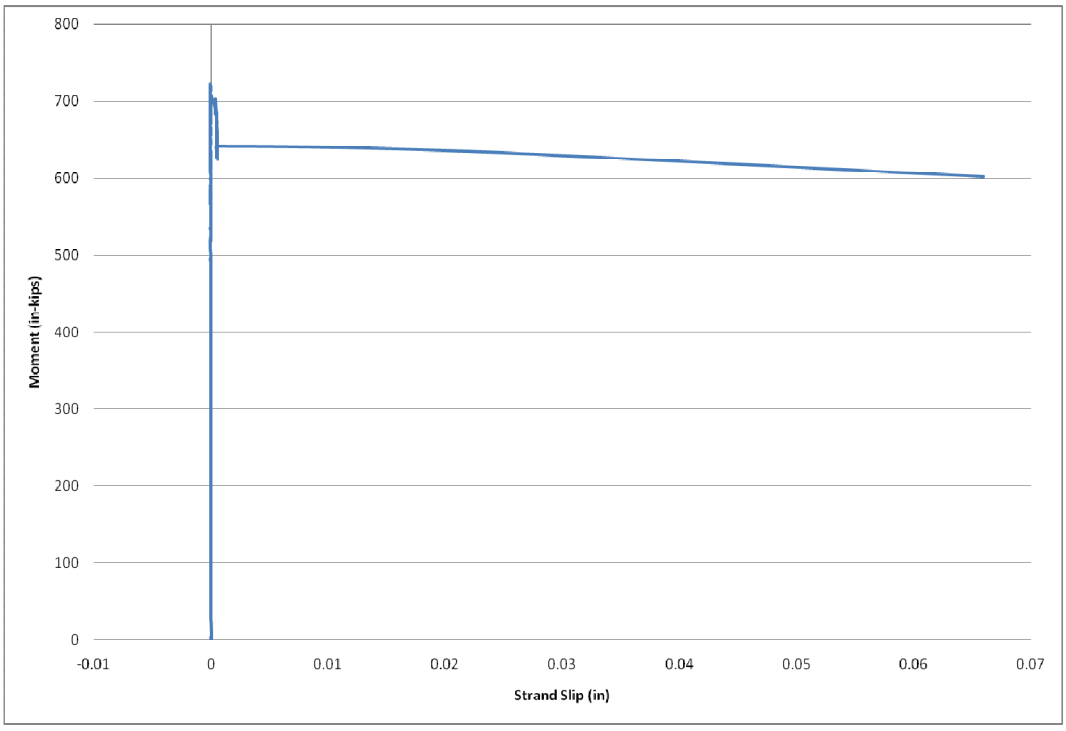

Figure C.22 Moment vs. Strand Slip for WT2B EE

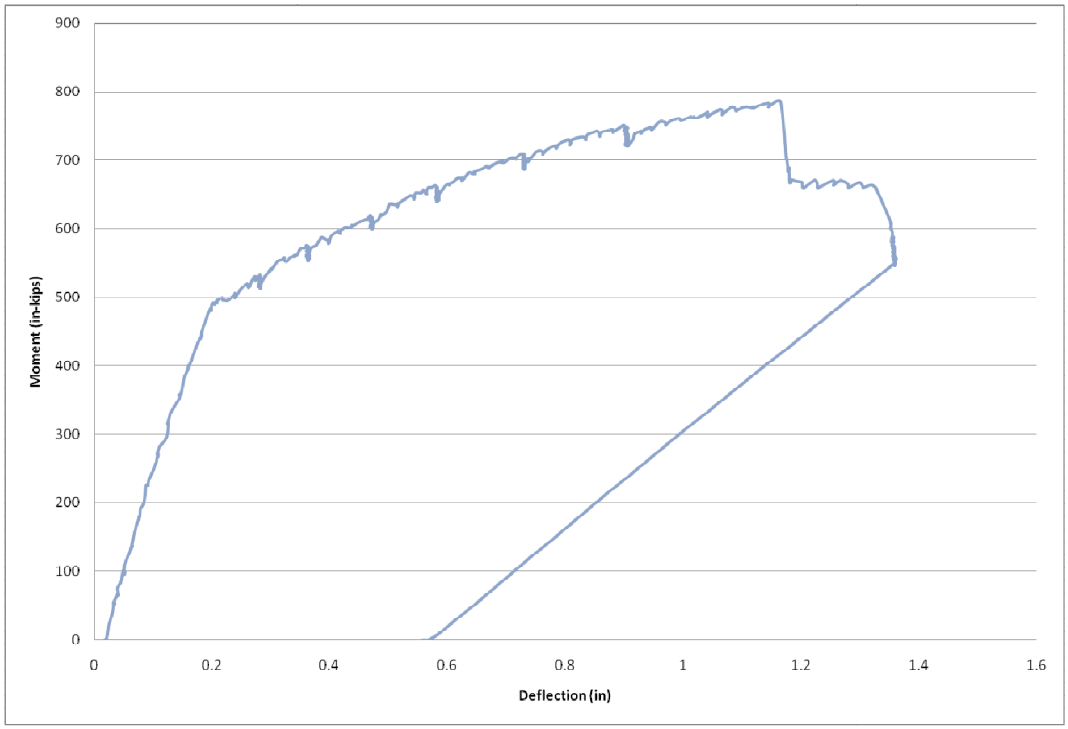

Figure C.23 Moment vs. Deflection for WT2B WE

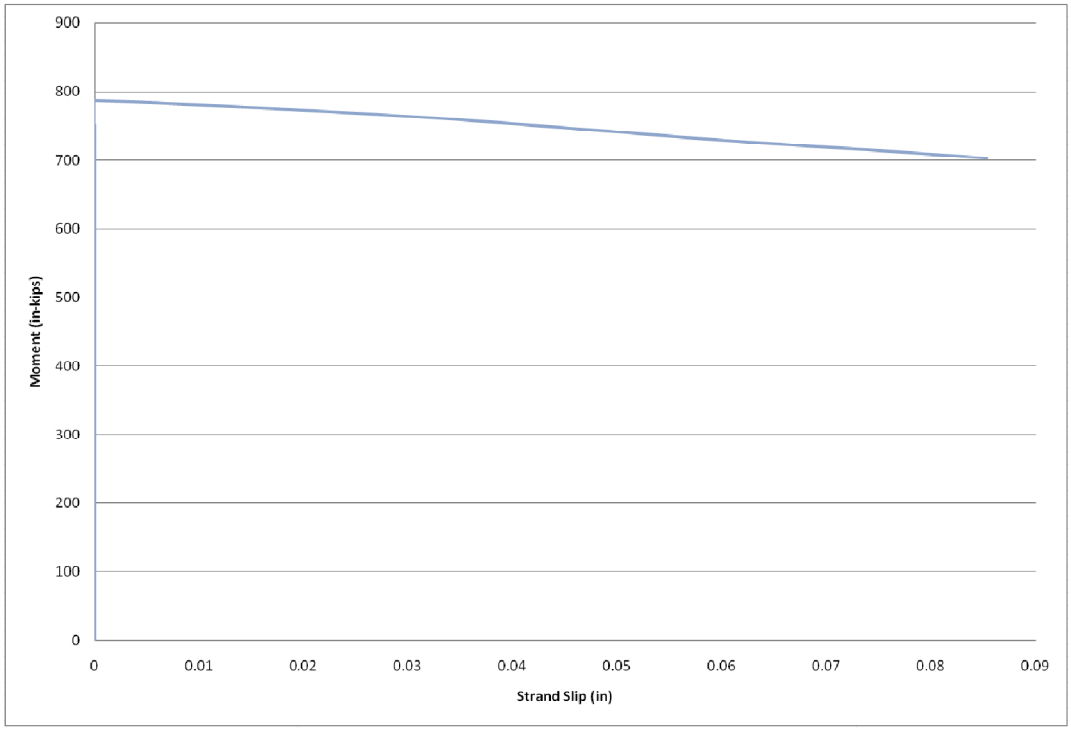

Figure C.24 Moment vs. Strand Slip for WT2B WE

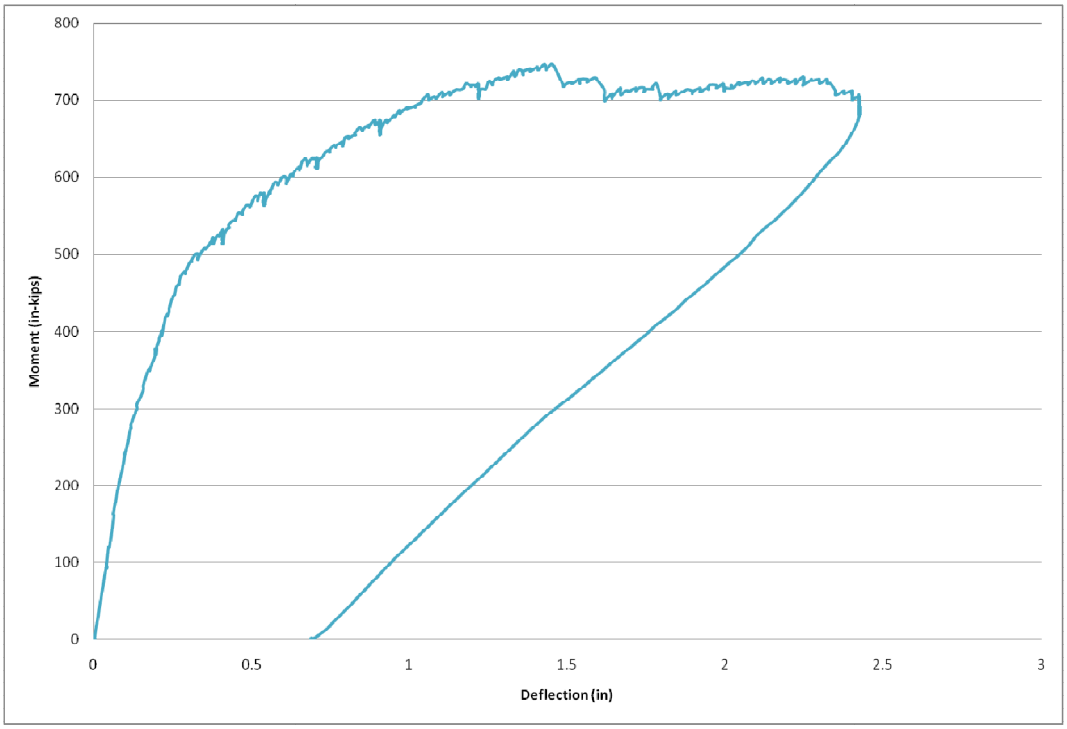

Figure C.25 Moment vs. Deflection for WT2C EE

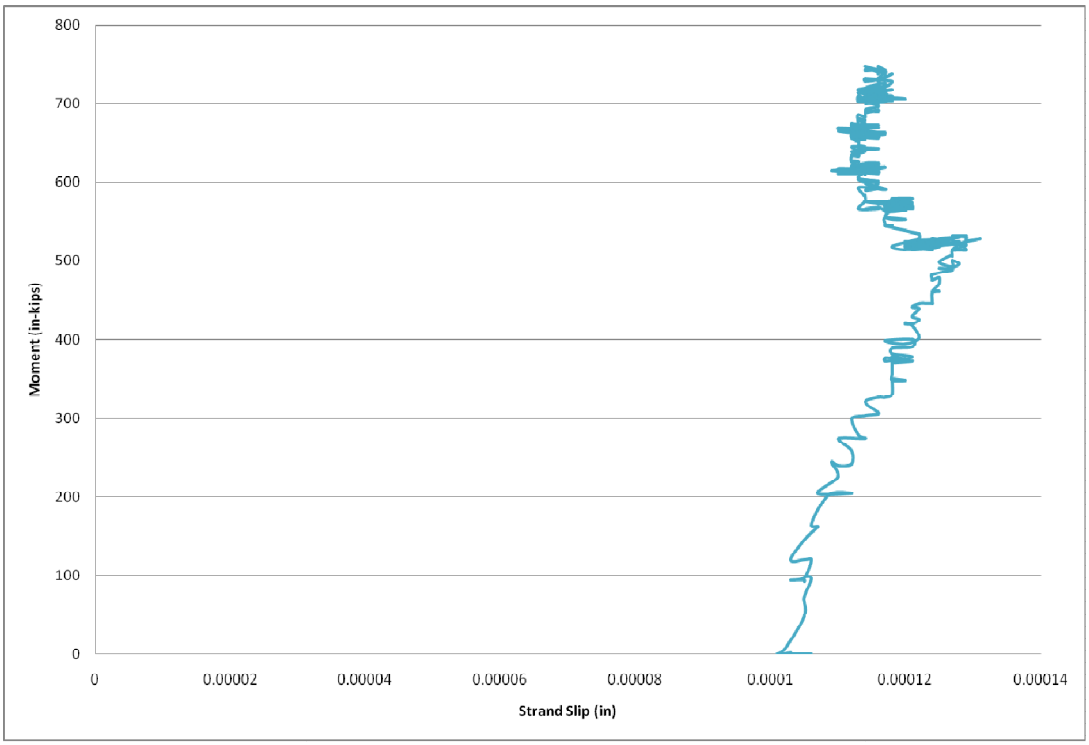

Figure C.26 Moment vs. Strand Slip for WT2C EE

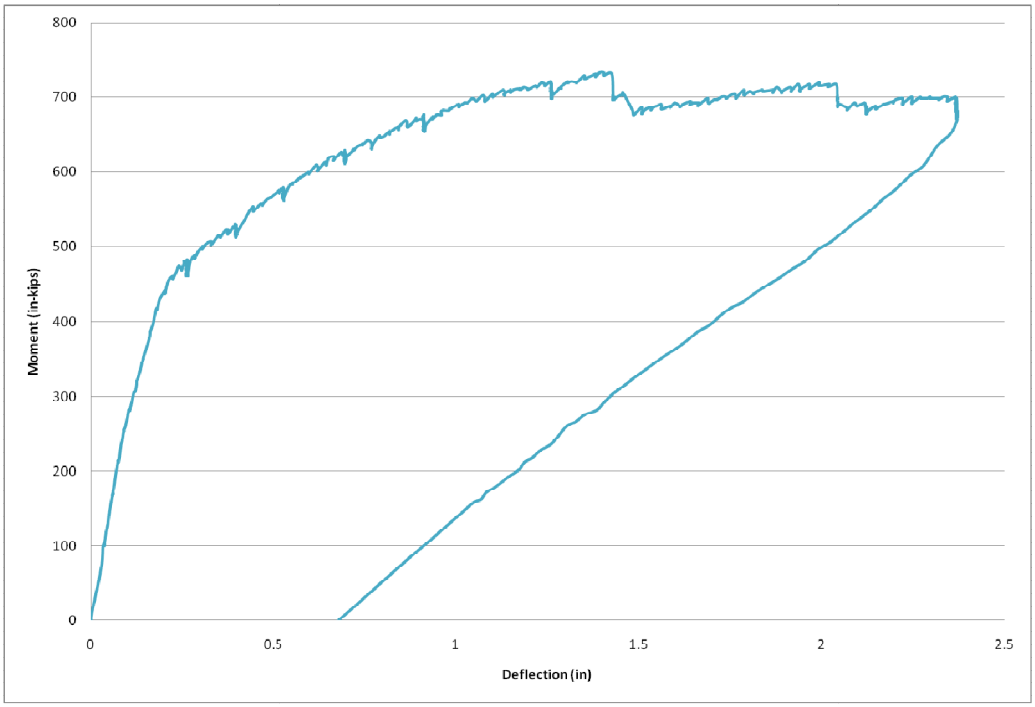

Figure C.27 Moment vs. Deflection for WT2C WE

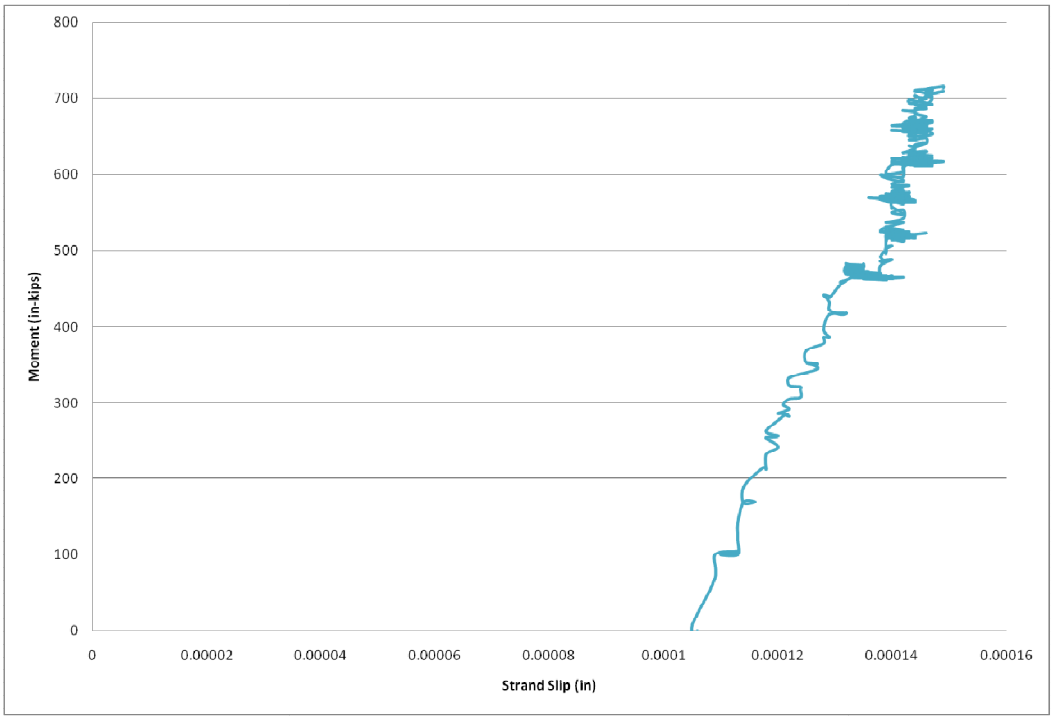

Figure C.28 Moment vs. Strand Slip for WT2C WE

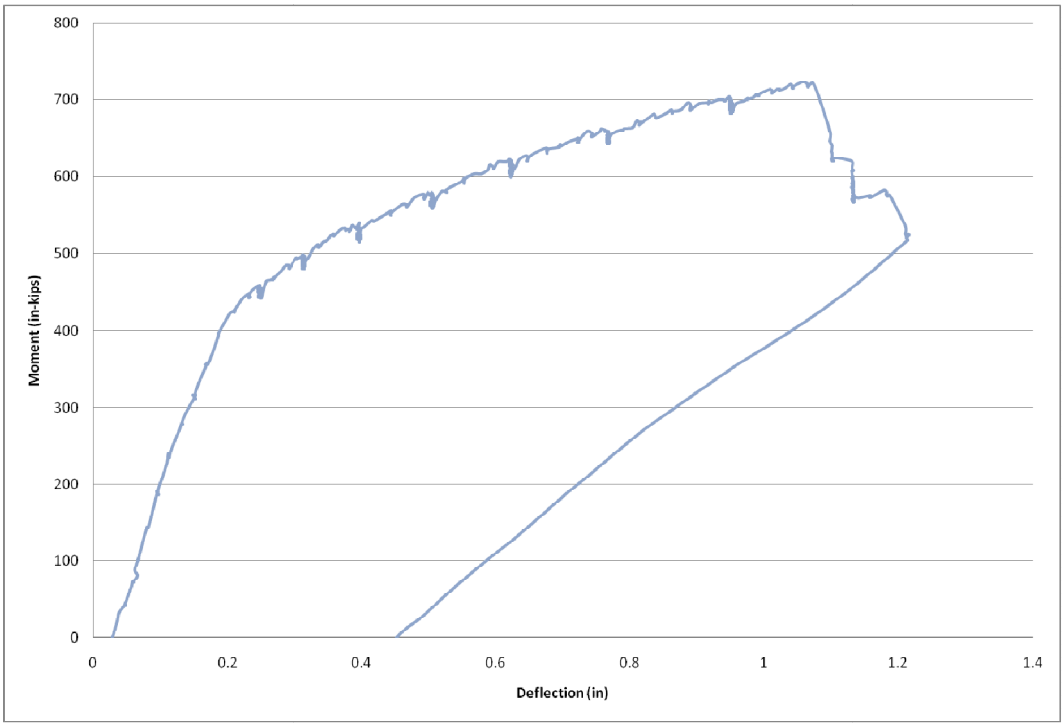

Figure C.29 Moment vs. Deflection for WT2D EE

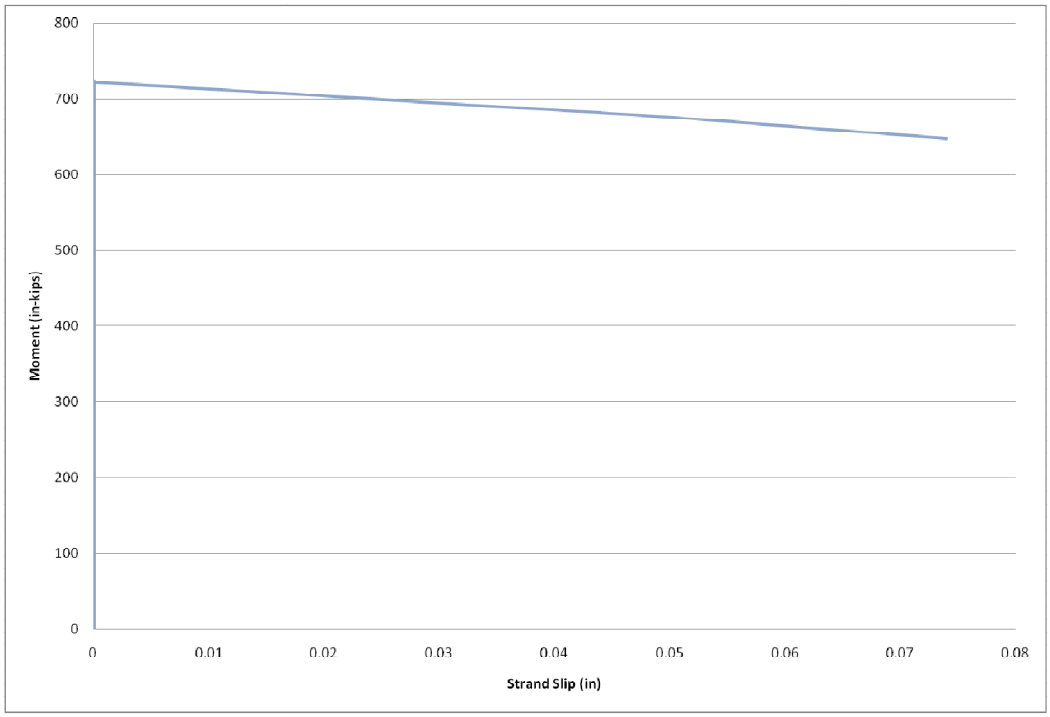

Figure C.30 Moment vs. Strand Slip for WT2D EE

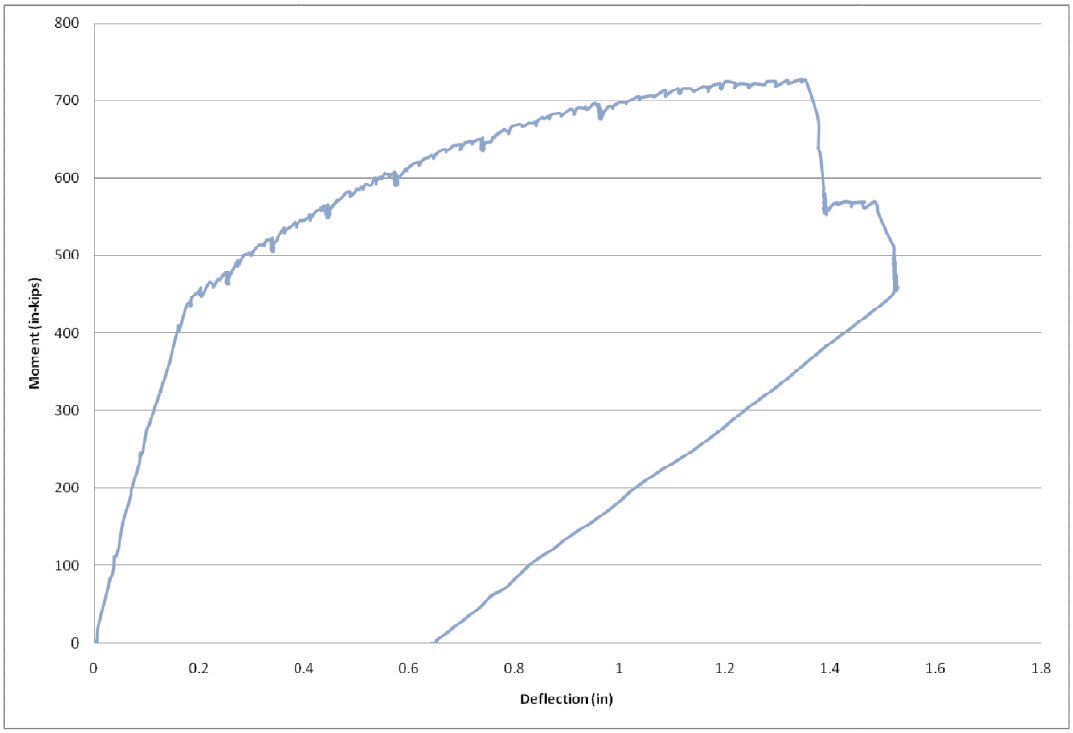

Figure C.31 Moment vs. Deflection for WT2D WE

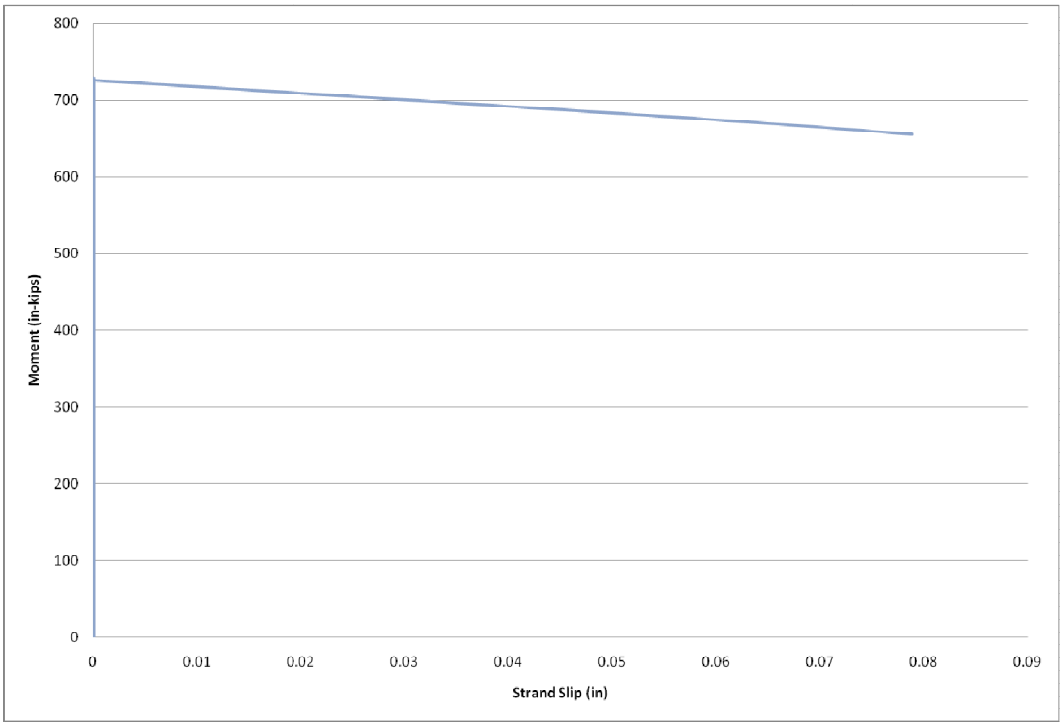

Figure C.32 Moment vs. Strand Slip for WT2D WE

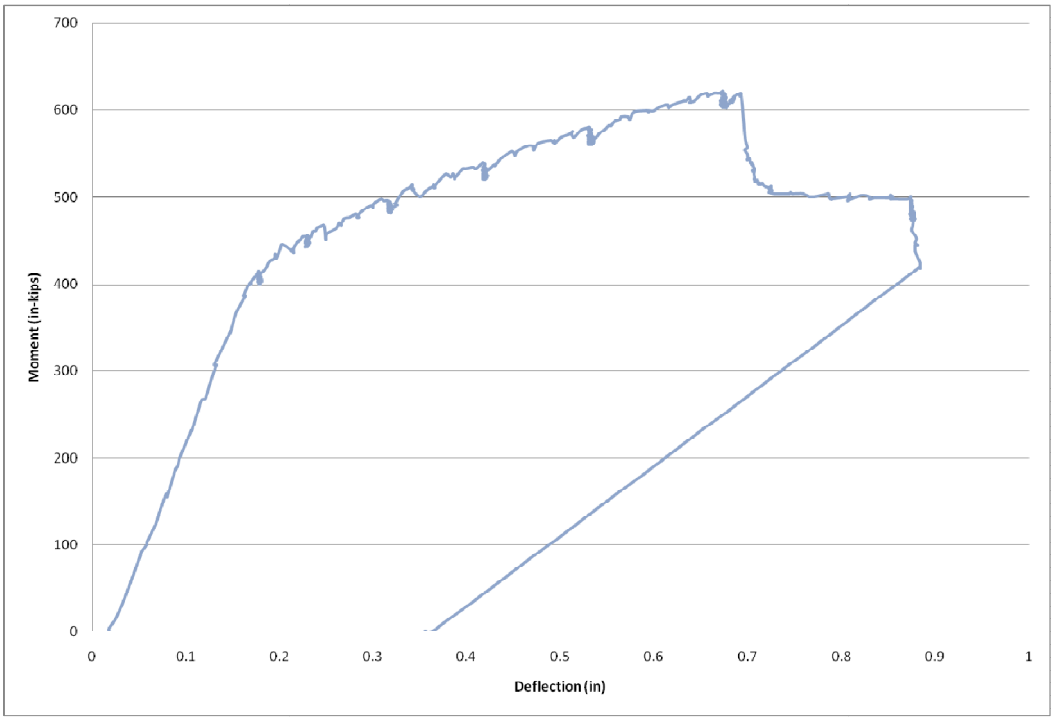

Figure C.33 Moment vs. Deflection for WT3A EE

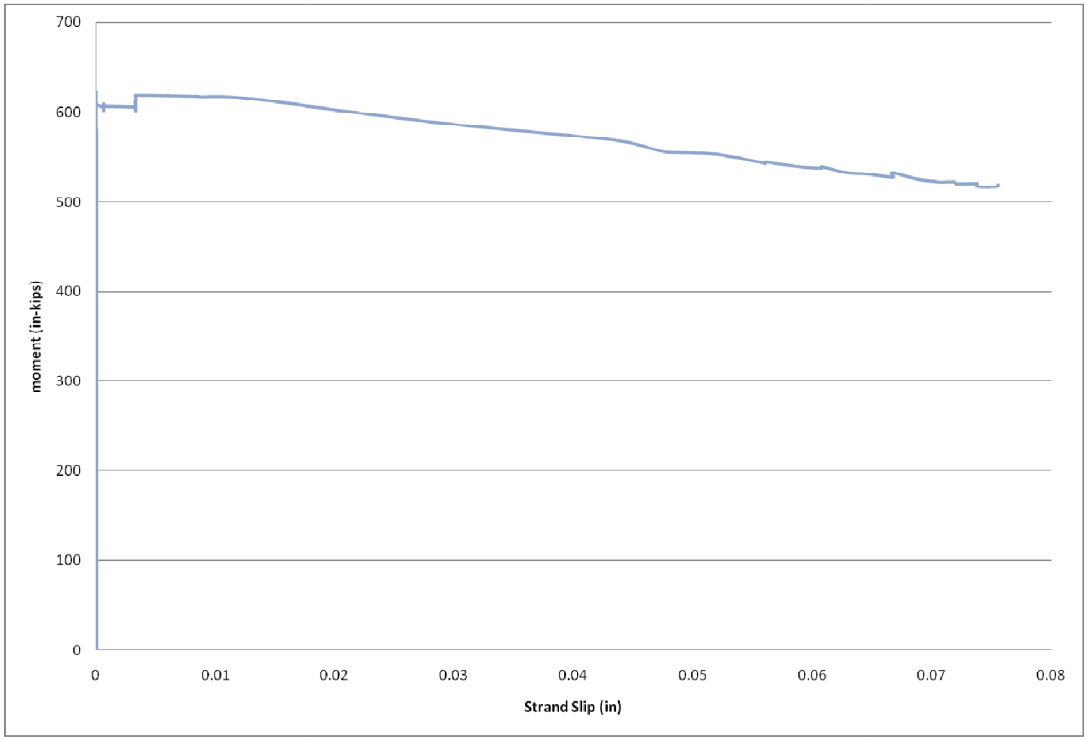

Figure C.34 Moment vs. Strand Slip for WT3A EE

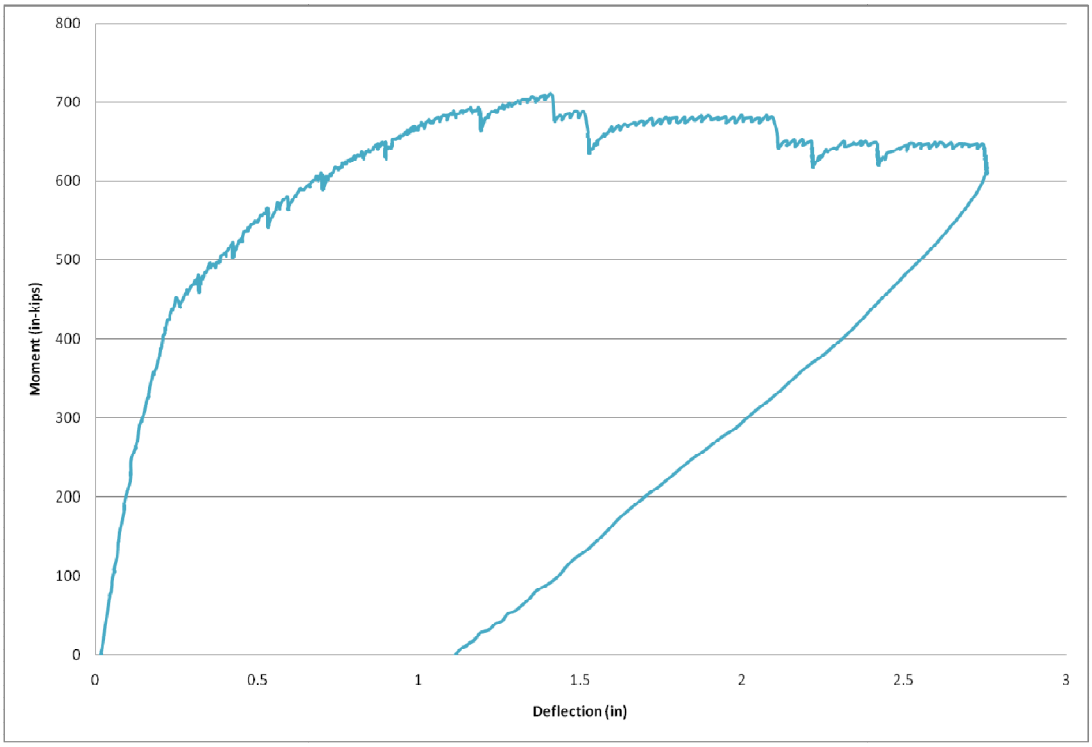

Figure C.35 Moment vs. Deflection for WT3A WE

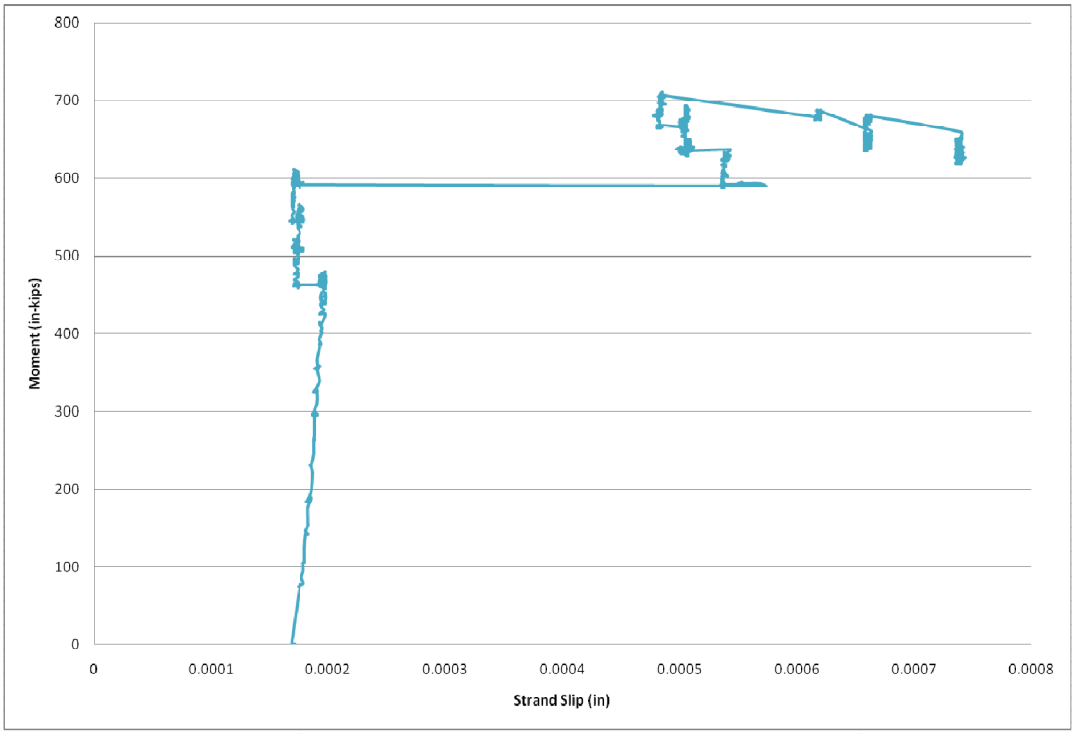

Figure C.36 Moment vs. Strand Slip for WT3A WE

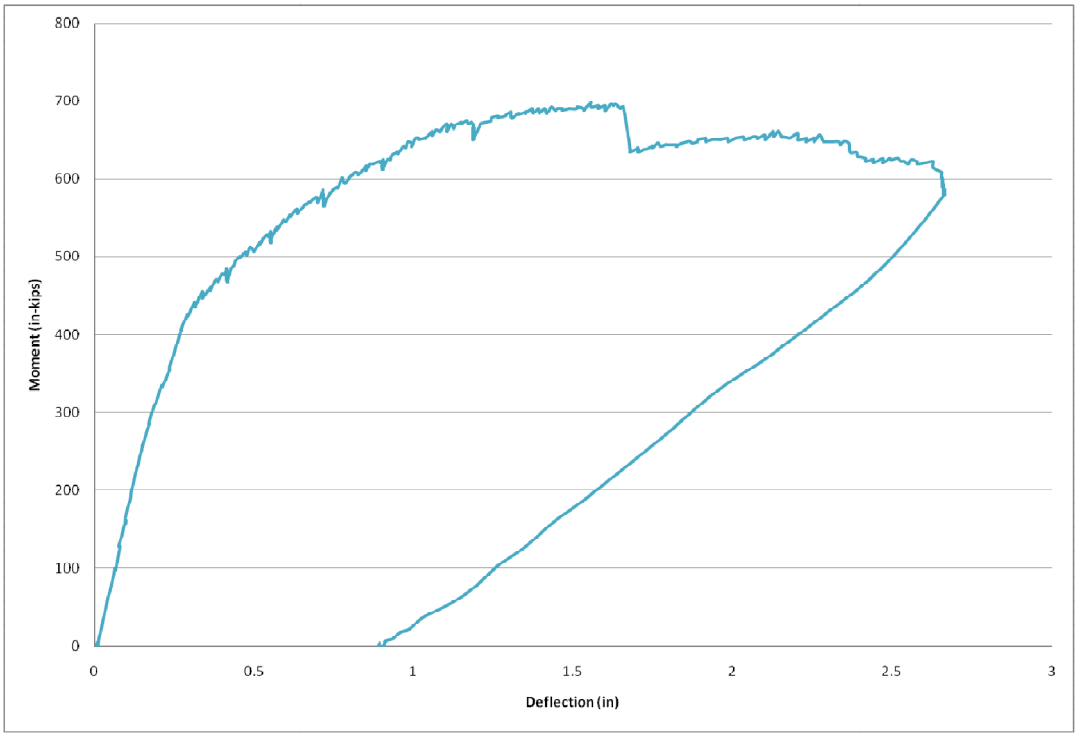

Figure C.37 Moment vs. Deflection for WT3B EE

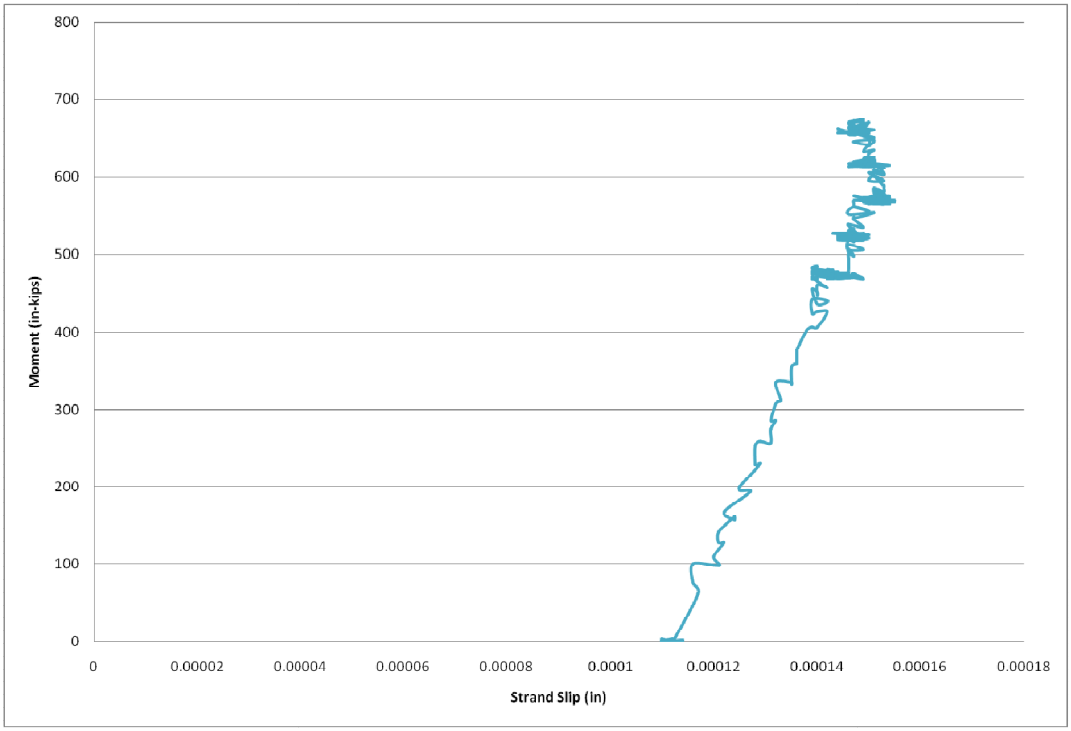

Figure C.38 Moment vs. Strand Slip for WT3B EE

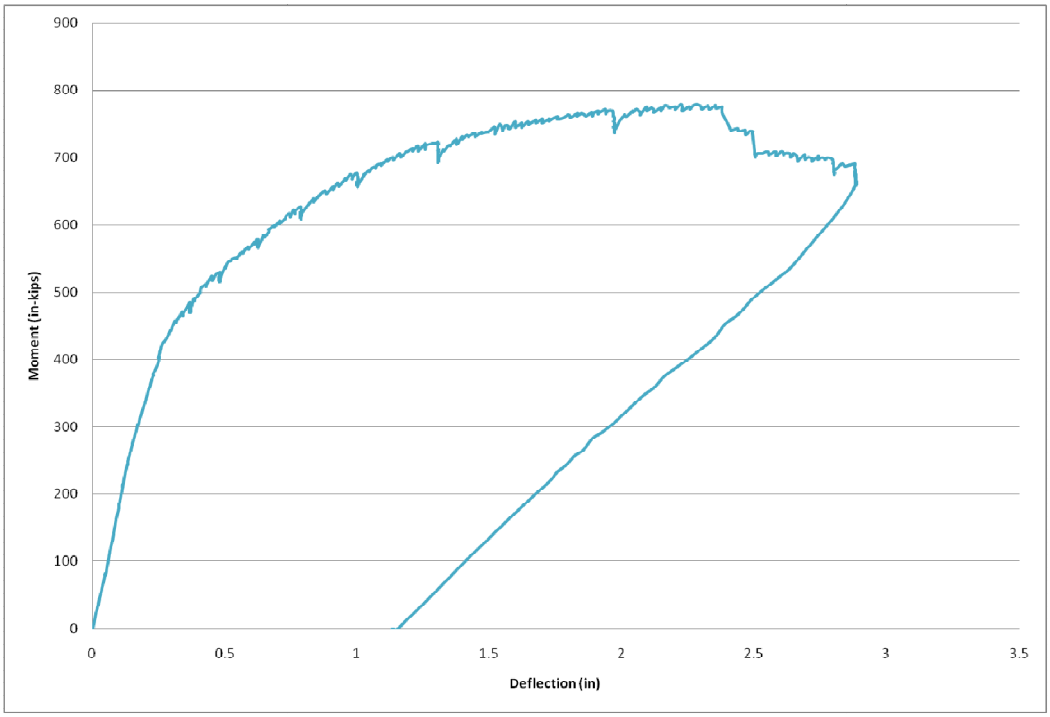

Figure C.39 Moment vs. Deflection for WT3B WE

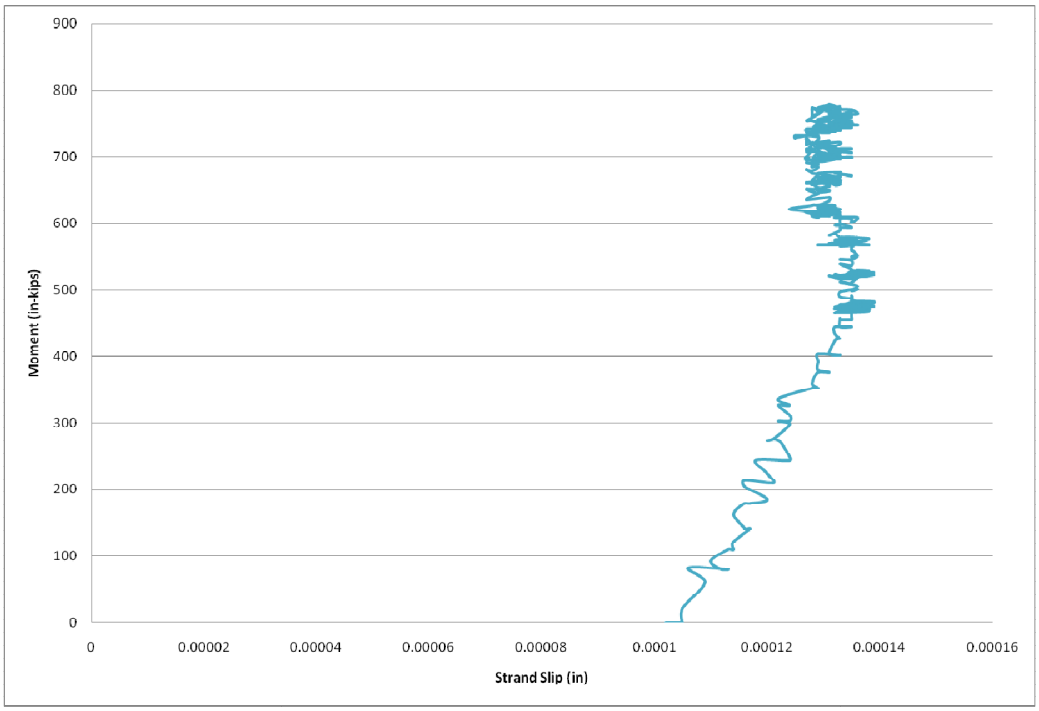

Figure C.40 Moment vs. Strand Slip for WT3B WE

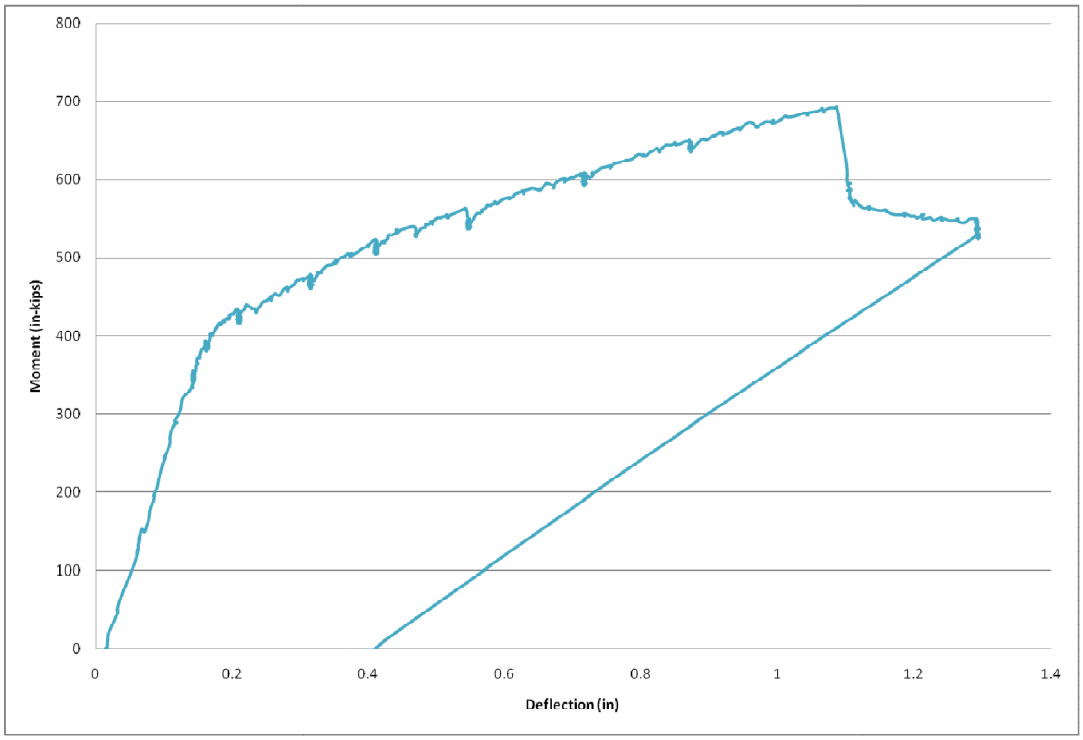

Figure C.41 Moment vs. Deflection for WT3C EE

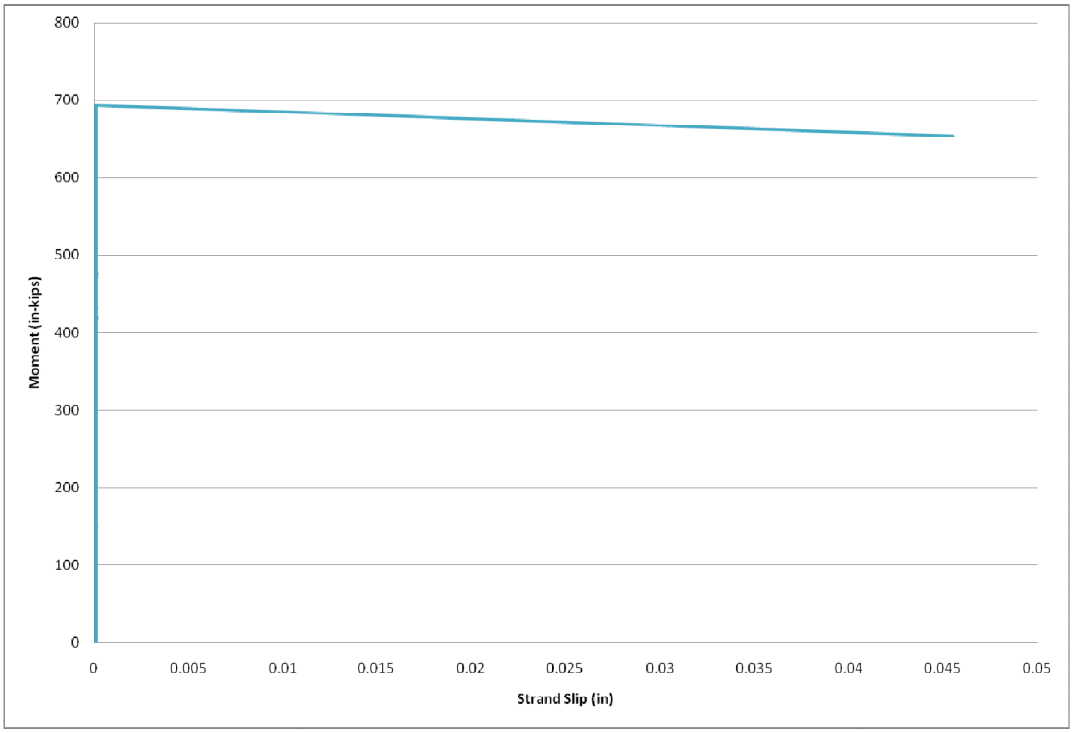

Figure C.42 Moment vs. Strand Slip for WT3C EE

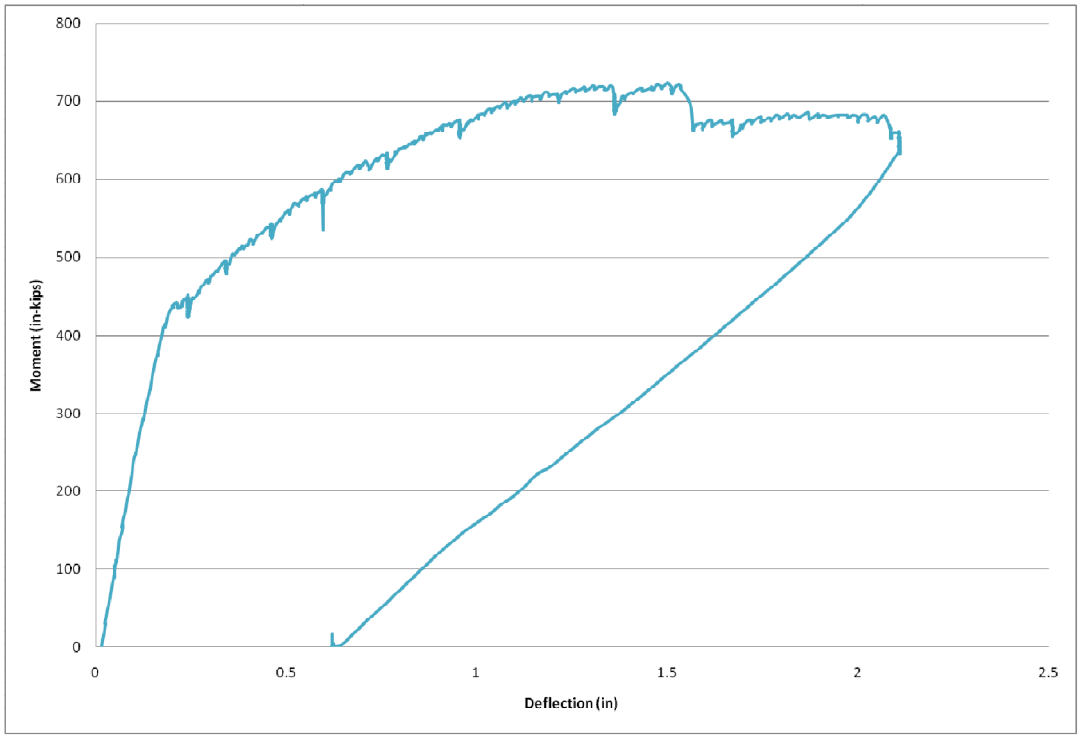

Figure C.43 Moment vs. Deflection for WT3C WE

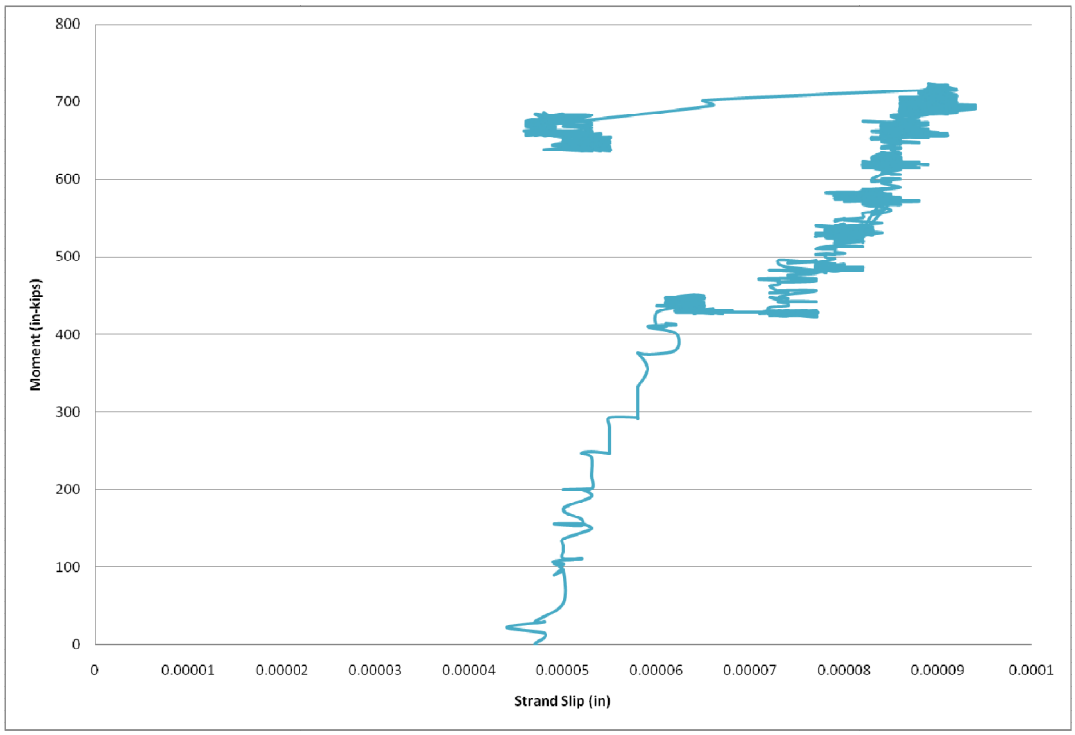

Figure C.44 Moment vs. Strand Slip for WT3C WE

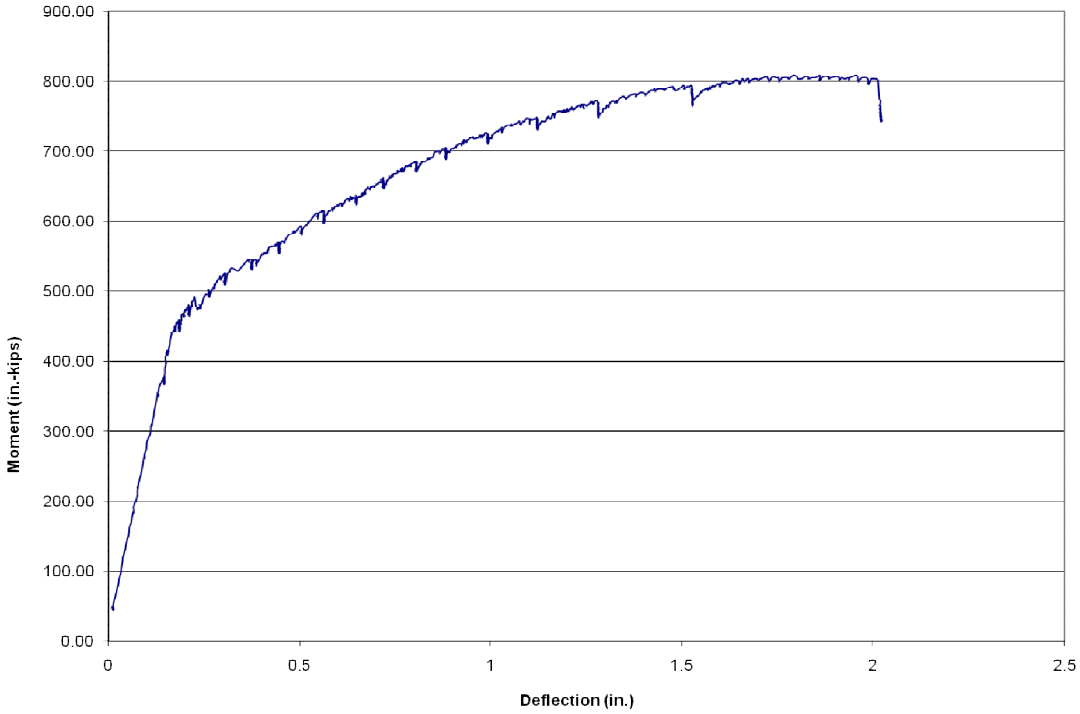

Figure C.45 Moment vs. Deflection for WT3D EE

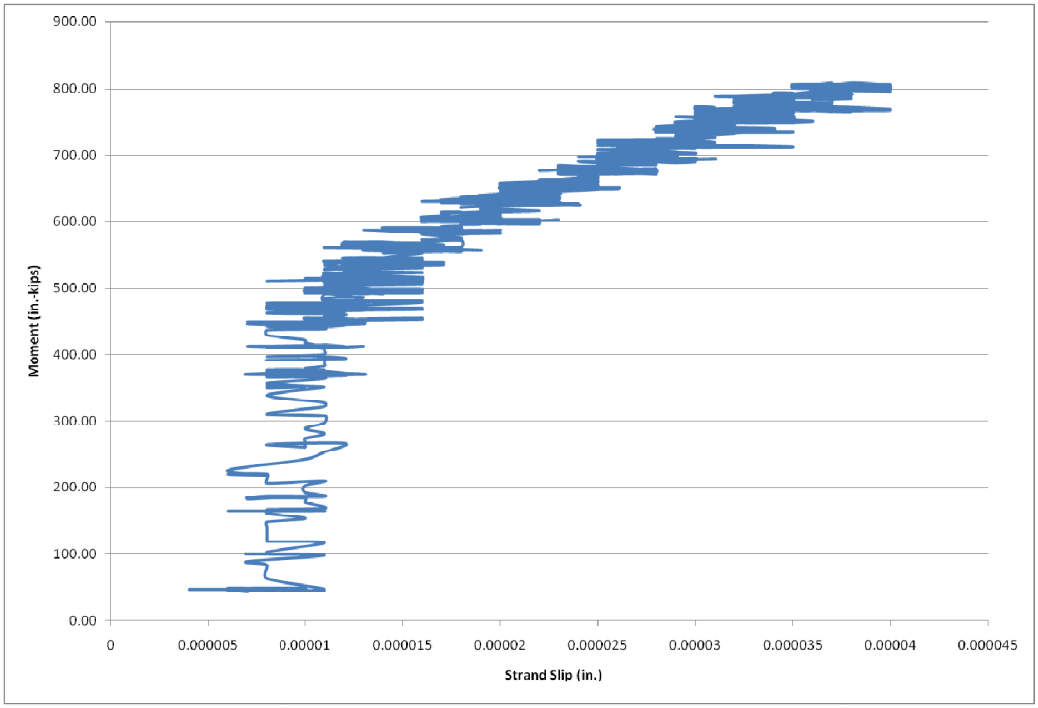

Figure C.46 Moment vs. Strand Slip for WT3D EE

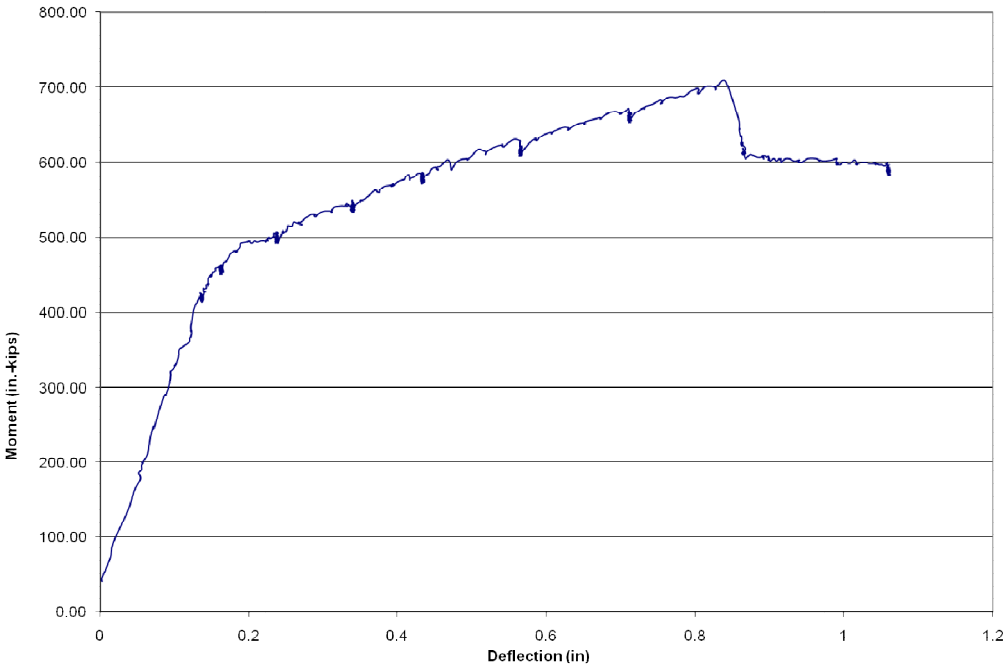

Figure C.47 Moment vs. Deflection for WT3D WE

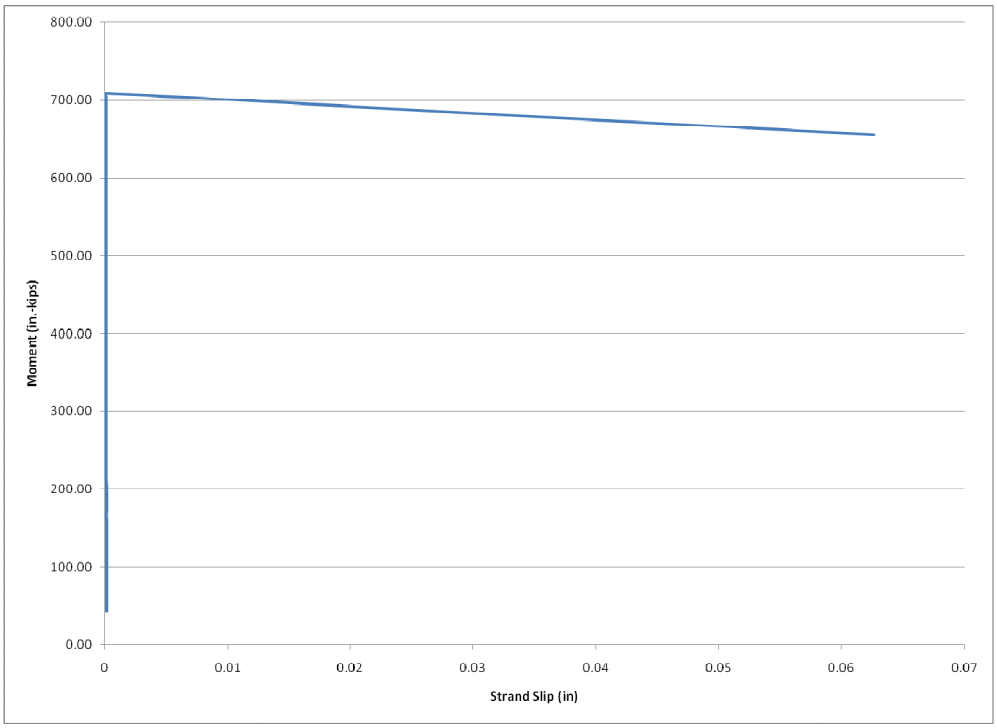

Figure C.48 Moment vs. Strand Slip for WT3D WE

APPENDIX D Crack Reopening Plots

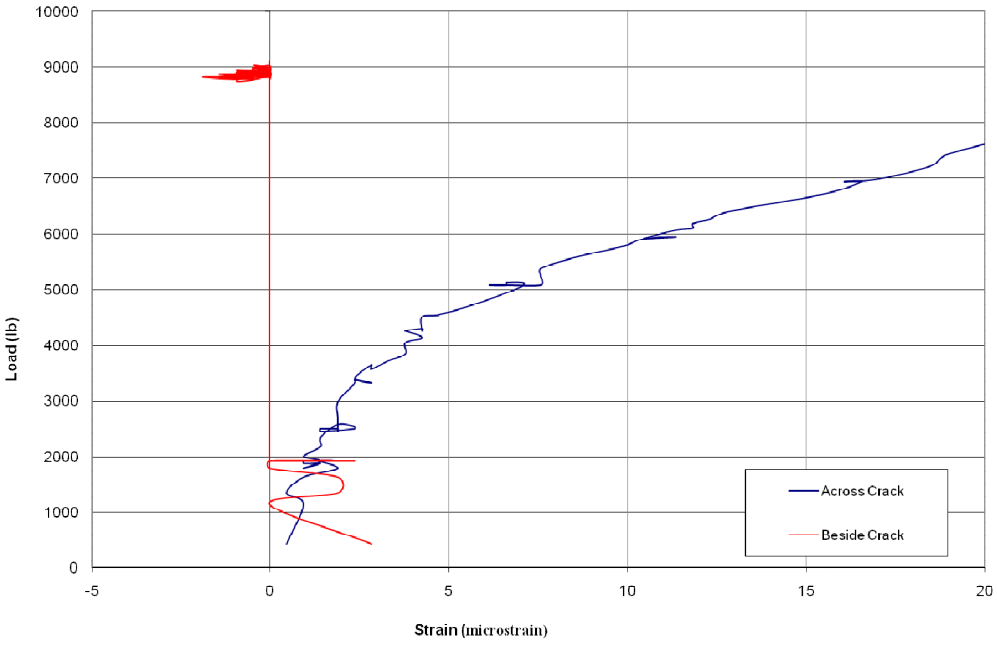

Figure D.1 Re-crack Plot for WT1A EE

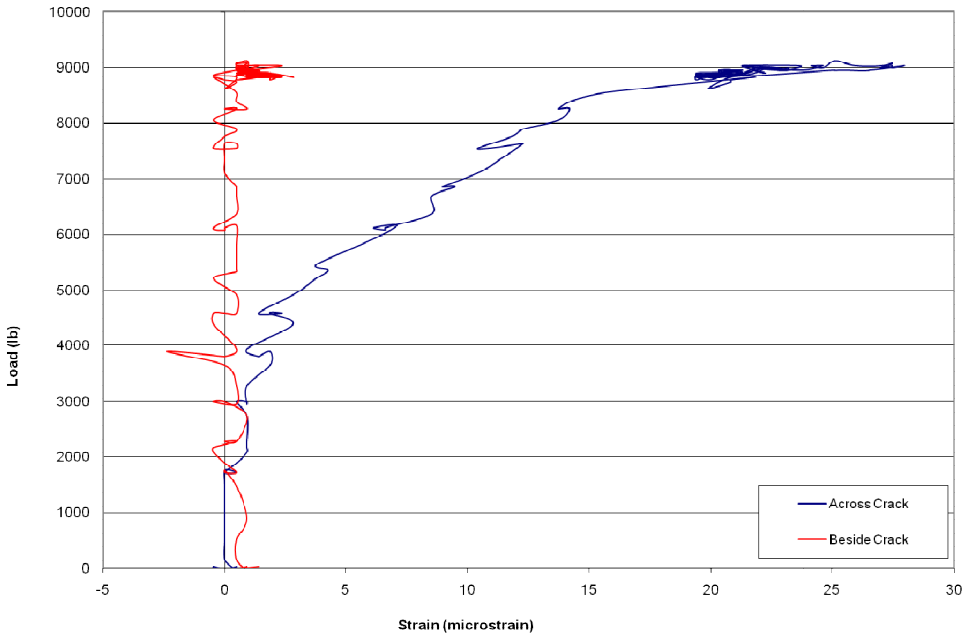

Figure D.2 Re-crack Plot for WT1A WE

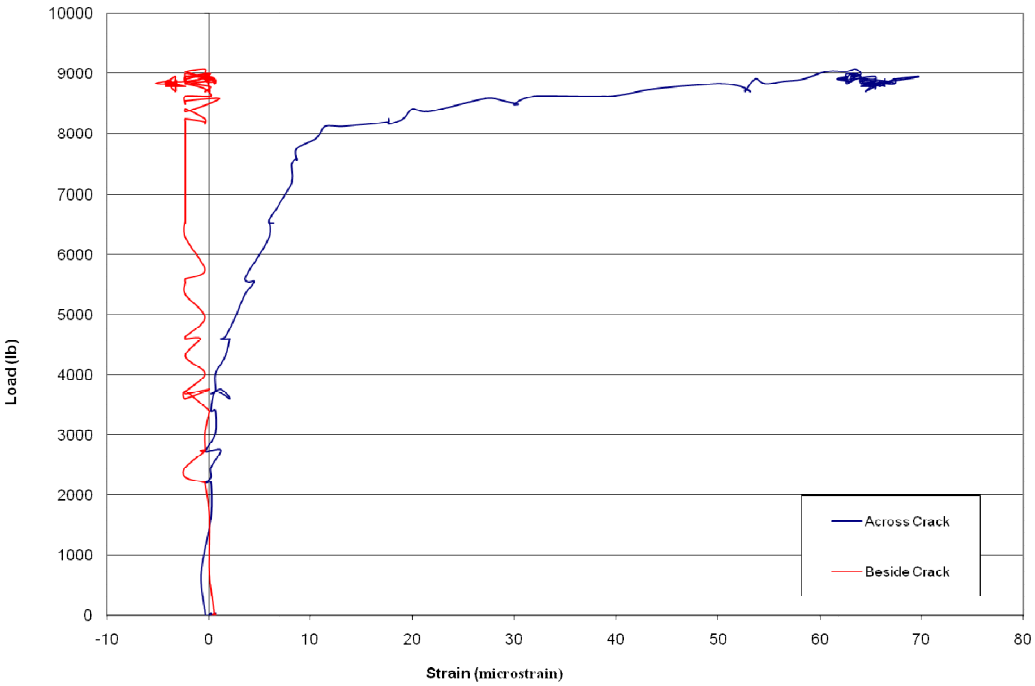

Figure D.3 Re-crack Plot for WT1B EE

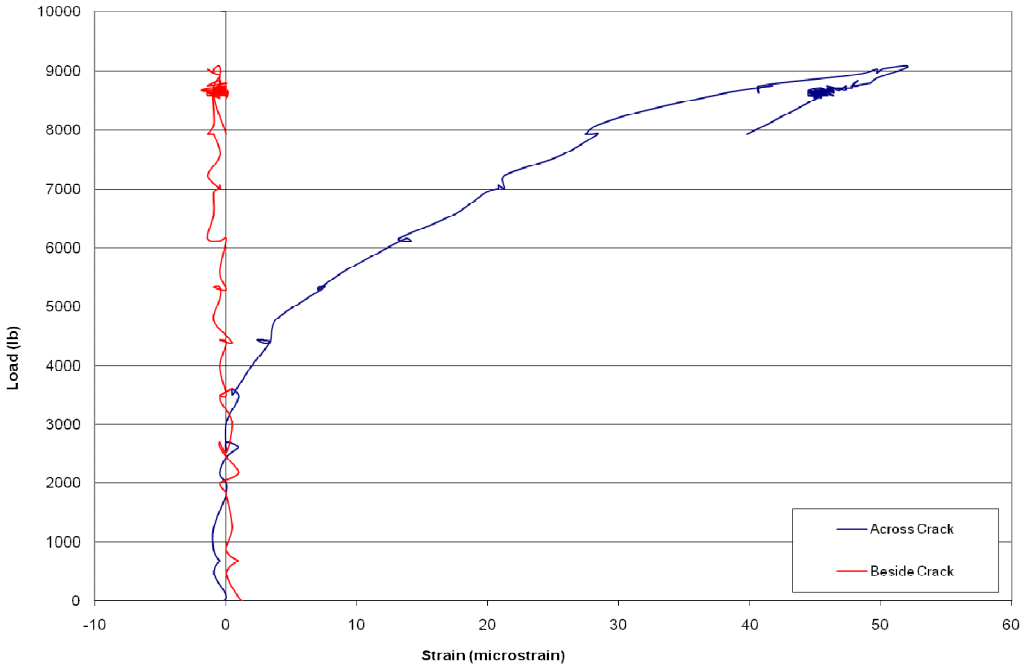

Figure D.4 Re-crack Plot for WT1B WE

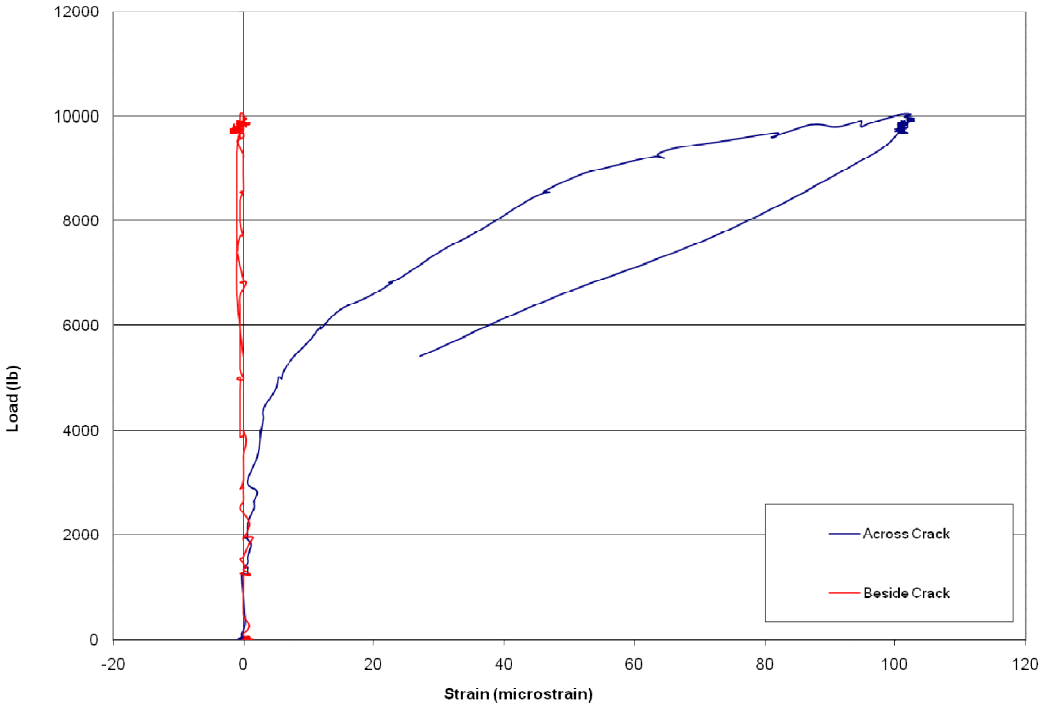

Figure D.5 Re-crack Plot for WT1C EE

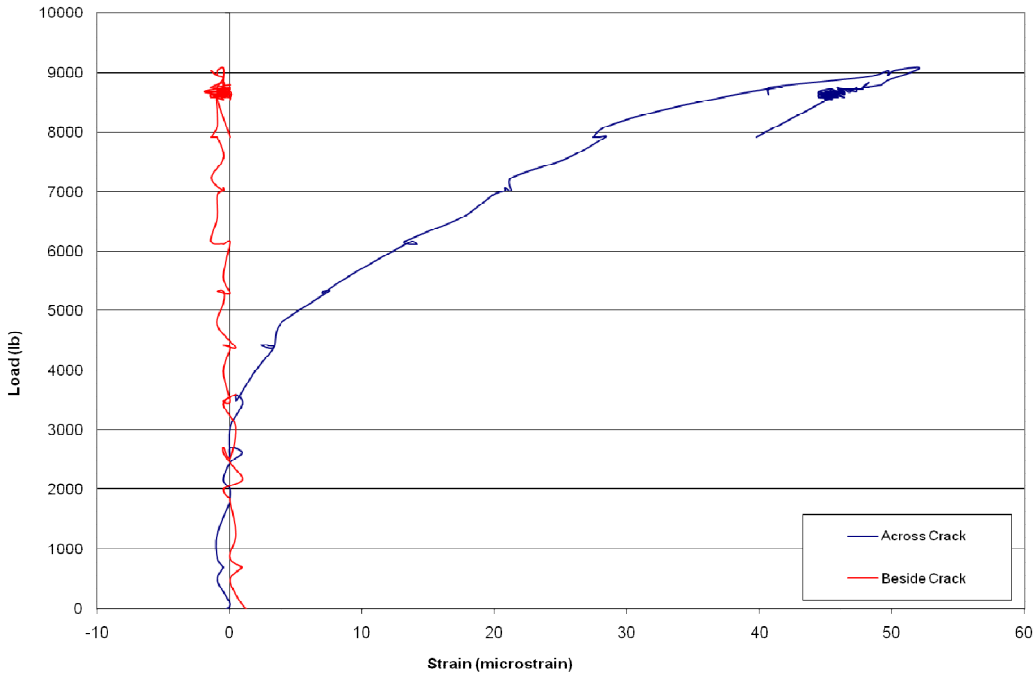

Figure D.6 Re-crack Plot for WT1C WE

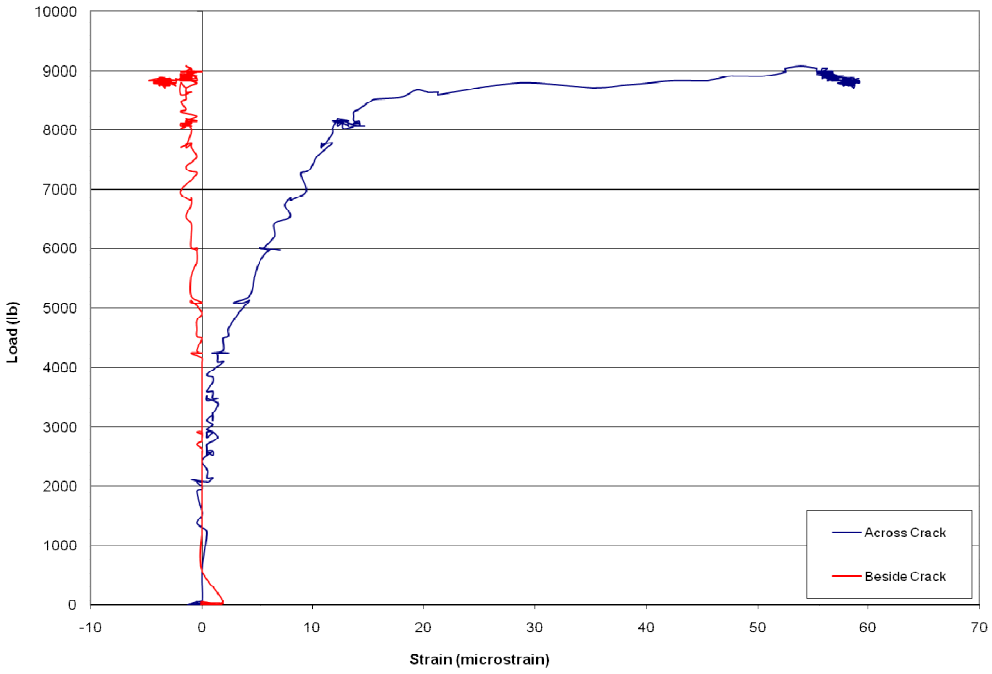

Figure D.7 Re-crack Plot for WT1D EE

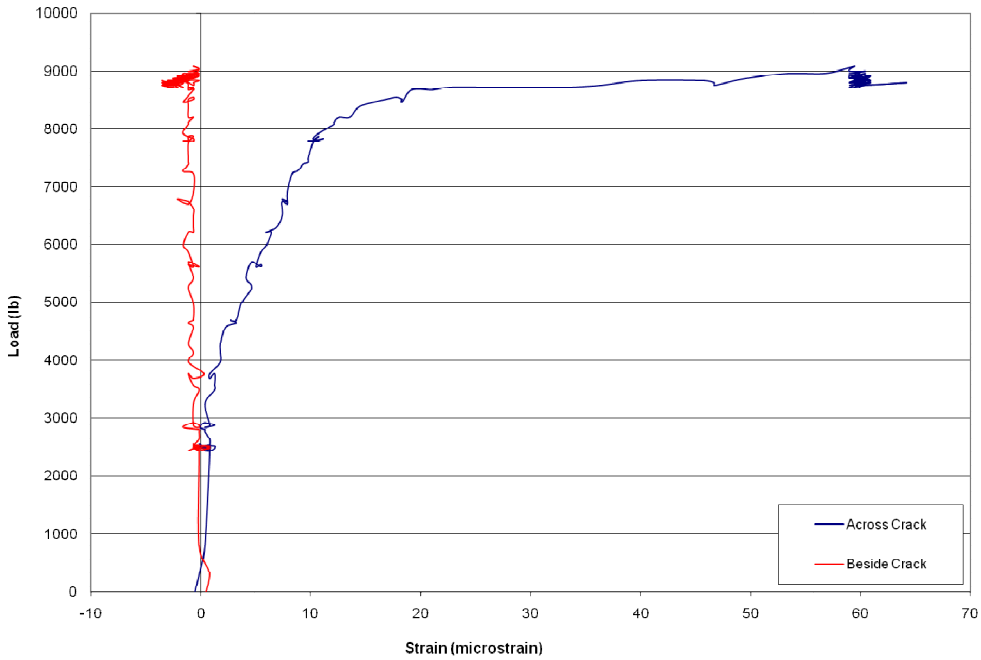

Figure D.8 Re-crack Plot for WT1D WE

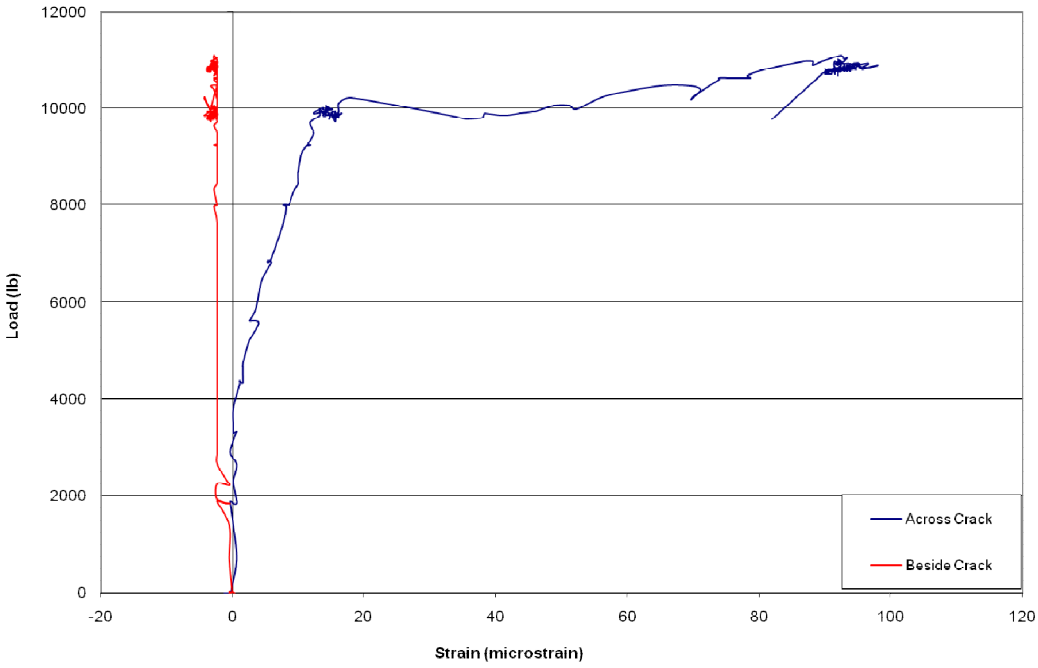

Figure D.9 Re-crack Plot for WT2A EE

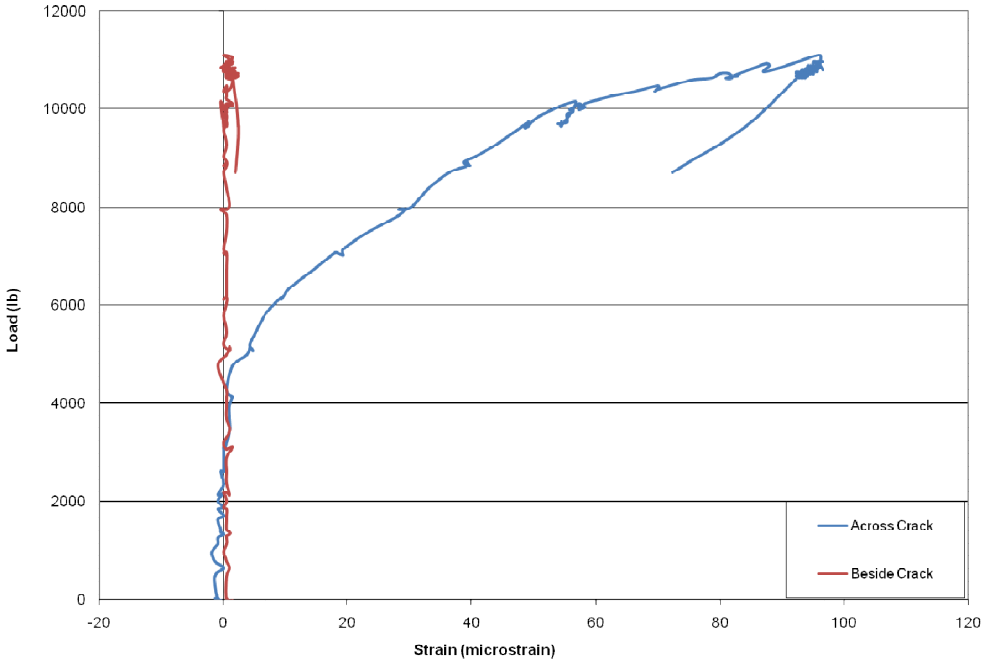

Figure D.10 Re-crack Plot for WT2A WE

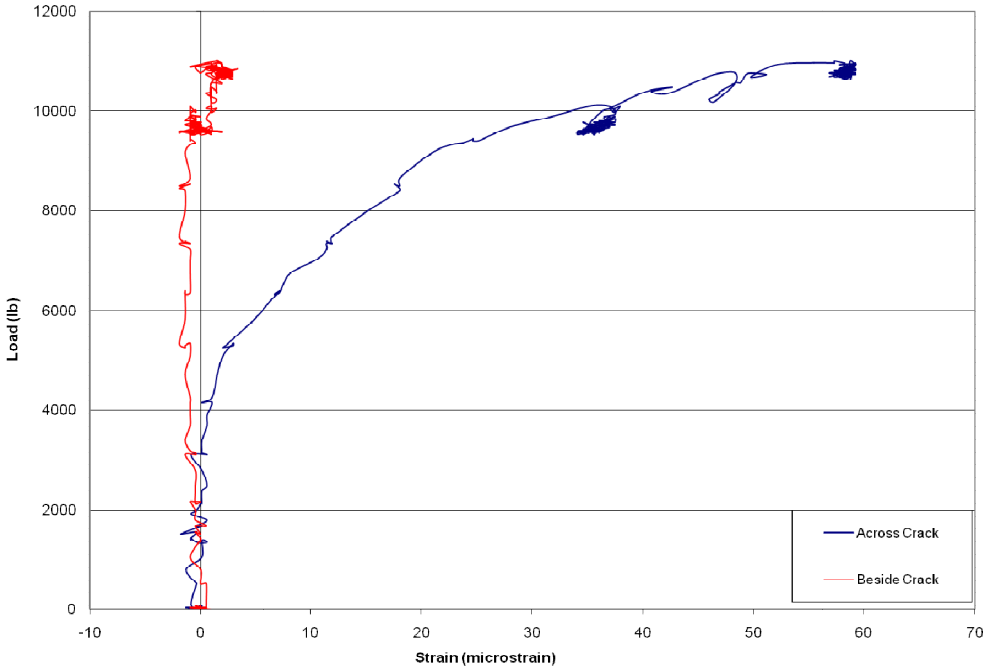

Figure D.11 Re-crack Plot for WT2B EE

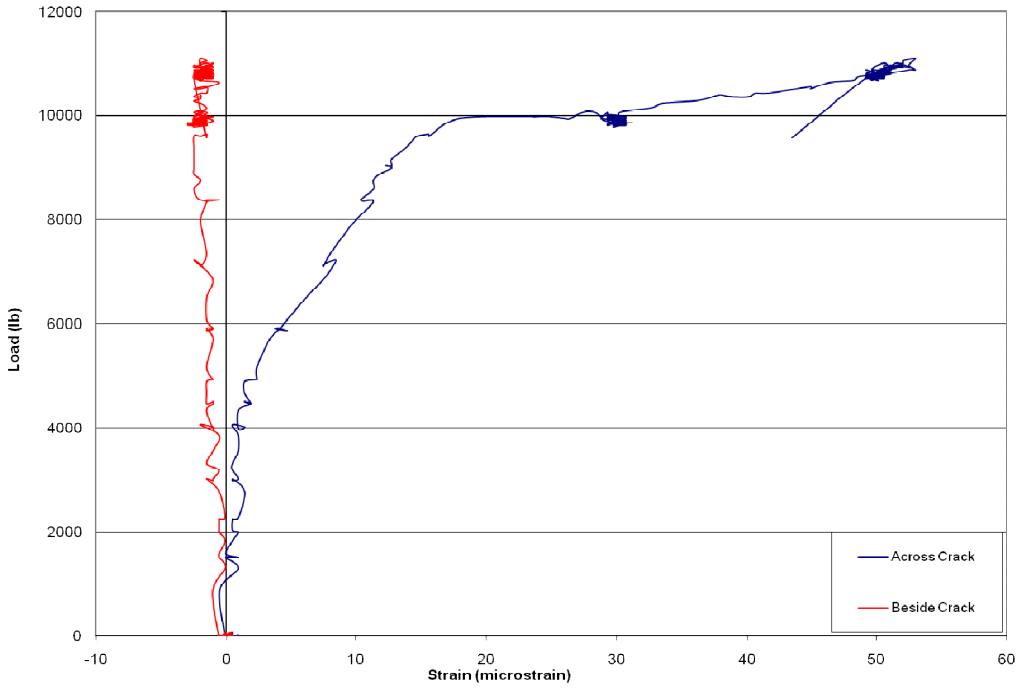

Figure D.12 Re-crack Plot for WT2B WE

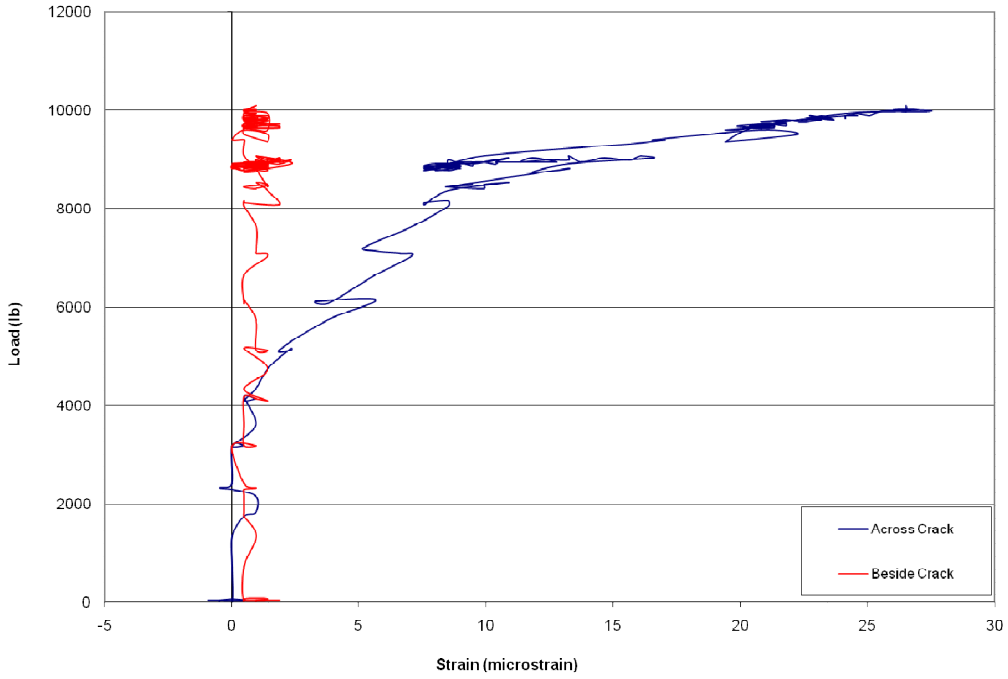

Figure D.13 Re-crack Plot for WT2C EE

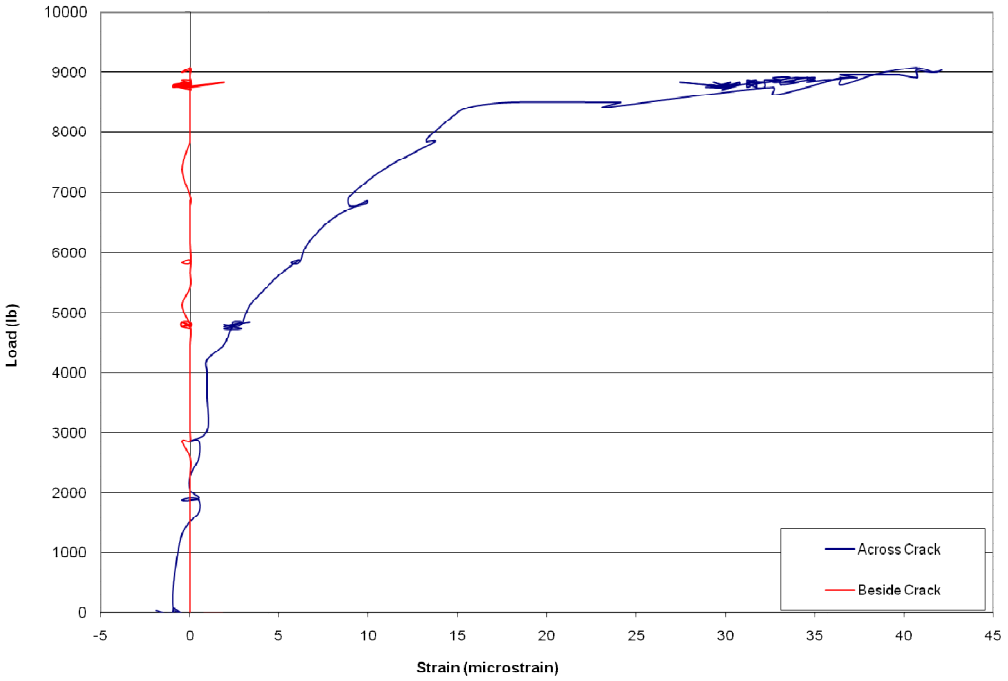

Figure D.14 Re-crack Plot for WT2C WE

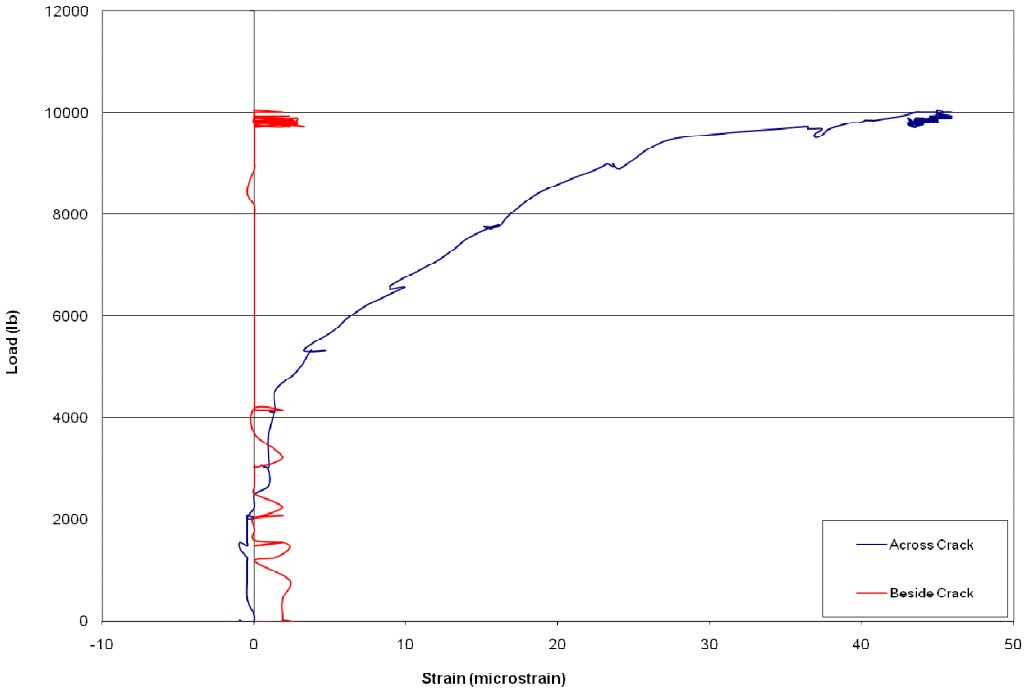

Figure D.15 Re-crack Plot for WT2D EE

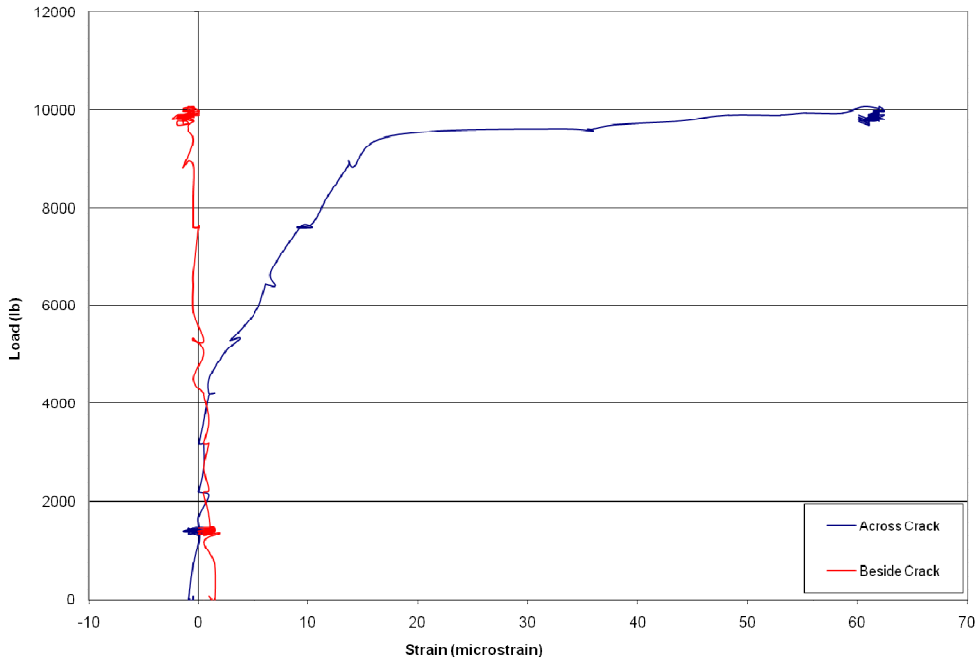

Figure D.16 Re-crack Plot for WT2D WE

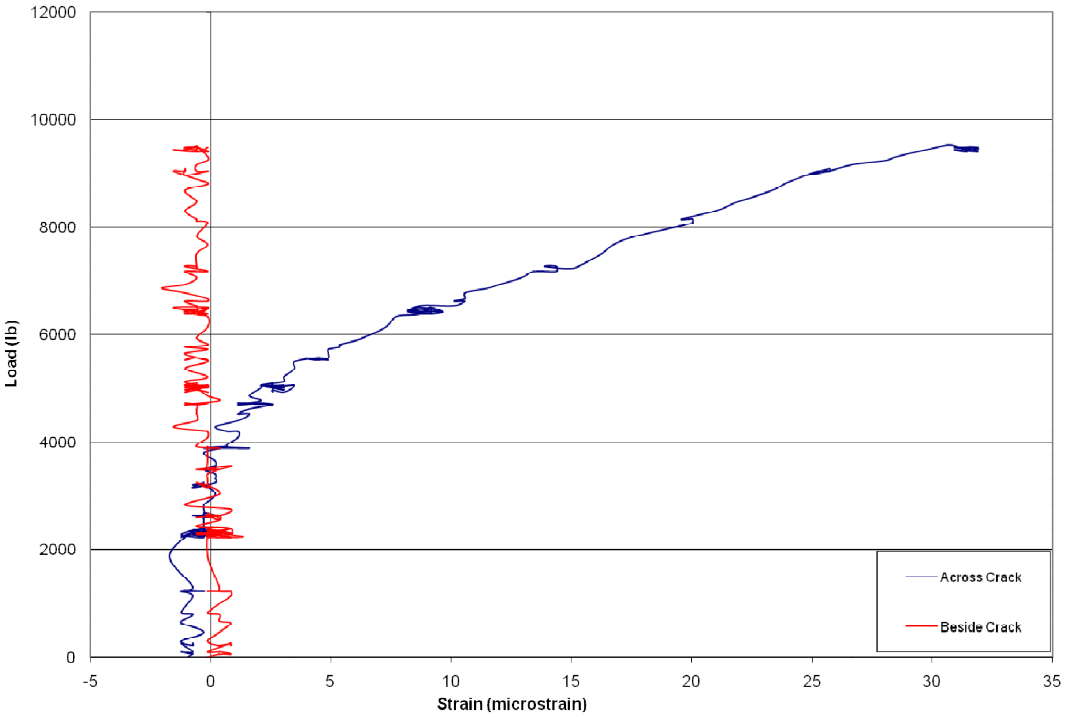

Figure D.17 Re-crack Plot for WT3A EE

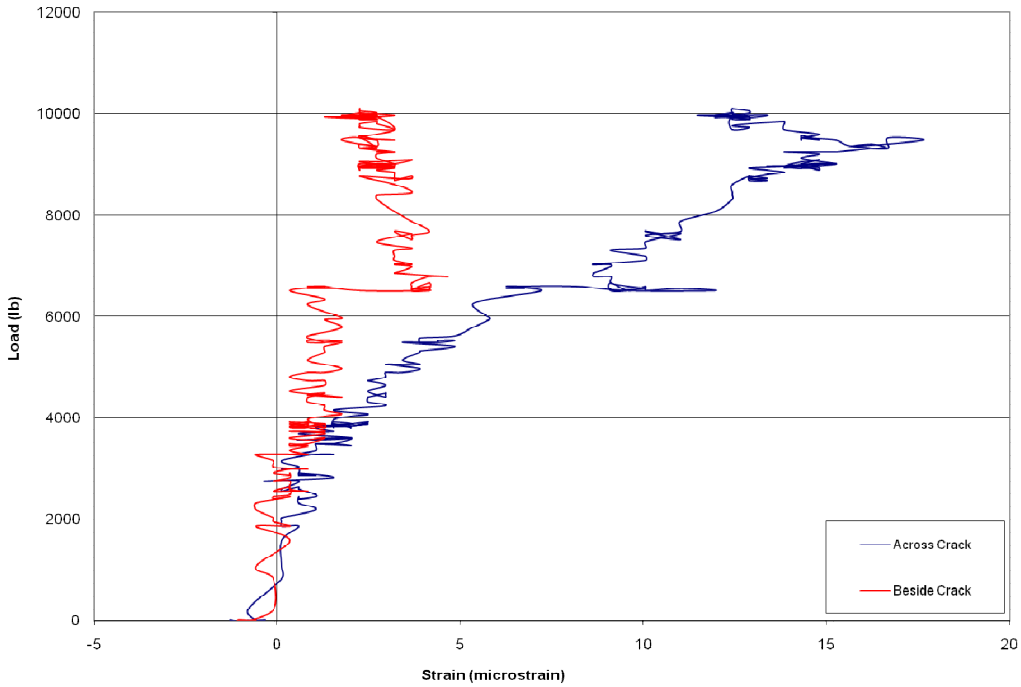

Figure D.18 Re-crack Plot for WT3A WE

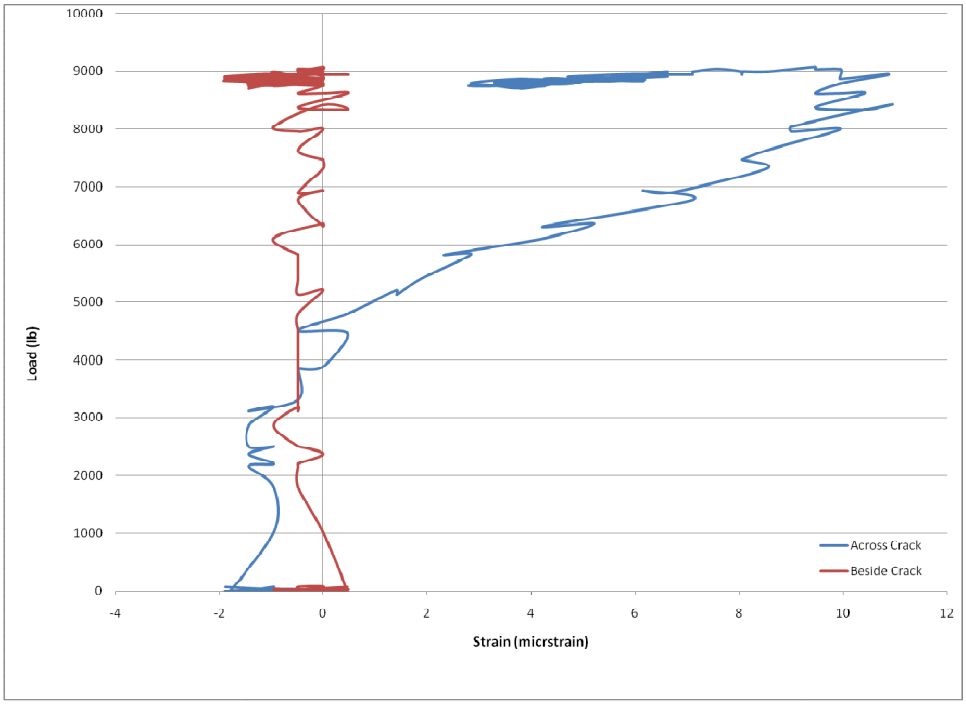

Figure D.19 Re-crack Plot for WT3B EE

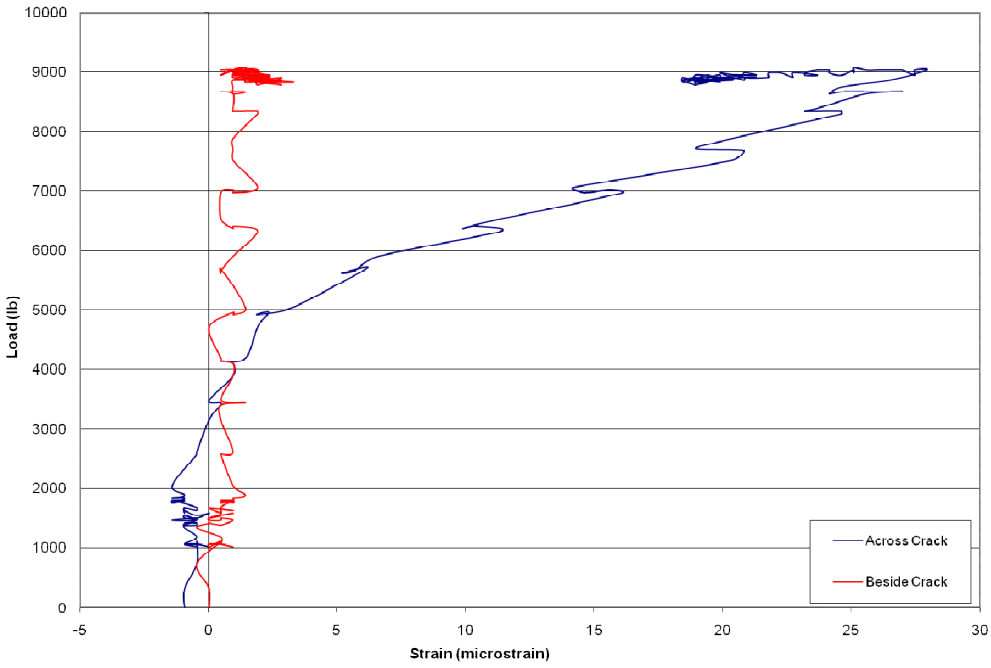

Figure D.20 Re-crack Plot for WT3B WE

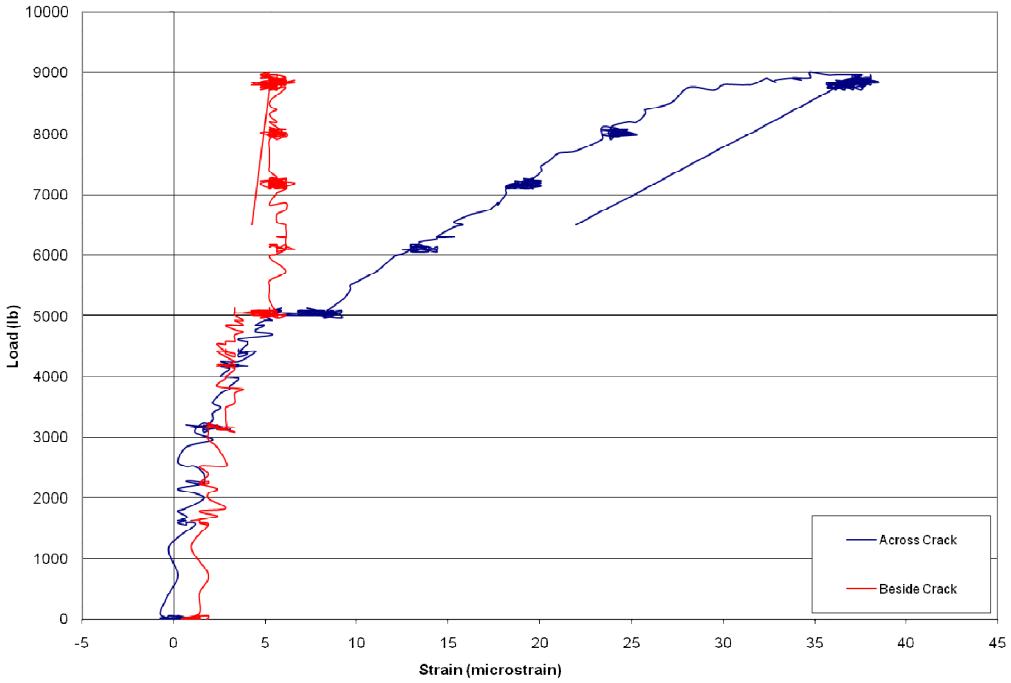

Figure D.21 Re-crack Plot for WT3C EE

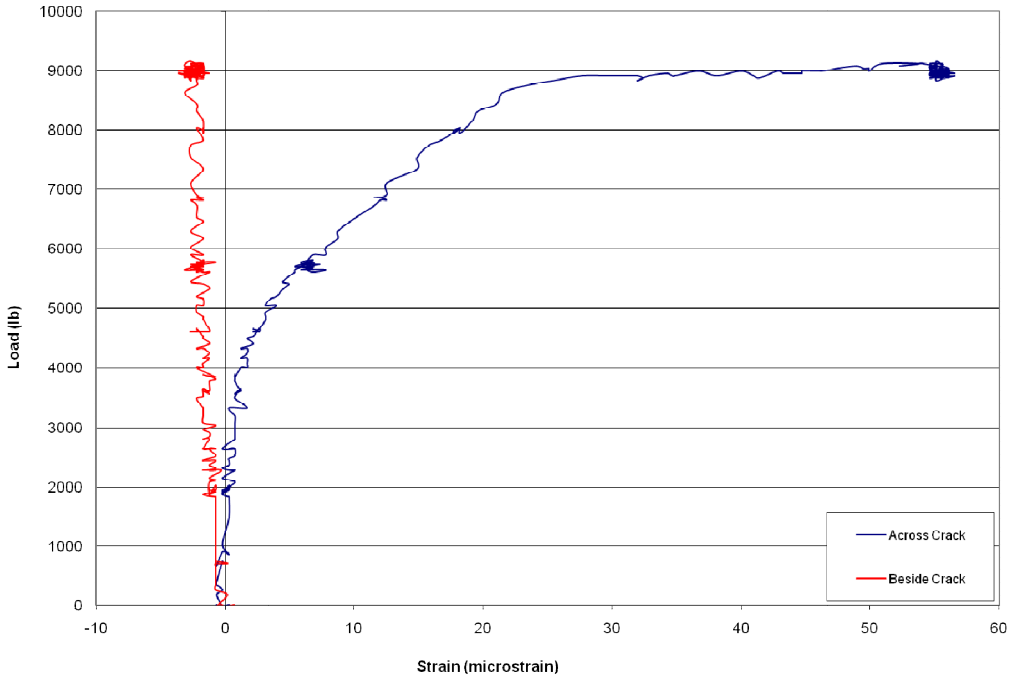

Figure D.22 Re-crack Plot for WT3C WE

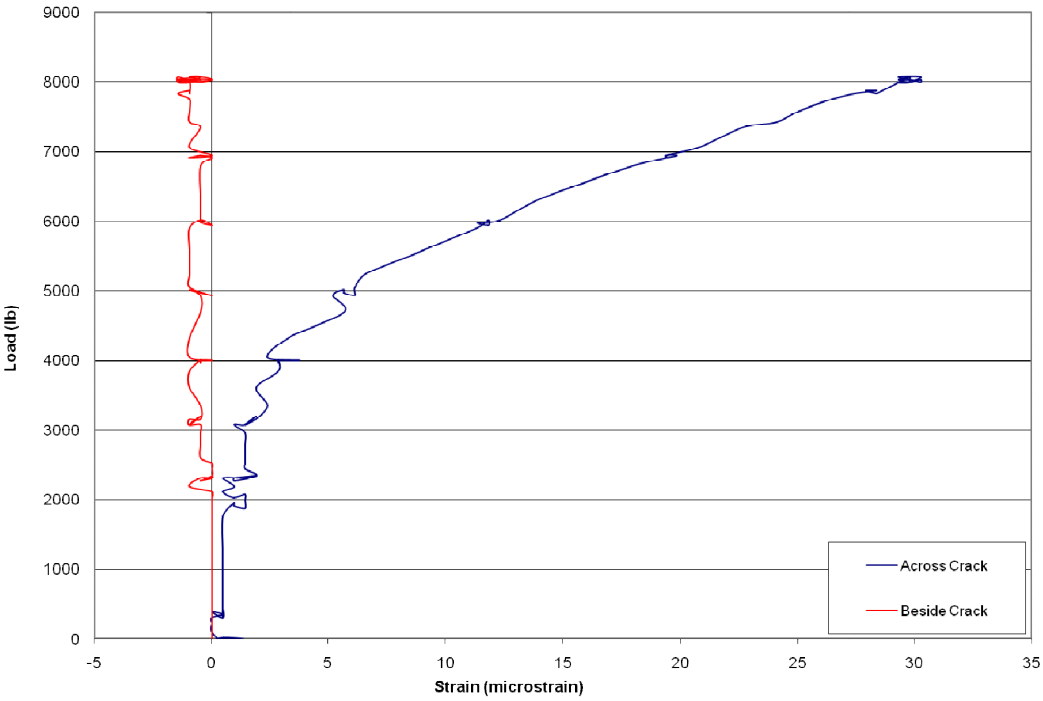

Figure D.23 Re-crack Plot for WT3D EE

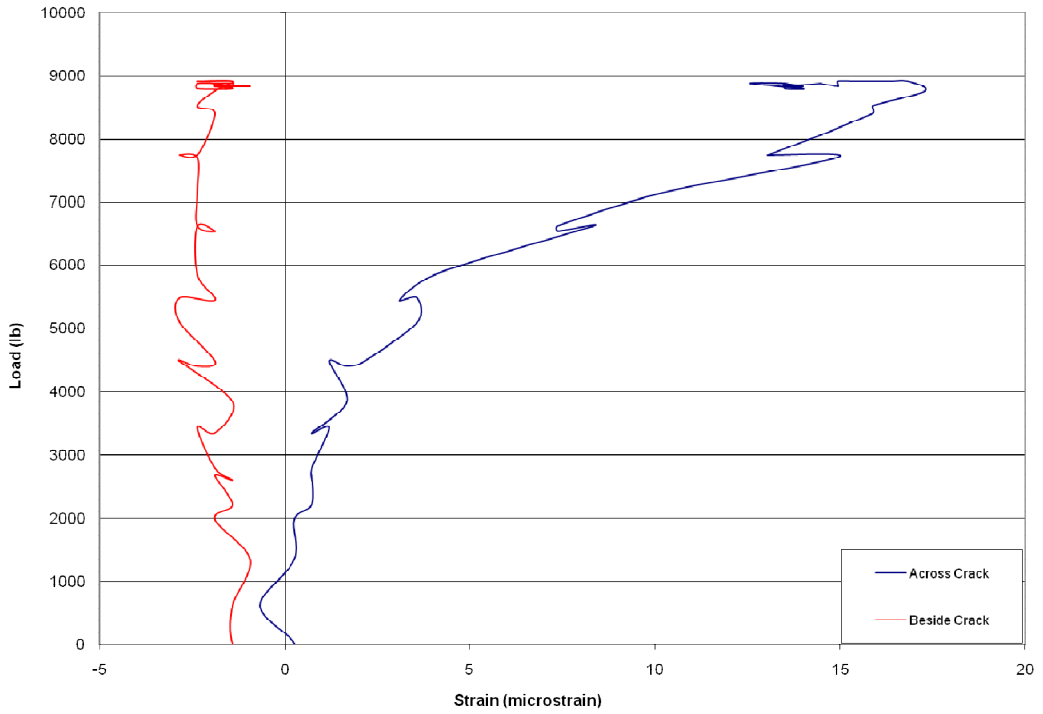

Figure D.24 Re-crack Plot for WTD WE